ABSTRACT

Title of Document: NORTH PACIFIC CLIMATE VARIABILITY
                                       AND ARCTIC SEA ICE

                                       Megan E. Linkin, Doctor of Philosophy, 2008

Directed By: Professor Sumant Nigam, Department of
                                       Atmospheric and Oceanic Science

Boreal winter North Pacific climate variability strongly influences North

American hydroclimate and Arctic sea ice distribution in the marginal Arctic seas. Two

modes of atmospheric variability explaining 53% of the variance in the Pacific Ocean sea

level pressure (SLP) field are extracted and identified: the Pacific-North American (PNA)

teleconnection and the North Pacific Oscillation/West Pacific (NPO/WP) teleconnection.

The NPO/WP, a dipole in North Pacific SLP and geopotential heights, is affiliated with

latitudinal displacements of the Asian Pacific jet and an intensification of the Pacific

stormtrack. The North American hydroclimate impacts of the NPO/WP are substantial;

its impact on Alaska, Pacific Northwest and Great Plains precipitation is more influential

than both the PNA and the El Niño-Southern Oscillation (ENSO). The NPO/WP is also

strongly associated with a contemporaneous extension of the marginal ice zone (MIZ) in

the western Bering Sea and Sea of Okhotsk and MIZ retreat in the eastern Bering Sea.

Wintertime climate variability also significantly impacts the distribution of Arctic

sea ice during the subsequent summer months, due to the hysteretic nature of the ice cap.

The North Atlantic Oscillation (NAO) is known for its effects on summer sea ice

distribution; this study extends into the Pacific and finds that circulation anomalies

related to Pacific sea surface temperature (SST) variability also strongly impact summer

Arctic sea ice. The NAO and ENSO are related to sea ice decline in the Eastern Siberian Sea, where the linear trend since 1979 is 25% per decade. PDV affects sea ice in the eastern Arctic, a region which displays no linear trend since 1979. The low frequency of PDV variability and the persistent positive NAO during the 1980s and 1990s results in natural variability being aliased into the total linear trend in summer sea ice calculated from satellite-based sea ice concentration. Since 1979, natural variability accounts for 30% of the negative trend in the Pacific marginal sea and offsets sea ice loss forced by additional factors in the Greenland Sea. Contemporaneous atmospheric variability during the boreal summer is not related to the sea ice trend, but does influence sea ice distribution in individual summers.

NORTH PACIFIC CLIMATE VARIABILITY AND ARCTIC SEA ICE

By

Megan E. Linkin

Dissertation submitted to the Faculty of the Graduate School of the
University of Maryland, College Park, in partial fulfillment
of the requirement of the degree of
Doctor of Philosophy
2008

Advisory Committee:
Dr. Sumant Nigam, chair, professor
Dr. James Carton, professor
Dr. Eugenia Kalnay, professor
Dr. Alfredo Ruiz-Barradas, assistant research scientist
Dr. James Farquhar, associate professor

Dedication

For my grandfathers, Anthony J. Kaminski and Harry E. Linkin
"So what would you think of me now? So lucky, so strong, so proud."

Acknowledgements

First and foremost, I need to thank my advisor, Dr. Sumant Nigam, for his unending patience, support, guidance and advice. His attention to detail and unparalleled scientific insight is truly inspirational; I was fortunate to have such a brilliant man and scientist as a mentor and the lessons which he taught me cannot be learned in any classroom.

Next, and just as significant, is my gratitude for my colleague, Dr. Alfredo Ruiz-Barradas. Alfredo, you taught me about being completely selfless, as you were always willing to sacrifice your own time and energy to help assist me in any way needed. Without his willingness to share data, programs and endless knowledge, this project would have never been completed.

I would like to thank Dr. Jim Carton, Dr. Eugenia Kalnay, Dr. Alfredo Ruiz-Barradas and Dr. James Farquhar for agreeing to sit on this committee.

Writing my dissertation would have been extremely difficult without the advice and suggestions of my colleague and friend, Dr. Scott Weaver. Scott always provided insightful and useful comments, and related to me in a way that only people from Middlesex County can.

My undergraduate professors have had a long-lasting impact on me. Dr. Alan Robock, Dr. Tony Broccoli, Dr. Georgiy Stenchikov and Mr. Bill Stern are fine teachers and exemplary scientists and were an inspiration for me during my undergraduate years at Rutgers University. I thank them for their guidance and advice during the formative years of my career.

I need to thank my friends and family for always believing in me and pushing me to be better. I need to thank my friends at the University of Maryland, especially Alan Cohn, Melanie Follette and Lisa Murphy, for the last 4 years and making Maryland feel more like home. I also need to thank Stephanie, Dave and my friends from college, who are an extension of my family, for their unconditional love and support. Now and forever, I will always think of you. I extend my deepest gratitude to my cousins, Jennifer and Frank, for opening their door to me and letting me live with them when I first moved to Maryland.

Finally I need to thank my parents, Robert and Nancy, and my younger brother, Michael. They are an unending source of love, encouragement and support. I am who I am, and I am where I am today because of them.

Table of Contents

List of Acronyms

AA	Aleutian Above
AB	Aleutian Below
ALB	Aleutian Blocking pattern
AMJ	April-May-June
AO	Arctic Oscillation
CPC	Climate Prediction Center
DJF	December-January-February
ECMWF	European Center for Medium-Range Weather Forecasting
EEOF	Extended Empirical Orthogonal Function
ENSO	El Niño Southern Oscillation
ENSO+	El Niño Southern Oscillation decay phase
ENSO-	El Niño Southern Oscillation growth phase
ENSO-NC	Non canonical mode of the El Niño Southern Oscillation
EOF	Empirical Orthogonal Function
ERA-40	ECMWF global reanalysis
HadISST	Hadley Centre global sea surface temperature and sea ice concentration
IGY	International Geophysical Year
IMSL	International Mathematical and Scientific Library
JAS	July-August-September
JJA	June-July-August
MIZ	Marginal ice zone

MJO	Madden Julian Oscillation
NAO	North Atlantic Oscillation
NARR	North American Regional Reanalysis
NASA	National Aeronautical and Space Agency
NCAR	National Center for Atmospheric Research
NCEP	National Center for Environmental Prediction
NPO	North Pacific Oscillation
NPO/WP	North Pacific Oscillation/West Pacific teleconnection
NP-PDV	North Pacific – Pacific Decadal Variability
NSIDC	National Snow and Ice Data Center
PC	Principal component
PDV	Pacific Decadal Variability
PP-PDV	Pan Pacific – Pacific Decadal Variability
PNA	Pacific North American teleconnection
SAT	Surface air temperature
SLP	Sea level pressure
SST	Sea surface temperature
SVD	Singular Value Decomposition
UEA	University of East Anglia
US-Mex	Merged precipitation from the United States and Mexico
WP	West Pacific teleconnection

List of Tables

List of Figures

Chapter 1: Introduction

1.1 Motivation – The North Pacific Oscillation/West Pacific Teleconnection

The Glossary of the American Meteorological Society defines the term

"teleconnection" as a:

> *1. A linkage between weather changes occurring in widely separated regions of the globe. 2. A significant positive or negative correlation in the fluctuations of a field at widely separated points. Most commonly applied to variability on monthly and longer timescales, the name refers to the fact that such correlations suggest that information is propagating between the distant points through the atmosphere.*

Glossary of Meteorology (2002)

Teleconnections are fundamental to the studies of weather and climate on a variety of spatial and temporal scales. Their presence in the atmosphere was noted even before the term "teleconnection," was coined in the latter 20th century. Since modern record keeping began in the 18th century, individuals have meticulously recorded observations of temperature and pressure at locations around the globe and remarked about apparent out-of-phase relationships between geographically remote regions (Van Loon and Rogers 1978). Hans Egede Saabye, a missionary stationed in Greenland during 1770-78, observed that, "In Greenland, all winters are severe, yet they are not all alike. The Danes have noticed that when the winter in Denmark was severe, as we perceive it, the winter in Greenland in its manner was mild, and conversely." Crantz (1765) also remarked about the opposition in winter temperatures between Greenland and Northern Europe in his book *History of Greenland* and a table (table 1) published by Gronau in 1811 describes the winter phenomenon back to 1709 (Dannmeyer 1948).

In the early 20th century, Sir Gilbert Walker and his colleague, E. W. Bliss, published an outstanding series of manuscripts that finally named this phenomenon and other out-of-phase temperature relationships. Sir Walker was perhaps the most astute climatologist of his time, as he was the first to calculate both contemporaneous and lag-lead correlations between variations of sea-level pressure (SLP), surface air temperature and precipitation at 17 "centers of action," selected based upon their proximity to semi-permanent pressure systems and monsoonal circulations (Walker 1923). A follow-up study (Walker 1926) explains the robust correlations between SLP, surface air temperature and precipitation at geographically remote areas by proposing that two oscillations in northern SLP change the circulation in the Atlantic and Pacific Oceans; he names these the North Atlantic Oscillation (NAO) and North Pacific Oscillation (NPO). The NPO is a meridional oscillation in SLP between the midlatitudes and the subtropics in the Pacific Ocean, whose signature is manifested in a displacement and an intensification of the Aleutian Low. The NPO is briefly described in Walker and Bliss (1928):

> *The essential feature in the N. Pacific oscillation is the opposition between pressure at Honolulu on the one hand and pressure at Alaska and temperature at Dutch Harbour in the Aleutian Islands on the other, increased circulation involving positive departures in the first and negative departures in the last two.*

> *Walker and Bliss, (1928), p. 104*

with a more thorough description of the NPO following in 1932. Walker and Bliss built their description of the NPO based on remarks made by observers with the United States Weather Bureau in 1916. Synopticians noted that:

> *... pressure variations in Hawaii were opposed to those over Alaska and Alberta, and that high pressure in Alaska meant a more southerly track of "lows" and*

more rain in parts of the United States and liability to cold weather east of the Rocky Mountains

As mentioned earlier, Sir Walker proposed that prevailing synoptic conditions were linked to persistent, super-synoptic (what we will refer to as subseasonal) SLP oscillations. In their fifth manuscript, Walker and Bliss pursued this notion of subseasonal variability by developing an NPO index from monthly-mean SLP and surface air temperature; monthly means were constructed from daily station data. Index correlations were then used to characterize the hemispheric-wide climate response of the NPO, which included notable precipitation and surface air temperature anomalies over North America. Warmer temperatures in interior North America coincided with lower pressure over Alaska, as did suppressed precipitation in much of western Canada. Significant correlations were also found over Asia and South America (figure 1.1).

Rogers (1981) performed a more recent analysis of the NPO using the magnitude and sign of surface air temperature anomalies between St. Paul, Alaska and Edmonton, Canada. He defined two phases of the NPO: Aleutian-Below (AB) and Aleutian-Above (AA). The AB phase of the NPO corresponds to an eastward shifted, intensified Aleutian Low, while the AA phase corresponds to oppositely signed anomalies (figure 1.2). The composite difference between the two phases is a SLP pattern nearly identical to the second eigenvector of Kutzbach (1970); the first vector was the North Atlantic Oscillation (NAO). During the eastward shifted Aleutian Low phase, Eastern Siberia and the southwest United States are anomalously cold, while much of coastal and interior North America is warm, with Alaska and the Great Plains receiving more precipitation;

consistent with the findings of Walker and Bliss (1932). Rogers's analysis is notable for linking the NPO circulation to movements of the sea ice edge in the Bering Sea, with the AB phase associated with a southward ice edge.

While Rogers was analyzing surface climate variability, climate teleconnections were being investigated in upper-air fields. The pioneering analysis of Wallace and Gutzler (1981; hereafter WG81) which identified five major teleconnection patterns in the 500 hPa geopotential heights during northern winter was published the same year as the Rogers' paper. The West Pacific pattern, one of the five, shows strong negative correlation between centers of action at 60ºN, 155ºE (65ºN,170ºE) and 30ºN, 155ºE (25ºN,165ºE) in the 500 hPa height (SLP) field; the base points for the WP (NPO) index. A composite based on the ten highest and lowest index values was used to characterize WP variability: A center over the Kamchatka peninsula and a broad low-latitude node straddling the 155ºE meridian, with a thickness pattern consistent with a cold core equivalent-barotropic structure. More importantly, WG81 noted the WP-NPO link (figure 1.2), writing the robust correlation between the WP base points and SLP "…is indicative of a close association between this pattern and the North Pacific Oscillation in the sea level pressure field identified by Walker and Bliss (1932)." A subsequent study by Barnston and Livezey (1987) extracted WP variability from rotated principal component analysis of 700 hPa hemispheric geopotential height anomalies. The WP pattern emerged as the 2nd or 3rd leading mode of variability in the 1950-84 record of monthly winter anomalies. In addition to the WP characteristics noted in WG81, an additional center of the same sign as the Kamchatka Peninsula center was found over the southwest United States in this analysis.

The vertical structure of the NPO and the WP was initially described by Hsu and Wallace (1985). Their "Pacific" pattern displays a unique vertical structure, influenced by both the Pacific Ocean and orography of the Rocky Mountains. Over the Pacific Ocean, the Pacific pattern is equivalent barotropic; similarly signed SLP anomalies are collocated with geopotential height anomalies in the mid to upper troposphere. Along the eastern slope of the Rockies, however, the vertical structure is highly baroclinic in nature. Positive SLP anomalies occur at the surface, while negative geopotential height anomalies are present at 500 hPa. The circulation features lee of the Rocky Mountains corroborates the findings of Walker and Bliss (1932); higher pressure in Alaska is linked with cold air outbreaks east of the Rockies.

Monthly means provide significant insight into the mature phase structure of teleconnections. However, the rapidly varying nature of the atmosphere necessitates the use of data with higher temporal resolutions to capture the nascent and decay phases of internal variability. Both observational analysis and modeling studies have demonstrated the rapidity with which teleconnections develop and decay. Esbensen's (1984) separate analysis of inter-monthly and interannual variability of 700 hPa geopotential heights showed the WP pattern to be operative on inter-monthly timescales. Feldstein (2000) investigated the preferred structure of variability at even finer resolution – in unfiltered daily data. His analysis of 300 hPa height anomalies shows the presence of NAO, Pacific/North American (PNA) and WP patterns, but all with e-folding timescales of 7-10 days, i.e., close to the synoptic time scale. NPO has also been linked to Alaskan blocking events (Nakamura and Wallace 1990; Renwick and Wallace 1996) and variations in the Pacific stormtrack (Lau 1988; Rogers 1990).

Dole (1986) found that persistent height anomalies over the North Pacific, North Atlantic and Siberia all exhibit a characteristic decay scale of approximately 15 days. Dole and Black (1990) and Black and Dole (1993) focused on the development of persistent negative height anomalies over the North Pacific and concluded that there is an important contribution from baroclinic cyclogenesis to the evolution of PNA-like height anomalies over the North Pacific.

Theoretical studies support the observational findings of a 10-15 day timescale for teleconnection evolution. Hoskins and Karoly (1981) used a linear steady-state five layer baroclinic model to simulate the response of the atmosphere to both orographic and thermal forcing. Energy associated with model generated Rossby waves propagated around the globe in approximately 15 days. Simmons et al. (1983) linearized a barotropic model about a 300 hPa January mean state and applied forcing in the form of localized perturbations throughout the tropics and subtropics. The patterns which result from these forcings appear to be associated with the most rapidly growing mode of barotropic instability associated with the mean state. This mode, which resembles the PNA and East Atlantic patterns (Wallace and Gutzler 1981), exhibits a period of ~50 days and an *e-folding* timescale of about one week. In localized regions, the growth rate is rapid, near the baroclinic instability growth rate.

Lag-lead regressions and correlations of time series derived from EOF analysis or singular value decomposition analysis on various atmospheric quantities provide insight into the precursor stages of teleconnection patterns. Correlations between pentad resolution geopotential height anomalies at 500 hPa and 1000 hPa and the time series of the Pacific pattern (Hsu and Wallace 1985; their Pacific pattern is the NPO/WP) reveal

that the Rocky Mountains impart a profound influence on the development of the NPO/WP. The presence of orography at lower levels results in 1000 hPa height anomalies that traverse a route parallel to the contours of elevation on the lee side of the Rocky Mountains; eventually reaching the southeastern United States. Conversely, at 500 hPa the impact of mountains is negligible and the development of the NPO/WP circulation anomalies is primarily controlled by low frequency Rossby wave dispersion. The differential evolution of the NPO/WP between the lower and upper troposphere gives the pattern a uniquely baroclinic structure lee of the Rockies and links the negative phase to cold air outbreaks in the eastern two-thirds of the United States.

Nigam (2003) analyzed weekly winter 200 hPa geopotential height anomalies using rotated principal component analysis; the leading variability modes were the same as discussed in earlier studies: NAO, NPO/WP and PNA. Focusing on the structural evolution of the PNA, a coherent signal in the extratropics is discernable two weeks in advance of the mature phase. The rotational component of the circulation development represents an eastward extension and meridional tightening of the Asian Pacific jet. The divergent circulation, diagnosed through divergence and diabatic heating anomalies, appears to be generated by the restoring forces of the thermal wind balance and secondary circulations. Most significantly, no obvious linkages to the tropics, either to ENSO or the Madden-Julian Oscillation (MJO; Madden and Julian 1971, 1972), are present, questioning the notion that the PNA is Rossby wave propagation in response to tropical Pacific forcing.

1.2 – The NPO/WP and Northern Hemisphere climate

The aforementioned studies discuss WP variability largely from the circulation viewpoint. The hydroclimate impact of this height variability pattern, especially over North America, was presented in Nigam (2003), who performed teleconnection analysis on an extended record (1958-98) of winter month anomalies in the full hemispheric domain (EQ-90ºN); as opposed to the 15-year (1962/63-76/77) extratropical domain (20º-90ºN) analysis of Wallace and Gutzler. A RPCA analysis of 200 hPa heights and of SST and heights together are both performed in that study. The WP pattern was identified as the 4th leading mode of variability, behind NAO, El Niño-Southern Oscillation (ENSO), and the PNA. Linear regressions of the WP principal component on SLP and zonal winds return a SLP signature similar to the NPO, much as in WG81, and link WP variability to meridional displacements of the Asian-Pacific jet. Nigam (2003) analyzed the WP links to North American precipitation and found significant correlations over the Pacific Northwest and the Great Plains, corroborating earlier findings of Walker and Bliss (1932) and Rogers (1981).

The NPO is also highly influential over the Pacific Ocean. Cayan (1992) found a tripole in turbulent heat flux anomalies is associated with the surface circulation around the two centers of the NPO. More significant, however, is the NPO's impact on Pacific sea surface temperature (SST). The southern lobe of the NPO is situated in the subtropical latitudes and the southern flank of the southern lobe extends into the trade winds. Relaxation of the trade winds is associated with one phase of the NPO (weakened Aleutian Low) and the weakened trade winds are a precursor of two coupled ocean/atmosphere phenomena: The Pacific Meridional Mode (Chiang and Vimont 2004) and ENSO (Vimont et al. 2001, 2002, 2003a, 2003b).

The Pacific Meridional Mode is an anomalous meridional SST gradient with an axis along the mean latitude of the Intertropical Convergence Zone. The variability peaks in boreal spring and is forced by anomalous trade winds in the northern subtropical ocean. Lagged regressions of the Pacific Meridional Mode principal component on SLP reveal that the NPO is the wintertime variability responsible for the trade wind slackening. Changes in the turbulent heat fluxes impart an SST footprint (Vimont et al. 2001) which persists into the boreal spring and in turn forces the tropical atmosphere.

The hypothesis that an SST footprint left by midlatitudes variability persists and forces the tropical atmosphere is referred to as the seasonal footprinting mechanism (SFM; Vimont et al. 2001). In a series of studies (Vimont et al. 2001, 2002, 2003a, 2003b) using the CSIRO coupled general circulation model, the authors are able to show that an NPO-related wintertime relaxation of the trade winds results in an anomalous SST pattern throughout much of the subtropical and tropical Pacific. The anomalous SST pattern persists for several months and forces a summertime circulation that imposes anomalous westerly wind stress at the equator. The anomalous westerly wind stress is determined to be a source of stochastic forcing for both ENSO and ENSO-like variability.

The response of sea surface temperatures (SST) and sea ice to teleconnection patterns is also discernable at subseasonal timescales. The PNA surface circulation imposes anomalous surface westerlies over the midlatitude and subtropical Pacific Ocean, leading to a wind driven SST response. Enhanced (diminished) westerlies (easterlies) increase (decrease) surface heat fluxes and vertical mixing at the air-sea interface. The changes in SST are consistent with a dynamic response to the atmospheric forcing; colder SST occurs north of 30ºN, with warmer SST confined to the south of

30ºN. Deser and Timlin (1997) also found strong atmosphere-ocean coupling on weekly timescales, specifically when the atmospheric circulation leads the SST by 2 weeks. In addition to atmospheric circulation responding to SST anomalies, the extratropical wintertime circulation anomalies cause SST anomalies, with the SST anomalies reaching their peak several weeks after the strongest atmospheric forcing. The pronounced weekly coupling of the air-sea system occurs in both the Atlantic and Pacific Oceans, and the leading pattern of Pacific atmosphere-ocean covariability on this timescale resembles the WP, leading to the possibility that the NPO/WP is the primary source of stochastic forcing of the oceanic mixed layer on weekly timescales.

The NPO/WP pattern has received little research attention in comparison with the NAO and PNA patterns, and ENSO's midlatitude teleconnection. This is not surprising given the larger influence of these patterns on winter continental precipitation (Nigam 2003). The NPO/WP pattern is however, if anything, more influential in the Pacific Northwest, especially in coastal regions, and in the south-central Great Plains. Moreover, just as the upward trend in NAO index in recent decades spurred interest in NAO research in view of potential links with global warming, Arctic sea-ice variability, especially, its recent decline, is generating new interest in NPO/WP variability.

1.3 Atmospheric Circulation and Arctic Sea Ice Variability

A combination of annual and perennial sea ice covers the Arctic Ocean, marginal seas and sub-Arctic marginal seas (figure 1.3), displaying a seasonal cycle (figure 1.4) which parallels the seasonal cycle of solar radiation. Sea ice begins to form during the month of October, when the surface layer of the ocean cools to the freezing point

(-1.8ºC). On a calm surface, a thin layer of tiny crystals form on the sea surface, growing

laterally. Lateral growth of the ice crystals yields them unstable, and dendrite arms of the

ice crystals break from even minimal turbulence. This suspension of broken ice crystals

on the surface is referred to as frazil ice (figure 1.5*a*), and in tranquil conditions, the

crystals freeze together into one continuous, centimeters-thick ice sheet. These thin

sheets of sea ice are termed nilas, and upon the sea ice reaching the nila stage, sea ice

growth changes; water freezes to the bottom of the ice sheet, increasing the thickness

below the ocean surface. This process is known as congelation growth. In rough water,

pancake ice (figure 1.5*b*) is formed from the frazil ice; pancake ice is a consolidated layer

of sea ice formed by rough seas promoting aggregation of sea ice crystals. The pancake

ice grows into pack ice (figure 1.5*c*), the sea ice type most commonly known.

The sea ice maximum is reached in April, and the melt season commences in

May. Melting is triggered by the formation of melt pools on the surface of the sea ice,

lowering the albedo and increasing the absorption of solar radiation. As solar radiation

increases during the summer months, the melt pools increase in surface area and depth,

draining into the underlying ocean via cracks in the sea ice . The melt continues until

September, the autumnal equinox (Wadhams 2003).

Sea ice measurements are presented using a variety of terms, defined below by the

National Snow and Ice Data Center:

- **Sea Ice Area** – Total area in km^2 of the globe covered by sea ice; quantity
  is calculated by multiplying each grid cell (25 km x 25 km true at 70ºN)
  by the fractional concentration of sea ice within that particular cell and
  summing the areas.

- **Sea Ice Extent** – Defines an area as being "ice-covered" or "ice-free," based upon a minimum concentration threshold, typically 15%. The area of grid cells where sea ice concentration exceeds the threshold is summed together. Extent is always larger than area; if sea ice concentration exceeds the threshold in the grid cell, then the entire area is considered ice covered. No weighting by the sea ice concentration is performed.

- **Sea Ice Concentration** – The fraction of a grid cell covered by sea ice.

All three terms are used throughout the analysis. Sea ice concentration is the only variable available on a 2-D grid. Sea ice extent and area are total quantities, rendering them 0-D (time series). Regardless of the sea ice variable chosen to represent anomalous sea ice coverage, all reveal the same thing: Arctic sea ice is unquestionably declining.

Since 1979, the first full year of satellite-based sea ice observations, Arctic sea ice extent exhibits a negative linear trend during the entire melt season (May-June-July-August-September). The trend is largest in September, the month of the annual sea ice minimum (Figure 1.6). With the beginning of the 21st century, the rate at which summertime sea ice is declining has increased (Solomon et al. 2007), surpassing the sea ice projections from coupled climate models. Furthermore, in September 2007, Arctic sea ice extent reached a minimum of 4.13 million km^2, 25% less than the previous record set in 2005 and the lowest since modern record keeping commenced (NSIDC 2007). This decrease in sea ice extent is also no longer confined to the summer months alone; since the early 2000s, sea ice extent during the winter months of January, February and March is also displaying a downward linear trend (Meier et al. 2005).

The alarming rate at which sea ice is shrinking, coupled to the appearance of a negative trend during the non-summer seasons, is the motivation behind numerous studies which strive to attribute the sea ice decline to natural variability, anthropogenic climate change or both. The pervasive hypothesis is that the current sea ice extent is evidence of anthropogenic climate change and the ice-albedo feedback. Increased atmospheric carbon dioxide concentration due to human activities augments downward longwave infrared radiation. To balance the enhanced radiation, surface temperature increases and melts the sea ice. The melting of the sea ice is amplified by changes in the surface albedo, as absorbing open ocean replaces reflective sea ice. Thus, more shortwave radiation is absorbed by the Arctic, further exacerbating sea ice melt. The increased fraction of thinner sea ice during the subsequent summer melt season results in a larger area of the sea ice melting, causing sea ice extent to plummet. The hysteresis of sea ice and the persistence of sea ice anomalies explain the trend in the subsequent autumn and winter seasons, as the time required for the sea ice to recover increases as summer sea ice extent decreases.

Imposed upon the linear trend, however, is substantial interannual variability. Prior to 2005, 2002 was the year of minimum September sea ice extent (NSIDC 2007). The summer of 1995 was the previous minimum for seasonal sea ice coverage before 2007, with the months of June, July and August all featuring below average sea ice extents (Singarayer et al. 2006). The presence of an interannual signal in the sea ice implies that natural variability is relevant in the state of Arctic sea ice.

The primary natural driver of sea ice, particularly on shorter timescales, is local atmospheric forcing (Thorndike and Colony 1982, Prinsenberg 1997). Changes in the

atmospheric circulation alter the surface wind distribution, and variations in the surface winds force ice drift (Thorndike and Colony 1982). This relationship is strongest along the marginal ice zone (MIZ), defined as the narrow transition zone between ice free and ice covered conditions (Fang and Wallace 1994), since thinner ice (lower internal stress) and lower sea ice concentration regions respond more strongly to atmospheric forcing (Shevchenko et al. 2004). Latitudinal displacements of the stormtracks can also impact the position of the MIZ, as poleward stormtracks increase the advection of warm moist air into the Arctic region (Pease 1980). During the winter months, the MIZ extends into the sub-Arctic Pacific and Atlantic seas. Figure 1.7 shows the climatological sea ice distribution and standard deviation for December-January-February 1958-2001 in the Bering Sea and Sea of Okhotsk. The MIZ is obviously far enough equatorward to respond to shifts in the positions of the Aleutian Low and Icelandic Low; furthermore, the standard deviation contours suggest that the variability of sea ice is confined to the MIZ.

The MIZ and NPO/WP variabilities have been linked (Johnson 1980, Rogers 1981, Parkinson and Gratz 1983, Cavalieri and Parkinson 1987), mostly using coarse sea-ice data from satellites, including Nimbus-7. Many of these studies suggest that a shift in the Aleutian Low results in a sea-ice dipole between the Bering Sea and Sea of Okhotsk. Rogers' (1981) analysis is the most thorough from the NPO/WP perspective, and concludes that the Bering Sea MIZ advances (retreats) during the positive (negative) phase of the NPO/WP.

Fang and Wallace (1994) utilize SVD analysis to obtain the leading covariability patterns of the atmosphere-sea ice system on weekly timescales. The strongest

correlations between sea ice and 500 hPa geopotential heights in the sub-Arctic Pacific seas occur when sea ice lags the atmosphere by 1 week (figure 1.8). The sea ice anomaly is a dipole pattern, with anomalies of opposite sign in the Bering Sea and Sea of Okhotsk. The corresponding 500 hPa height pattern features a dominant center over Alaska, with weaker opposing centers over Siberia and the western United States. This height pattern is not the PNA, but bears a stronger resemblance to the NPO. Blocking over Alaska is linked with a retreat (advancement) of sea ice in the Bering Sea (Sea of Okhotsk). When the opposite is true, the sea ice grows (retreats) in the Bering Sea (Sea of Okhotsk).

The linkages between the NAO and the wintertime MIZ have been more extensively studied, due to the presence of transcontinental shipping traffic in the North Atlantic. Van Loon and Rogers (1979) correlated various seasonal indexes of sea ice severity with the winter NAO and find that the positive phase is associated with heavy summer sea ice in the Davis Strait, more springtime icebergs near Newfoundland and light ice conditions in the Baltic Sea. A more extensive study is performed in Deser et al. (2000), who found that during winter, the positive phase of the NAO is connected to an out-of-phase dipole between the Labrador Sea and Greenland-Barents Seas. Enhanced cyclonic anomalies in the North Atlantic force an extension (retreat) of the MIZ in the Labrador (Greenland-Barents) Sea. Moreover, an intensified, poleward stormtrack increases the number of storms penetrating into the Arctic, bringing warm, moist midlatitude air into the polar regions and causing the break-up of sea ice due to large, wind driven waves destroying the sea ice edge.

As briefly mentioned earlier, the global climate is a hysteretic system, where the current state of the climate reflects not only the current conditions and inputs, but also the

history of how the system was driven to its current state. Arctic sea ice anomalies are an example of the "memory" of the climate system; certain winter circulation patterns are conducive to the development of thinner sea ice and the transport of multiyear ice out of the Arctic through the Fram Strait into the Atlantic.

The linkages between the wintertime atmospheric circulation and the summer sea ice anomalies led some to propose that the trend in summertime sea ice extent was not due entirely to anthropogenic changes, but partially explained by a trend towards a persistent positive phase of the Arctic Oscillation (AO; Thompson and Wallace 1998) during the latter part of the 20th century. The positive phase of the AO is associated with cyclonic anomalies over the polar ice cap. The cyclonic anomalies of the high-index phase of the AO force Ekman divergence (figure 1.9) of the sea ice, opening leads and fractures in the sea ice pack. The presence of open leads will promote the development of thin sea ice and enhanced heat flux from the ocean. A reduction in the strength of the anticyclonic Beaufort gyre will decrease sea ice recirculation, further contributing to sea ice loss (Rigor et al. 2002). A comparison of seasonal summer sea ice concentration trends with the regression of seasonal summer sea ice concentration on the previous winter AO index (figure 1.10) reveals significant spatial similarity between the two plots, especially along the Siberian coast, implicating the persistent positive phase of the AO during the 1980s and 1990s as a contributor to the observed summer sea ice decline.

Since the turn of the century, the AO displays no trend, becoming neutral in recent years. Arctic sea ice, especially in the summer, continues to decline rapidly. The paradox between the winter AO conditions and the thinning summer Arctic sea ice led many to suggest that the Arctic climate reached a tipping point and that high latitude

circulation was no longer the primary driver of sea ice variability (Lindsay and Zhang 2005). Maslanik et al. (2007) identified three additional atmospheric circulation patterns, focused regionally, which are also conducive to thinning sea ice in the western Arctic. All three circulation variabilities, found previously in earlier studies by Gudkovich (1961), Rogers and McHugh (2002), Wang et al. (2005) and Wu et al. (2006), were active and in phase during the peak AO period. In recent years, the patterns have diverged, and only two, as opposed to all three, are contributing to thinning sea ice. The coincidence of two out of three circulation patterns, instead of all three, reduces the value of the hemispheric-wide AO index but continues to promote thinner winter Arctic sea ice.

Summertime circulation also imparts a signal on the sea ice. The AO occurs in all calendar months, explaining 36% of the SLP variance over the Arctic during the summer months (Rigor et al. 2002). Regressing July-August-September SLP onto an index developed from detrended sea ice concentration returns a pattern similar to the summer AO, whose summertime index is correlated with September sea ice concentration at 0.51 (Ogi et al. 2004). Anticyclonic anomalies are conducive to sea ice thinning in the Siberian and Alaskan marginal seas (figure 1.11), with easterlies advecting ice away from the coast into the interior Arctic (Ogi and Wallace 2007). This is in stark contrast to the relationship between the winter AO and summertime sea ice concentration, where cyclone circulation anomalies promote decreased sea ice.

The importance of the wintertime circulation variability on the summertime distribution is clearly evident based on the above discussion. However, much of the focus is on the Atlantic and the Arctic. The current study extends the region of focus to the Pacific, investigating how the high-latitude circulation anomalies associated with the

PNA and NPO/WP impact both the contemporaneous MIZ during the winter months and

sea ice distribution during the following summer. Additionally, we seek to further the

understanding of the relationship between summertime sea ice conditions and the

contemporaneous atmospheric circulation by extracting and defining the various summer

circulation regimes and dominant modes of sea ice variability.

1.4 Research Questions

The presented research attempts to definitively answer the following questions:

- What is the spatial structure, both horizontally and vertically, of the mature phase NPO/WP? What are the characteristics of the rotational and divergent components of the circulations?

- How does the NPO/WP impact the Asian-Pacific jet stream and the Pacific Basin stormtrack? Are the impacts analogous to the impacts of the NAO on the Atlantic jet stream and stormtracks? What are the other similarities/differences between the NPO/WP and NAO? Does the weekly analysis reveal any interbasin links indiscernible on monthly timescales?

- How does the NPO/WP impact North American hydroclimate? How significant is the impact in the Pacific Northwest, where the precipitation displays a strong seasonal cycle? How does the NPO/WP hydroclimate response compare to that of ENSO and the PNA?

- What is the response of the MIZ, especially in the Pacific sub-Arctic seas, and SST to NPO/WP variability? Are any linkages to ENSO noted?

- What are the defining characteristics of the nascent and decay phases of the NPO/WP when weekly anomalies are used? How do the jet anomalies evolve?

- Does the MIZ respond almost immediately, as suggested in Fang and Wallace (1994)?

- How do the wintertime teleconnections (NPO/WP, PNA and NAO) and Pacific SST variability affect summertime distribution of sea ice in the Arctic Ocean? Is there a trend in any of the climate indexes that explains a fraction of the trend in sea ice concentration?

- What are the dominant modes of summer atmospheric variability? Are any of them highly influential for sea ice distribution?

- How much of the sea ice decline observed in 2007 can be attributed to atmospheric circulation and natural climate variability?

1.5 Data and Methodology

1.5.1 Datasets – monthly NPO/WP analysis

Climate studies, mainly those involving climate variability, have been revolutionized by the introduction of comprehensive gridded global reanalyses. The first was introduced by the National Center for Environmental Prediction and the National Center for Atmospheric Research (NCEP/NCAR). The NCEP/NCAR reanalysis (Kalnay 1996), hereafter the NCEP reanalysis, is a multiyear 1949-present dataset generated with a fixed assimilation system. A decade later, the European Center for Medium Range Weather Forecasting (ECMWF) introduced its reanalysis, beginning in September 1957 (the International Geophysical Year; IGY) and ending in August 2002 (Uppala et al. 2005). The ability of these reanalyses to capture long-term climate variability is without equal; however, the minor drawback of these is the relatively coarse spatial resolution and the large quantity of variables which are model output, as opposed to assimilated observations (i.e. precipitation).

Much of our analysis is performed with the ECMWF 45 year global reanalysis, ERA-40. ERA-40 analysis is produced at 6 hourly intervals for the entire 44 year period and is archived on 2.5° longitude x 2.5° latitude horizontal grid with 23 isobaric vertical levels. Monthly mean quantities were retrieved directly from the ECMWF website

(http://data.ecmwf.int/data/d/era40_mnth/). Anomalies were calculated by removing the 1958-2001 climatology.

To test the robustness of our results, we supplemented our analysis with the NCEP reanalysis. As with the ERA-40 reanalysis, the NCEP reanalysis is produced at 6 hourly intervals using a T62 global spectral model with 28 levels in the vertical. The NCEP data was available in-house, archived on a 5º longitude x 2.5º latitude horizontal grid with 17 levels in the vertical. We used the overlapping ERA-40 period, calculating the anomalies by removing the 1958-2001 climatology.

Diabatic heating, a significant influence on tropical and extratropical circulation by forcing divergent circulation anomalies, was diagnosed in-house using the ERA-40 isobaric reanalyses at 2.5º resolution (Chan and Nigam 2007). Heating was diagnosed as a residual in the thermodynamic equation (e.g., Hoskins et al. 1989; Nigam 1994), using monthly-averaged data and sub-monthly transient fluxes; just as it was earlier for NCEP and ERA-15 reanalyses (Nigam et al. 2000). The diagnosis involves the thermodynamic equation and analyzed vertical velocity (ω):

$$\overline{Q} = \frac{\Delta T}{\Delta t} + \overline{\vec{v}} \cdot \vec{\nabla}\overline{T} + (p/p_o)^{(R/C_p)}\overline{\omega}\frac{\partial\overline{\Theta}}{\partial p} + (p/p_o)^{(R/C_p)}[\vec{\nabla}\cdot\overline{\vec{v}'\Theta'} + \frac{\partial\overline{(\omega'\Theta')}}{\partial p}]$$

Monthly means are denoted by an overbar and the quantities with primes are the departure of the 6-hourly analysis from the monthly mean quantity. This method does not allow for separation of the residual into contributing constituents, i.e. sensible, latent and radiative heating components, however, all three of these are provided in both the ERA-40 and NCEP reanalysis.

Monthly precipitation and surface air temperature data from the University of East Anglia (UEA) are used to characterize the hydroclimate impact. The global 1901-2002 station data is available on a 0.5° lon x 0.5° lat grid (Mitchell and Jones 2005). Monthly snow cover is also used, available between 1971 and 1994 and provided by the NOAA/OAR/ESRL PSD, Boulder, Colorado, USA, from their Web site at http://www.cdc.noaa.gov/ (Dewey and Heim 1981, Dewey and Heim 1982). Monthly SST data comes from the 1870-2002 Hadley global SST data set (HadISST), on a 1º lon x 1º lat grid (Rayner et al. 2003). Monthly sea ice concentration comes from the updated HadISST1.1, covering 1870-2007 (Rayner et al. 2006), retrieved from the NCAR Research Data Archive, found at: http://dss.ucar.edu/. The sea ice concentration is primarily derived from satellite-based observations from 1979 onward; prior to 1979, sea ice concentration is calculated from shipping maps, observations and a variety of other sources. In an effort to assure ourselves that the sea ice concentration values during the pre-satellite era are representative, we use only the data during the post-IGY period, January 1958 onward. Additionally, we compare the December-January-February (DJF) 1979-2004 climatology with the DJF 1979-2004 climatology of satellite derived sea ice concentration (Cavalieri et al. 1997, updated 2006). Figure 1.12*a* and 1.12*b* show the climatology comparison, with the difference plotted in panel *c*. The climatologies compare remarkably well, with differences of approximately ~10% occurring in the vicinity of Greenland and the Sea of Okhotsk.

The ability of the HadISST1.1 to capture the variation of the sea ice, primarily at the MIZ, is paramount, as the focus of this study is largely on climate *variability*. To assess the degree to which the HadISST1.1 correctly captures sea ice variability, the DJF

1979-2004 standard deviation is calculated for both the HadISST1.1 sea ice concentration and satellite derived sea ice concentration. Variability of the ice pack is largely confined to the MIZ, positioned in the Bering Sea, Sea of Okhotsk, Barents/Greenland Seas and Labrador Sea during the winter months, with sea ice concentration varying up to 30% (figure 1.13*a* and 1.13*b*). No significant difference (panel *c*) occurs between the two data sets, bolstering our belief that the HadISST1.1 is a reasonable representation of observed sea ice concentration. While the use of satellite observations, as opposed to in situ observations, to validate a reanalysis product which uses surface-based observations is unusual, satellite-based sea ice concentration data is the most complete record of sea ice observations with the finest horizontal resolution. Alternative sources of sea ice observations which assimilate no satellite data are horizontally coarse and spaced at irregular intervals, rendering them difficult to use as baseline comparison data.

For reference, the DJF 1958-2001 climatology and standard deviation are plotted in figures 1.12*d* and 1.13*d*. The characteristics of the longer climatology and standard deviation are similar to the shorter period, not surprising given the lack of any distinguishable trend in winter sea ice prior until 2002 (Meier et al. 2005).

1.5.2 Datasets – weekly NPO/WP analysis

The weekly analysis is similar to the monthly mean analysis. Once again, both the NCEP and the ERA-40 reanalyses are used to examine the spatio-temporal structure of the NPO/WP. Sunday-to-Saturday weekly averages (centered on Wednesday) are generated from daily values retrieved from the Lamont-Doherty Earth Observatory (LDEO) Climate Data Library

(http://ingrid.ldgo.columbia.edu/SOURCES/.NOAA/.NCEP-NCAR/.CDAS-1/.DAILY/)
and the ECMWF website (http://data.ecmwf.int/data/d/era40_daily). The overlapping
period between the two data sets, January 1958-December 2001, is used, and winter is
defined as the 18 week period beginning on the Wednesday closest to December 1.
Anomalies are calculated by removing the *weekly* climatology from all winter weeks
between 1958 and 2001.

Hydroclimate impact is assessed using the 1000 hPa reanalysis temperature and
the daily precipitation analysis over the United States and Mexico (US-Mex), produced
by the Climate Prediction Center (CPC). The US-Mex is a retrospective analysis of
precipitation over the continental United States and Mexico derived from the CPC
Unified Precipitation Data Set and station gauges throughout Mexico (Higgins et al.
2000). As with the atmospheric quantities, Saturday-to-Sunday weekly means are
generated from the daily values and centered on Wednesday. The minor caveat of the
US-Mex precipitation is its truncation at the US-Canadian border, precluding analysis of
the response of Canadian and Alaskan hydroclimate on weekly timescales. The North
American Regional Reanalysis (NARR; Mesinger et al. 2003) would be ideal in this
situation, however, it currently extends back only to 1979.

Weekly SST anomalies are from the updated version of the Reynolds-Smith SST
dataset (Reynolds et al. 2002). SSTs are calculated using an optimal interpolation
scheme on a blend of in situ and satellite observations. The anomalies are calculated
using 1971-2000 as the base period climatology, and weekly values are available
beginning in November 1981. Access to the data and a more thorough technical
description is available at:

Sea ice concentration is generated from brightness temperature data provided by the Nimbus-7 Scanning Multichannel Microwave Radiometer (SMMR) and Defense Meteorological Satellite Program (DMSP) -F8, -F11 and -F13 Special Sensor Microwave / Imager (SSM/I) radiances at a 25 km x 25 km horizontal resolution. The product provides consistent time series of sea ice concentration as fraction (or percent) of the grid cell covered by ice. The sea ice concentration data is archived on a 1ºlon x 1ºlat grid in polar regions, at daily resolution during the January 1979 – December 2004 period. The period overlapping with the ERA-40 data set (January 1979 – December 2001) is analyzed in this study. Monthly means are generated from daily sea ice data, and anomalies are computed with respect to calendar-month climatologies, as before. More information on the data is available at http://www.nsidc.org/data/nsidc-0051.html, or in Cavalieri et al. (1997, updated 2006). As with the atmospheric and precipitation quantities, weekly sea ice values span Sunday-to-Saturday and are centered in Wednesday.

1.5.3 Datasets – Sea Ice-Atmosphere analysis

Both sea ice datasets are utilized in this section of the study. All 26 years of the satellite-derived sea ice concentration data is used, and the HadISST1.1, is used for both comparative purposes between 1979 and 2004 and for a longer analysis between 1958 and 2007. Extending the analysis through 2007 allows us to include the record-breaking year of 2007. As previously mentioned, September sea ice extent reached an all-time record low, and the mechanisms behind this dramatic decline are currently an active area

of research. All of the atmospheric analysis is performed using the NCEP reanalysis.

The NCEP dataset is extended to include monthly means through December 2007 and the

resolution is increased from 5º longitude x 2.5º latitude to 2.5º longitude x 2.5º latitude.

1.5.4 – Methodology

Much of the methodology is rooted in applied statistical techniques. The mean

state of the atmospheric circulation (SLP, geopotential height) and the sea ice is assessed

by calculating annual, seasonal and monthly averages from monthly mean quantities.

Anomalies are calculated by removing the annual, seasonal, monthly or weekly

climatology, depending on what the end goal of the analysis is. These anomalies provide

the basis for rudimentary and advanced statistical analysis, such as linear regression,

correlation and empirical orthogonal function (EOF) analysis.

The simplest way to glean the amount of association between two variables (i.e.

SLP and sea ice concentration) is to calculate regression and correlation coefficients. The

coefficients are calculated as followed:

$$Regression\ of\ A\ on\ B:\ \frac{\sum_{i=1}^{N} A'B'}{\sqrt{\sum_{i=i}^{N} A'^2}} \qquad Correlation\ of\ A\ with\ B:\ \frac{\sum_{i=1}^{N} A'B'}{\sqrt{\sum_{i=1}^{N} A'^2}\ \sqrt{\sum_{i=1}^{N} B'^2}}$$

Regression relates the amplitude of the anomaly for a unit departure of the normalized

time series or principal component; correlation conveys the significance of the anomaly.

Regression coefficients retain the unit of the field anomaly, while correlation coefficients

are unitless. Regression and correlation analysis are powerful tools are ascertaining the

linkages between two variables, at times leading to the deduction of causal relationships.

However, this simplistic analysis does not allow for the separation of the various modes of natural variability; a more sophisticated technique is necessary.

Empirical Orthogonal Function (EOF) analysis, also known as Principal Component Analysis (PCA), is a statistical technique that takes advantage of the fact that many geophysical variables are highly correlated in space (Kutzbach 1967; Preisendorfer 1988, Björnsson and Venegas 1997). The goal of an EOF/PCA analysis is to take a set of two or more variables and reduce the data set to a small set of modes that retains most of the original variance. EOF analysis is based in linear algebra; a covariance matrix, F, is formed from the anomaly field. Gridded anomaly fields are typically area weighted by the cosine of the latitude to account for longitudinal convergence towards the poles. The covariance matrix R forms the basis for the eigenproblem.

$$RC = C\Lambda$$

Λ is a diagonal matrix containing the eigenvalues, and C is a matrix whose columns contain eigenvectors of R corresponding to the eigenvalues. For each eigenvalue, there is a corresponding eigenvector; the eigenvectors are maps, and are the EOFs sought in the analysis. The eigenvectors are ordered according to the magnitude of the eigenvalues, thus, EOF1 corresponds to the largest eigenvalue and explains the maximum variance of the total field. The remaining eigenvalues are processed accordingly; higher numbered EOFs explain a smaller fraction of the variance.

An EOF represents a standing oscillation, and provides no insight into the fluctuations of the pattern in time. To obtain the pattern vacillation, the principal component (PC) time series are constructed by projecting the original anomaly matrix on

the eigenmatrix *C*. The original data can be reconstructed from the EOFs and the PCs, so that

$$F = \sum_{j=1}^{p} \vec{a}_j (EOF_j)$$

The reconstructed data, if preferred, contains more signal than noise by truncating the number of EOFs used in the above sum; since the first few EOFs contain much of the variance, only they truly capture the dynamical behavior of the system. Higher numbered EOFs eventually become noise.

Singular value decomposition (SVD) analysis is a close cousin of EOF analysis, and removes some of the redundancy associated with EOF analysis by further simplifying the matrices going into the calculation. This thesis research utilizes SVD analysis as a way to calculate the EOFs and associated PCs; the analysis is performed using the FORTRAN routines available in the International Mathematical and Science Library. A further description of the derivation and technique can be found in Appendix A of Nigam and Shen (1993).

The aim of EOF analysis, ideally, is to extract preferred modes of variability that correspond to known physical variations in the climate system. However, since EOF analysis is a pure statistical technique, the possibility exists that first several EOFs are not representative of actual physical modes of variability. The disadvantages of EOF analysis, discussed by Richman (1986), are listed below.

- **Domain Shape Dependence** – If the domain over which the EOF analysis is being performed is large, the EOFs are representative of the shape of the domain rather than the covariance of the data.

- **Subdomain Instability** – Richman and Lamb (1985) found that the EOFs returned from an analysis of hemispheric data were significantly different than the EOFs returned when the northern and southern halves were analyzed separately. This raises the concern that the EOFs are not particularly robust or physical.

The physicality of teleconnections extracted via EOF or SVD analysis is frequently questioned due to the limitations listed above. This issue is addressed in two ways; the size of the domain is limited or the EOFs are rotated (Richman 1986). Rotated EOFs are weighted by their corresponding eigenvalue, revealing the actual connection between the spatial patterns and anomaly field. The rotated EOFs are then more representative of distinct teleconnections, and are not merely statistical artifacts. Several different methods to rotate EOFs are contained in the literature; the most popular of these is the VARIMAX rotation (Kaiser 1958). Where rotation is necessary, this approach is used.

Canonical EOF analysis, regardless of rotation, provides a "snapshot" of a teleconnection, returning the mature phase. The temporal variability of the system is neglected in EOF analysis; the analysis is keyed to extract modes of spatial variability. Lag-lead regressions using a principal component time series then are shape sensitive and tend to seek out patterns that are spatially similar to the mature phase variability. The information pertaining modal development obtained from this method must be regarded tepidly, since important temporal variability of the system can not be gleaned from this method.

Extended empirical orthogonal function (EEOF) analysis takes advantage of the fact that atmospheric and oceanic quantities are not only highly correlated in space, but in time as well. The covariance matrix constructed for the aforementioned analysis is lagged; the elements which comprise the matrix are covariances at grid point i and grid point j at time t as well as the covariances between the same grid points at some time t_2 in the future or past. Consequentially, the solution to the eigenproblem is a set of linear functions which explain the largest percent of variance over all specified times (Weare and Nasstrom 1982). The EOFs derived from this analysis are thus the various modes of spatio-temporal variability, and insight into modal development and the mechanisms behind teleconnection evolution and decay can be identified.

1.5.5 Thesis Organization

The thesis is divided into three parts: analysis of monthly mean SLP, analysis of weekly SLP and analysis of summertime sea ice concentration. Chapter 2 focuses on the mature phase structure of the NPO/WP and its links to jet and stormtrack displacement, hydroclimate, SST and the position of the marginal ice zone. The NPO/WP is placed in context of the better known Northern Hemisphere teleconnections (NAO, PNA and ENSO). Chapter 3 investigates the development and decay of an NPO/WP episode and examines the response of the climate on subseasonal timescales. Interbasin connections to the NAO are sought, as are lagged relationships with the PNA. Chapter 4 looks into the declining summertime sea ice extent, and attempts to relate a fraction of the trend to circulation anomalies associated with the NPO/WP and other known atmosphere and ocean teleconnections. Conclusions and future research plans are discussed in Chapter 5.

Chapter 1 Tables and Figures

YEAR	WINTER	
	GREENLAND	GERMANY
1709	Very mild	Extremely severe
1740	Very mild	Unusually cold
1746	Mild	Cold
1756	Very harsh and severe	Very mild
1758	Hardly winter at all	Very cold
1759	Not really cold	Very cold
1764	Very cold	Very mild
1765	Very cold	Moderate
1766	Very mild	Very cold
1767	Mild	Very cold
1768	Mild	Cold
1790	Cold	Mild
1792	Very mild	Very cold
1799	Extremely mild	Unusually cold
1800	Extremely mild	Unusually cold

Table 1.1: Reproduction of a table first complied by Gronau in 1811, later published in Dannmeyer (1948) and Van Loon and Rogers (1978), detailing winter conditions in Greenland and Germany. Note the contrast between winter severity at the two locations; the phenomenon behind this out-of-phase relationship would later be identified as the North Atlantic Oscillation. Years and descriptive terms taken from Van Loon and Rogers (1978).
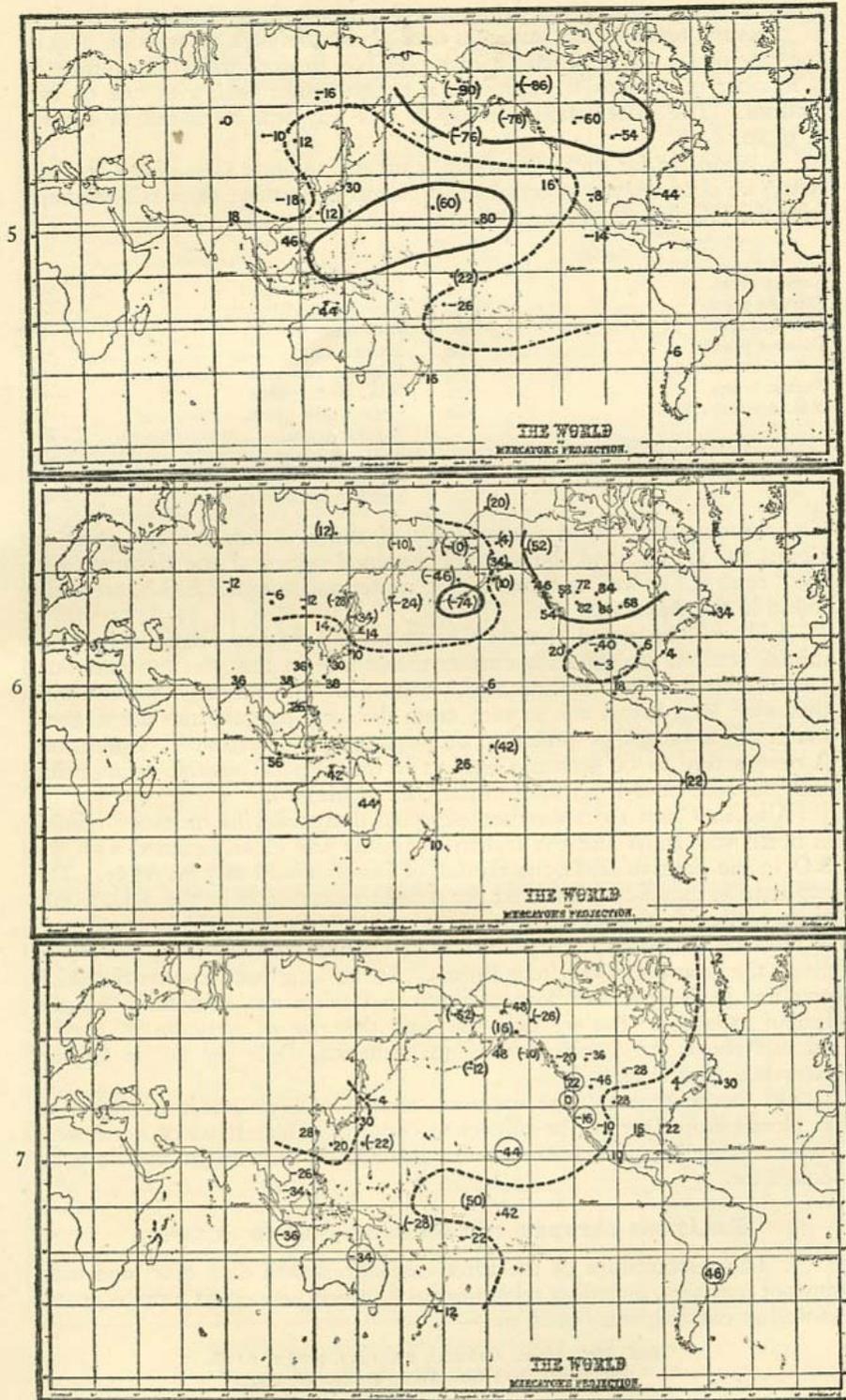
Figure 1.1: Correlations of the Walker and Bliss NPO time series with station based SLP (top), precipitation (center) and SAT (bottom) during DJF. Reproduced from Walker and Bliss (1932).
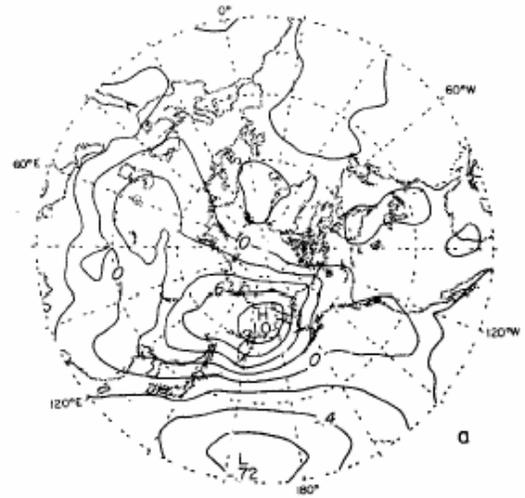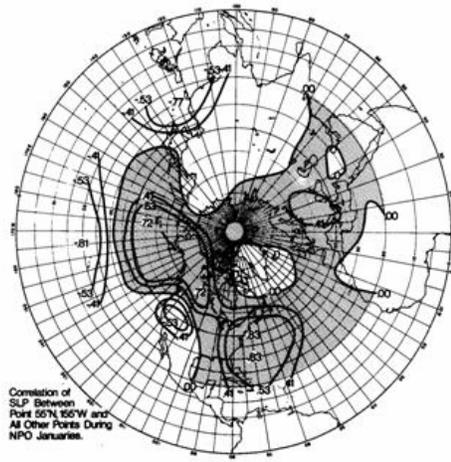
Figure 1.2: Correlations of SLP at the NPO base points defined by Rogers (left) and Wallace and Gutzler (right) with January Northern Hemisphere SLP. Images reproduced from Rogers (1981) and Wallace and Gutzler (1981).

Figure 1.3: Polar stereographic projection of the North Pole. Continents, oceans and marginal seas are all named on the map. Map obtained from **http://www.gajason.org/PastExpeditions/Frozen_worlds/maps/Arctic_Ocean_map.gif**
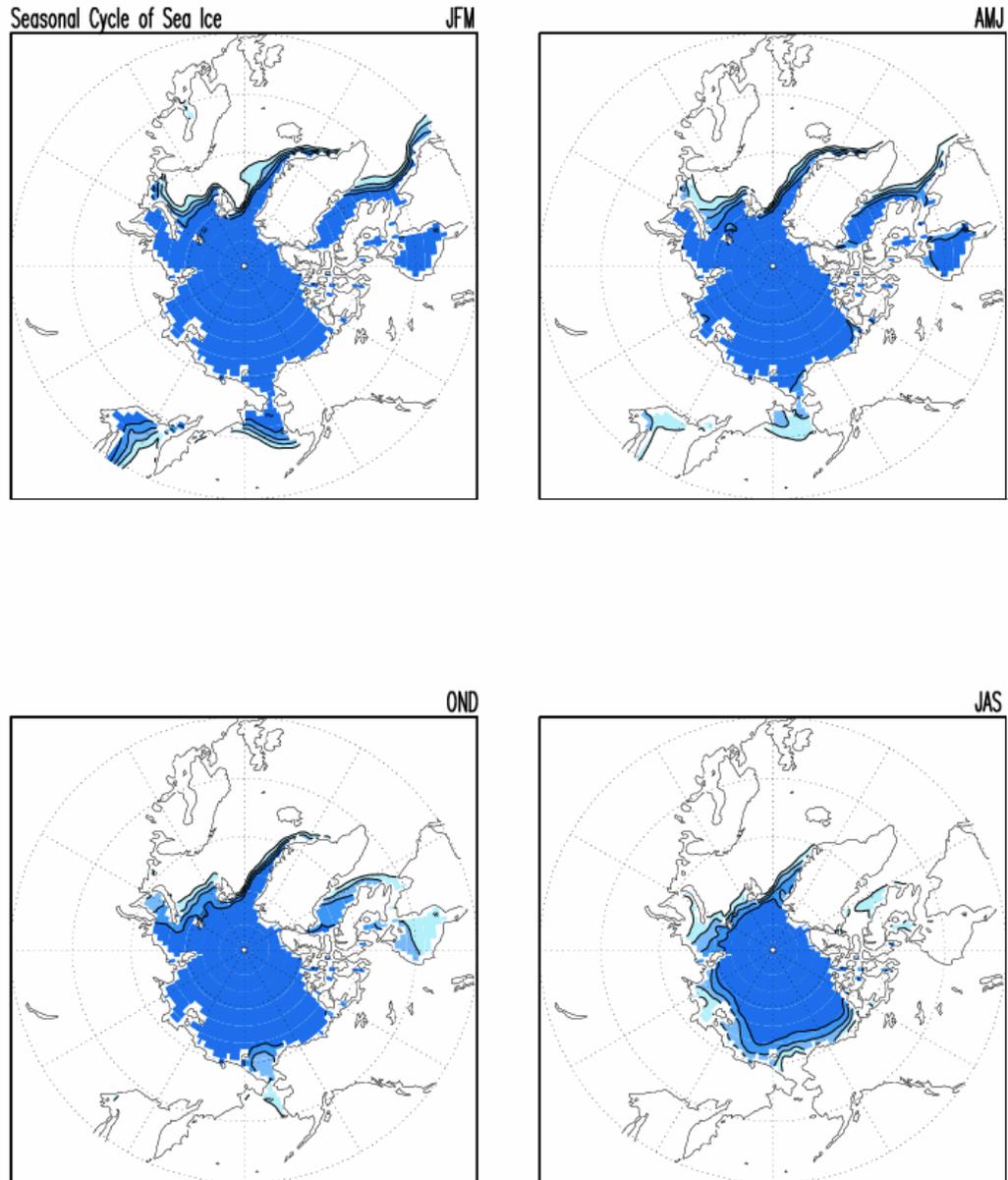
Figure 1.4: Seasonal cycle of Northern Hemisphere Arctic sea ice. The seasons are defined as follows, beginning in the upper left corner and moving clockwise around the page; winter (January-February-March), spring (April-May-June), summer (July-August-September) and autumn (October-November-December). Seasonal cycle defined using 1979-2000 climatology of NASA satellite-based sea ice concentration. Sea ice values are contoured/shaded at 20%.

a) Frazil Sea Ice

b) Pancake Sea Ice

c) Pack Sea Ice

Figure 1.5: Sea ice during the various stages of development. Panel a is frazil ice, panel b is pancake ice and panel c is pack ice. All images provided by the Virginia Institute of Marine Science at the College of William and Mary and are available at http://www.vims.edu/bio/microbial/NBPice.html
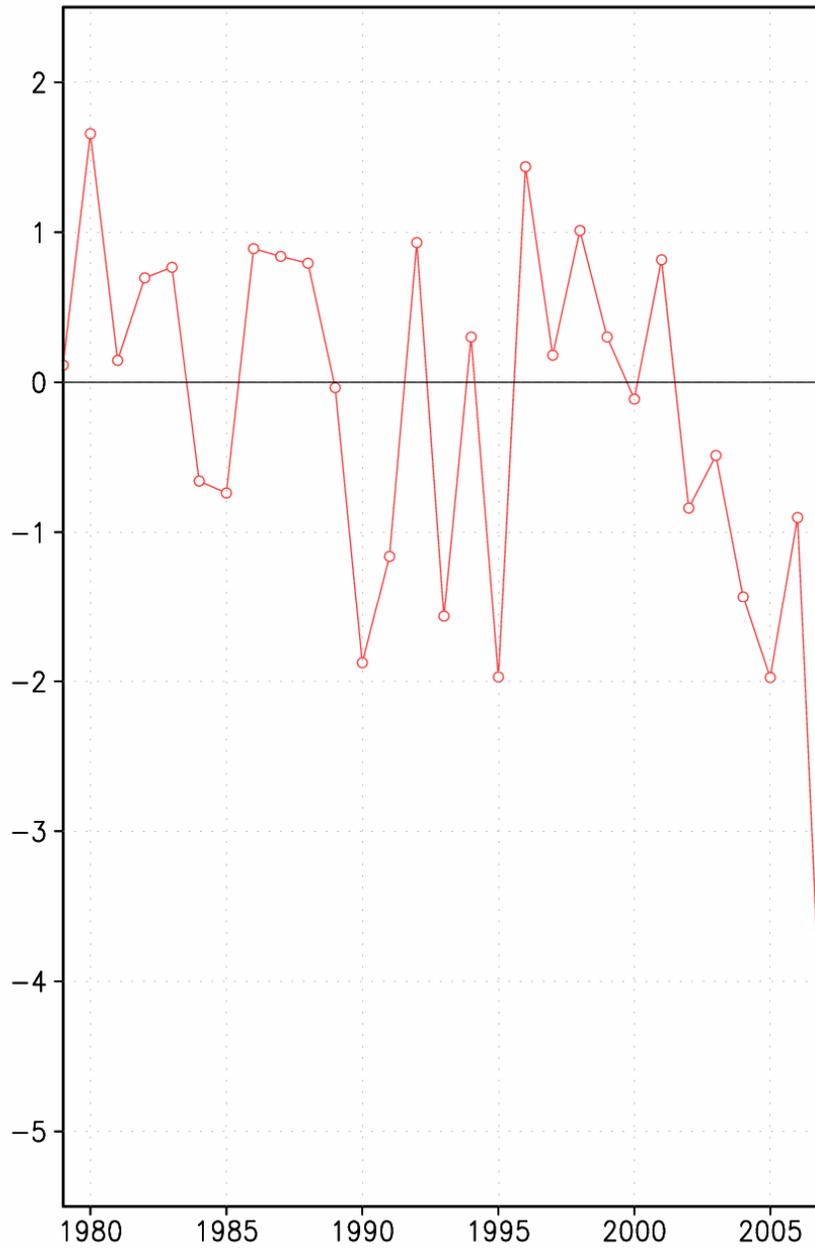
Figure 1.6: Normalized Arctic sea ice extent anomalies from the Hadley Center HadISST1.1 for Septembers 1979-2007. Normalized anomalies are calculated by removing the September 1979-2000 climatology and dividing the anomaly by the standard deviation of the same 22 year period.
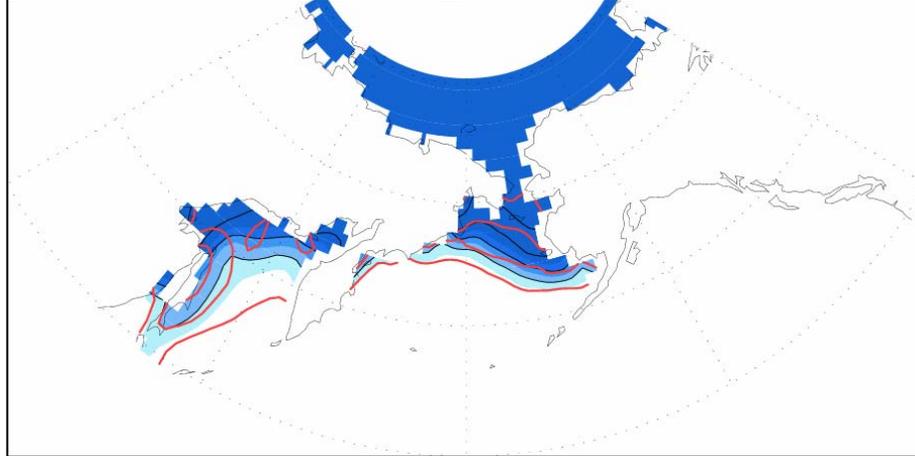
Figure 1.7: December-January-February 1958-2001 climatological sea ice concentration (shaded/contoured) and standard deviation (red contours) in the Bering Sea and Sea of Okhotsk. Climatology is contoured/shaded at 20%; standard deviation is contoured at 10%.
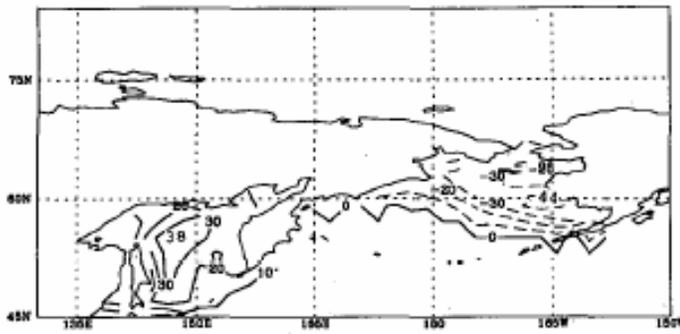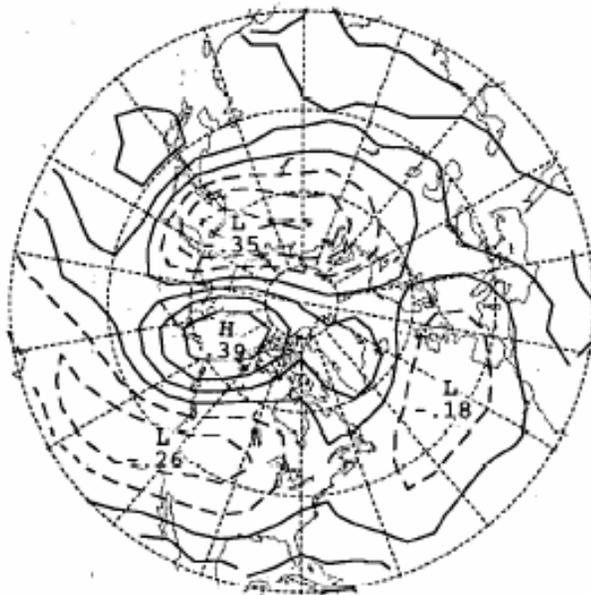
Figure 1.8: The leading covariability mode of weekly winter sea ice concentration and 500 hPa geopotential height from Fang and Wallace (1994). Dashed (solid) contours correspond to negative (positive) correlations. Reproduced from Fang and Wallace (1994).
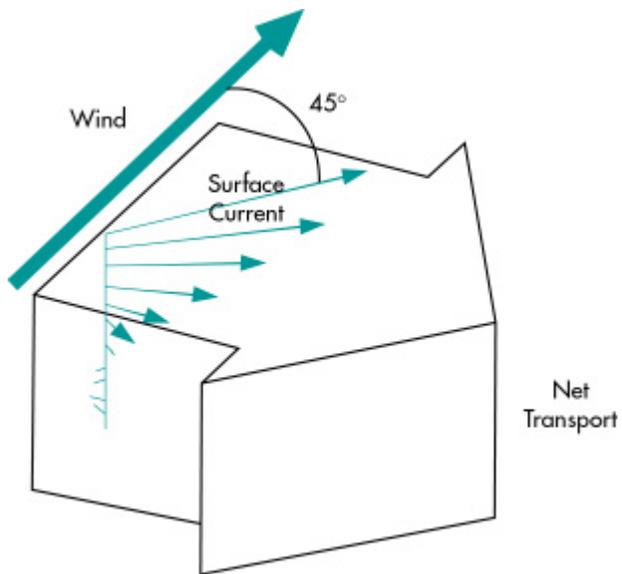
Figure 1.9: Basic schematic of Ekman motion in the Northern Hemisphere. Sea ice floats on the ocean surface; sea ice motion will be directed 45º to the right of the surface wind in the Northern Hemisphere. Figure obtained from
http://seacoos.org/Data%20Access%20and%20Mapping/currents/ekman

a) JAS 1979−1999 Trend
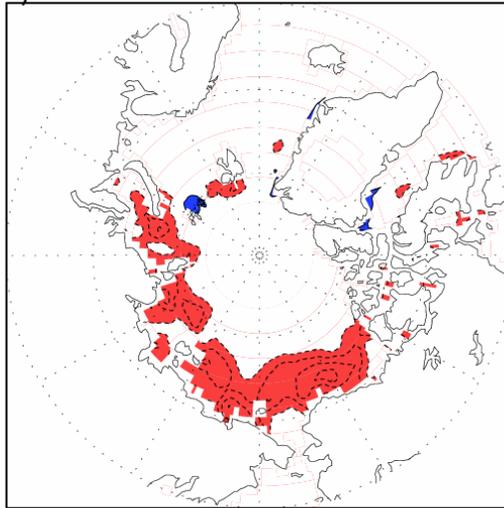
b) JFM AO regressed on JAS SIC
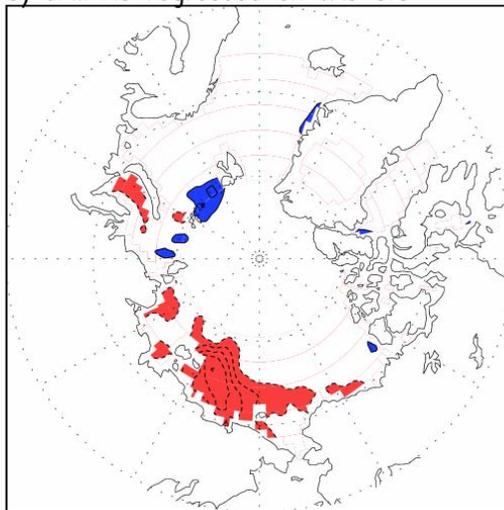
Figure 1.10: Linear trend (a) in seasonal July-August-September sea ice concentration between 1979 and 1999 and the regression pattern (b) of the seasonal January-February-March Arctic Oscillation index regressed on seasonal July-August-September sea ice concentration for the same 21 years. Sea ice concentration derived from NASA satellite-based brightness temperature; AO index from NOAA's Climate Prediction Center. Dashed (solid) contours and red (blue) shading indicate negative (positive) values; contour interval is 5% (per decade for panel a).
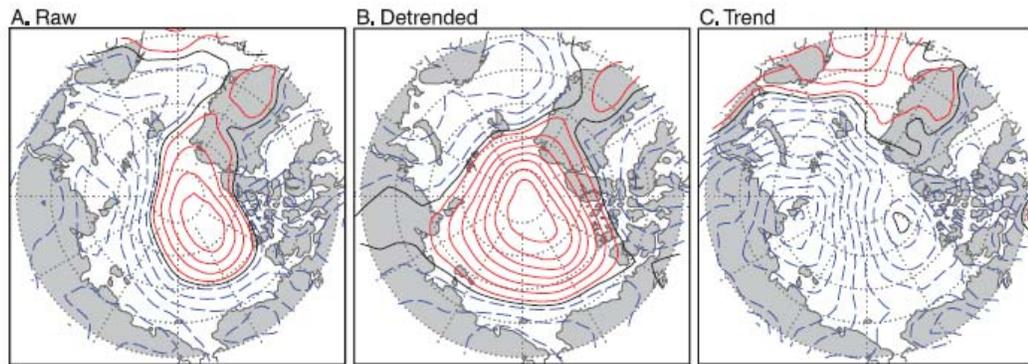
Figure 1.11: Sea level pressure anomalies obtained from regressing summer (July-August-September) SLP on an inverted index of raw September Arctic sea ice extent (panel *a*), an inverted index of detrended September sea ice extent (panel *b*) and the trend in summer SLP during 1979-2006. Contouring begins at 0.1 hPa and is contoured at 0.2 hPa; solid (dashed) contours indicate positive SLP departures. Panel *b*, the negative AO, is linked with less sea ice in the western Arctic marginal seas. Image reproduced from Ogi and Wallace (2007).
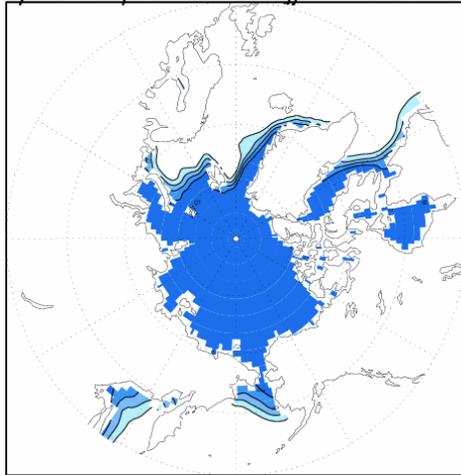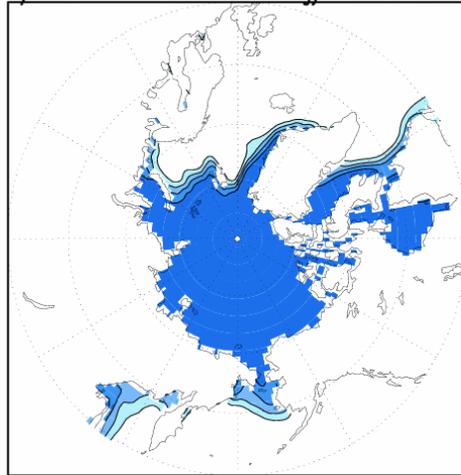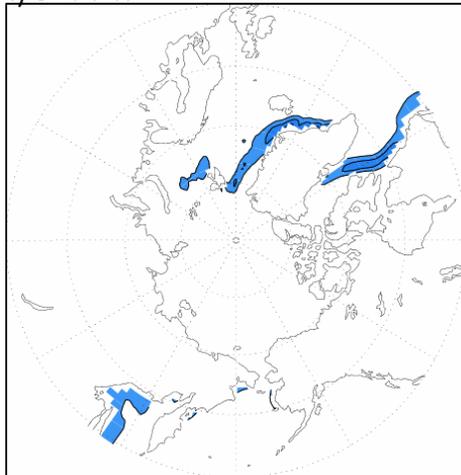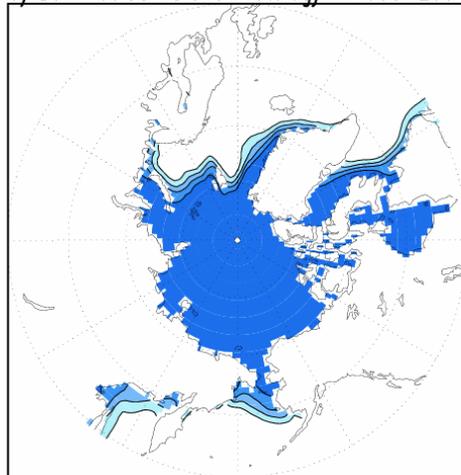
Figure 1.12: Climatological December-January-February sea ice concentration between 1979 and 2004 from (a) satellite-based brightness temperatures and (b) HadISST1.1. Difference between the two climatologies is plotted in panel c. DJF 1958-2001 climatology plotted in panel d. Climatology is contoured/shaded at 20% intervals, panel *c* is contoured/shaded at 10% intervals. .
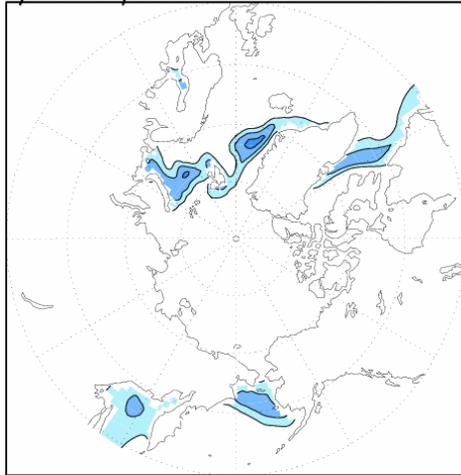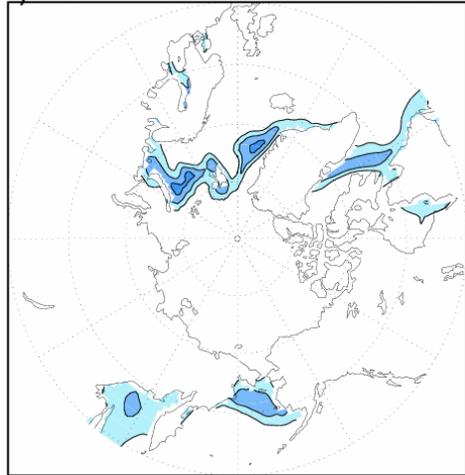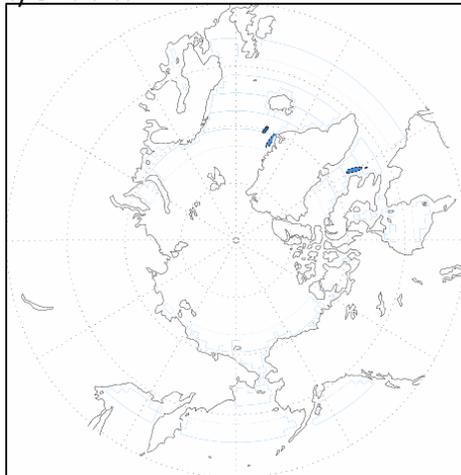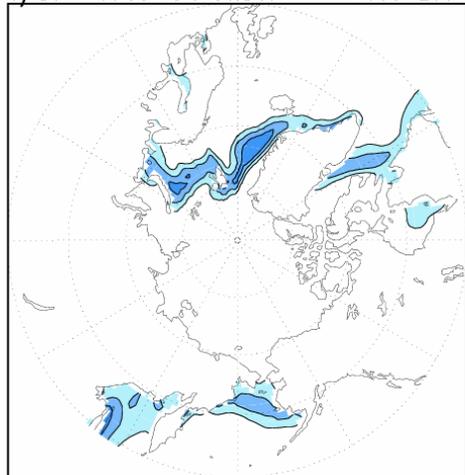
Figure 1.13: As in figure 1.12, except for standard deviation. Shading/contouring in all plots is 10%.

Chapter 2: The North Pacific Oscillation/West Pacific Pattern – Mature Phase Structure

This chapter presents the NPO/WP in its mature phase. Following up on the work of Walker and Bliss (1932), WG81, Rogers (1981), Horel (1981) and Barnston and Livezey (1987), we extract the mature phase NPO/WP from the SLP field using a variety of statistical techniques. The 3-D structure of the mature phase NPO/WP is discussed; as is the hydroclimate and oceanic impact of NPO/WP. Finally, the NPO/WP is placed in context of its better-known counterparts: the PNA, ENSO and NAO.

2.1 – Statistical analysis of the NPO/WP

2.1.1 – One point correlation analysis

In an attempt to connect with previous NPO studies, one-point correlation analysis is conducted on SLP anomalies. The SLP base points in Figure 2.1 are 55°N, 155°W and 65°N, 170°E; the first from Rogers (1981) and the second from WG81. The correlation maps, computed using longer, more consistent records here, contain the same features as in Rogers (1981, figure 2.1) and WG81 (their figure 10a): A large region of positive correlation extending into eastern Alaska and western Canada along with negative correlations to the south in the Hawaiian latitudes, with a secondary feature near Japan. The WG81 base point (65ºN, 170ºE) returns a qualitatively similar dipole, except for the longitudinal shift. The difference between the two one-point correlation maps is likely attributable to the aliasing of PNA and ENSO influence. Both PNA and ENSO affect the North Pacific SLP in a similar manner (positive phases of each linked to lower pressure, see Nigam 2003) and one-point correlations cannot separate these influences.

The meridional pressure swing manifest in these patterns is in general accord with the NPO descriptions of Rogers (1981) and Walker and Bliss (1932). Correlation patterns obtained from NCEP and ERA-40 data sets are virtually identical; and only the ERA-40 based analysis is displayed.

2.1.2 – EOF analysis of monthly mean SLP

Recurrent modes of winter SLP variability are computed from covariance based EOF analysis. Winter is defined to be the four month December-March period (hereafter DJFM). The inclusion of March into the definition of winter, as opposed to the traditional meteorological definition of winter as the months December-January-February (DJF), does not affect the stability of the modes. An identical analysis is performed on monthly DJF SLP anomalies; the order, magnitude and spatial characteristics of the leading modes are indistinguishable. The SLP anomalies are weighted by $(\cos \theta)^{1/2}$ to account for the decrease of grid area towards the pole. The need for EOF rotation is obviated by confining the analysis to the Pacific basin: 120°E-120°W, 20°N-85°N. The second principal component (PC) of SLP is used as the NPO/WP index; the first PC is a marker of PNA variability. Regressions of the second PC on geopotential height, zonal and meridional wind, precipitation, diabatic heating, meridional heat flux, surface air temperature, SST and sea ice concentration are used to characterize NPO/WP variability.

The second EOF describes the NPO: a meridional dipole in north Pacific SLP (Fig. 2.2*a*); EOF1, a monopole in SLP in the Gulf of Alaska, is the surface signature of the PNA. The spatial structure of EOF2 is consistent with the earlier descriptions in Walker and Bliss (1928, 1932) of the NPO as an out of phase oscillation between SLP in Alaska and Hawaii. The northern node has twice the magnitude of the southern one,

leading to NPO's considerable influence on the position and strength of the Aleutian Low. The mode explains 20.7% of the monthly winter variance in ERA-40's SLP. The displayed EOF structure is similar to the second eigenvector of hemispheric SLP in January (Kutzbach 1970). The related circulation anomalies and thermal advection can generate high latitude temperature anomalies consistent with Rogers' (1981) analysis.

The upper right panel in Figure 2.2 shows the 2nd EOF from weekly SLP analysis in the same spatio-temporal domain; once again, the surface PNA is mode 1. Not surprisingly, the amplitude is stronger now, especially of the southern lobe, but the meridional dipole structure manifest in monthly analysis is robustly returned. The variance explained by monthly and weekly modes is also nearly identical.

The top two panels Figure 2.3 shows 2nd EOF of ERA-40 and NCEP DJFM SLP; no significant difference between the two reanalyses is obvious. Furthermore, the principal component time series (Figure 2.3c) are correlated at 0.99. The lack of any significant differences between the two reanalyses allows us to rely on the ERA-40 analysis from here on out.

2.1.3 – NPO + WP = NPO/WP

The above described SLP variability – the NPO – is linked with the upper-air West Pacific teleconnection pattern in this section. Temporal correlation of the SLP principal component (Fig. 2.2e) and the WG81 WP index, spatial correlation of the SLP EOF (i.e., NPO) and the WP height pattern (Fig. 2.2d), and SLP regressions of the WG81 WP index (Fig. 2.2c) all help to make the case. The WP index is calculated from the normalized 500 hPa height anomalies at the two centers of action noted earlier; as in WG81. The use of the WG81 WP index, as opposed an index extracted from EOF

46

analysis performed on 500 hPa heights, is utilized in an effort to connect with the earlier descriptions of the WP. No statistical difference between the WG81 WP index and NOAA's Climate Prediction Center (CPC) WP index, derived from rotated EOF analysis on monthly 500 hPa height anomalies, is found. The temporal correlation of the SLP PC and the WP index is 0.83, as is the spatial correlation of SLP EOF and the WP height pattern; both significant at the 99% level. Winter SLP regressions of the WG81 WP index (Fig. 2.2c) are also in remarkable agreement with the NPO (SLP EOF) structure. Given these significant temporal and spatial correlations, the North Pacific Oscillation and the West Pacific teleconnection pattern are considered to be the same mode of variability, whose SLP footprint is the NPO and whose upper-air signature is the WP teleconnection pattern. This view is reflected in our use of the NPO/WP acronym to describe this mode of winter variability in the remainder of the thesis.

If the SLP PC2 is taken as marker (or index) of NPO/WP variability, one can ascertain NPO/WP links with other modes of winter variability. Given the large sub-seasonal variability, as reflected in the within season sign-change in 34 of the 44 analyzed winters, linkage with ENSO is unlikely. The small 0.16 correlation between the SLP PC and Nino3.4 SST index confirms this to be the case. Links with decadal and interdecadal SST variability are sought as well. Di Lorenzo et al. (2008) find that the surface wind anomaly pattern which forces the North Pacific Gyre Oscillation (NPGO) is structurally similar to the NPO. The correlation between our NPO index and the NPGO index developed by Di Lorenzo et al. (2008) is only 0.19 for the winter months, a relatively small value. The correlation with the Pacific Decadal Oscillation (PDO; Mantua et al. 1997) index is even smaller, with a correlation of 0.02 during the four

month winter season. Of more interest are inter-basin links in the extratropics, especially, with NAO variability. Although correlation with Hurrell's (1995) NAO index is small (0.22), inter-basin connection remains an interesting open issue as links may be manifest not contemporaneously, but at lead/lags. The presence of interbasin connections is discussed in a subsequent chapter.

2.2 – Upper Air Analysis of the NPO/WP

2.2.1 – Upper Air Signature and Vertical Structure

The geopotential height signature of the NPO/WP at 300 and 700 hPa levels is shown in Figure 2.4. In addition to the characteristic Pacific features noted earlier (e.g., Fig. 2d), the full hemispheric view shows a dual centered ridge, whose western lobe is positioned over Canada and the eastern lobe just upstream of Western Europe. This upper-air signature is consistent with the WP descriptions in literature (WG81, Horel 1981, Hsu and Wallace 1985, Barnston and Livezey 1987, Nigam 2003). Its equivalent barotropic structure is in accord with WG81's description of the pattern having a cold-core low over the Aleutians. Between the surface and 700 hPa though, there is some shift in the pattern centers: The westward tilt is slight over the North Pacific with the surface pressure anomaly centered over the western tip of Alaska and the Bering Strait and the corresponding 700 hPa center positioned over Eastern Siberian and the western and central Bering Sea. Over to the east, the shift is much greater. The pronouncedly baroclinic vertical structure over western/central North America (cf. panels 2.4*b-c*) has, of course, been noted before by Hsu and Wallace (1985).

Interestingly, the NPO/WP pattern bears some resemblance to the component of climatological stationary waves forced by transient fluxes of heat and momentum. Nigam and Deweaver (2003) analyzed the forcing of these waves using a linear stationary wave model, and show the wave response forced by orography, diabatic heating, and transient fluxes. The 300 hPa geopotential height pattern forced by transient fluxes consists of a low over the north Pacific and a dual centered ridge, with lobes over the Canadian Maritimes and Great Britain (Nigam and DeWeaver 2003; their figure 13D). The correspondence in features suggests that NPO/WP variability is, perhaps, linked with Pacific stormtrack fluctuations; a linkage investigated in the next subsection.

The vertical structure of NPO/WP variability is examined more closely in Figure 2.5. A latitude-height cross section between 20ºN and 90ºN and 1000 hPa and 100 hPa along the 180º meridian – the longitude of maximum geopotential amplitude – is presented. The height perturbations maximize near the tropopause, with the trough amplitude (~80 m) being twice as large as of the subtropical ridge. The temperature field is hydrostatically consistent with the height distribution: Maximum warming beneath the upper level ridge and maximum cooling in the vicinity of, but not directly underneath, the trough.

Temperature anomalies in this region, in fact, display a northward tilt with height. This feature results from the presence of cold temperatures to the south in the lower troposphere. Colder temperatures in this region must arise from zonal cold advection, originating from the NPO/WP circulation itself. The circulation consisting of anomalous westerlies here can lead to cold advection from the cold Asian continent. The cooling is confined to the lower troposphere as the climatological land-sea thermal contrast – the

basis for cold advection – is generally not evident in the middle and upper troposphere except in mountainous regions. This NPO/WP circulation induced thermal advection results in a quadriture relationship between geopotential and temperature in the lower, but not in the upper, troposphere.

The NPO/WP zonal wind is shown atop the climatological field in Figure 2.6*a*; all at 300 hPa. The wind anomaly has a meridional dipole structure and is longitudinally confined to the sector past the climatological jet-core, leading to northeastward nudging of the Asian-Pacific jet in the depicted phase. Panel *b* shows the related upper-level divergence atop the zonal wind anomaly. The location of divergence features vis-à-vis the jet anomaly indicates the presence of the thermal-wind restoring divergent circulation. The counteracting influence of this circulation on the jet anomaly suggests that the latter is likely forced by other dynamical processes (e.g., anomalous vorticity transients associated with jet displacement).

To put the NPO/WP jet fluctuation in perspective, the zonal wind anomaly associated with PNA variability is shown in Figure 2.6*c*. This PNA anomaly is also a meridional dipole but with a stronger southern lobe that is located squarely in the Asian-Pacific jet latitudes. Longitudinally, the anomaly is focused in the jet-exit region, leading to eastward extension of the jet in the depicted phase. The NPO/WP and PNA jet fluctuations are thus in near-quadriture. The PNA anomalies have an interesting structure in the Atlantic as well, reminiscent of the local NAO anomalies; both leading to meridional displacement of the Atlantic jet. However, different jet-sectors are targeted: PNA anomalies are focused in the jet-core sector, while the NAO ones in the jet-exit (and further downstream) region (cf. following Fig. 2.18).

The meridional divergent circulation which maintains thermal wind balance in response to perturbation of the Asian-Pacific jet is shown in Figure 2.7. The vertical cross section is taken along the 180º meridian, i.e., at the core of the zonal wind anomalies. The divergent circulation accompanying the jet anomaly is evidently deep and thermally indirect, in that rising motions occur near ~60ºN while sinking takes place at ~30ºN. The Coriolis force due to equatorward flow in the upper midlatitudes opposes the westerly anomaly, while related ascent (descent) to the north (south) generates adiabatic temperature changes needed to accommodate the greater vertical wind shear; that is, restore thermal wind balance. Of particular note is the meridional location of low-level convergence – just northward of the westerly anomaly core – which should be influential on cyclone storm development.[1]

2.2.2 – Linkages to Pacific Stormtrack

The NPO/WP links with Pacific storm tracks are investigated in Figure 2.8 using meridional wind variance, meridional heat flux, and lower-troposphere diabatic heating anomalies.[2] Regressions of PC2 (NPO/WP) on 300 hPa meridional wind variance display a tripole pattern, with the location of the largest anomalous wind variance occurring where the climatological wind variance is largest. To its north and south, wind variance is diminished, indicating decreased cyclone activity and a narrower stormtrack. The NPO/WP variability is thus linked with a meridionally tighter and eastward extended stormtrack. Comparison of the 700 hPa NPO/WP related meridional heat flux (from

---

[1]For discussion of the dynamical interactions between jets, divergent circulations, and stormtrack feedbacks, see Lau and Nath (1991), Orlanski (2005), and references therein.

[2]Submonthly variance of the unfiltered meridional wind is commonly used to monitor stormtrack variability (e.g., Chang 1993, Chang et al. 2002, Orlanski 2005). Other markers, such as meridional heat flux, may require band-pass filtering of data in order to focus on synoptic variability.

submonthly fluctuations) with the climatological heat flux distribution (Fig. 2.8*b*) also suggests that NPO/WP variability is associated with a focused stormtrack, assuming dominance of synoptic contributions in the meridional heat flux.[3] It is noteworthy that the Asian-Pacific jet, itself, has not strengthened since the positive NPO/WP zonal wind anomalies occur in the poleward flank of the jet (and not jet-core latitudes; cf. Fig. 2.6*a*). The jet anomaly, as such, would be more consistent with meridional displacement rather than tightening / zonal extension of the stormtracks.

The NPO/WP link with lower troposphere diabatic heating anomalies is displayed in panel *c*, with the contoured climatological heating providing positional context. The largest heating anomalies (~0.4 K/day) occur not where the climatological heating is a maximum, but to the northeast of this region. The climatological heating here is 1.5-2.0 K/day; and the anomalies thus significant. The anomalies are generated both from anomalous fluxing of cold air from the Siberian peninsula onto the warmer Pacific, leading to low-level sensible heating and, of course, from the changes in latent heating associated with stormtrack modulation. The lower troposphere diabatic heating anomalies straddle the axis of maximum climatological diabatic heating, implying a meridional displacement of the stormtrack. This different view of stormtrack modulation – meridional displacement as opposed to previous indications of in-place meridional focusing – must result from the presence of more than just latent heating in the residual diabatic heating; for example, sensible heating component. This will preclude characterization of stormtrack changes from the structure of diabatic heating anomalies.

---

[3]The meridional heat flux is maximum slightly to the southwest of the jet-anomaly core (not shown); a dynamically favored sector for synoptic development in view of the presence of a thermally direct divergent circulation, including low-level convergence, in the region upstream of the jet-core. Meridional heat-flux convergence is thus large poleward of the jet anomaly.

Is the NPO/WP stormtrack signal manifest in direct analyses of Pacific stormtrack variability (e.g., Lau 1988)? Lau (1988) extracted the primary modes of oceanic stormtrack variability from bandpass (2.5 – 6 day) filtered geopotential height and found that most modes of stormtrack variability are tied to the teleconnection patterns derived from monthly mean statistics. The first four leading eigenvectors of Pacific stormtrack variability explain approximately half the variance. Lau links a monopolar intensification of the stormtrack to the WP as defined in WG81. This location of the intensification is close to the axis of the climatological stormtrack and is a manifestation of the increased eddy activity in this region driven by enhanced midlatitude westerlies.

Visual inspection of the Pacific eigenvectors precludes a definitive link between one single stormtrack eigenvector and the NPO/WP. Lau's eigenvectors P1, P2 and P3 all contain some salient features of the NPO/WP stormtrack response. While we also find a basin-wide intensification/tightening of the stormtrack associated with the NPO/WP, a meridional displacement occurs in tandem with the northward shifted jet stream. The structure of lower tropospheric diabatic heating anomalies is dipolar in nature, straddling the climatological stormtrack axis. Furthermore, dual maxima in diabatic heating anomalies occur in the central and eastern Pacific, with one maximum occurring just to the west of 180º and the other occurring at approximately 130ºW. The elongation of the stormtrack is due to the presence of lower heights over the Bering Strait and higher heights over the subtropical western Pacific. The geopotential gradient accelerates the midlatitude westerly flow, increasing eddy activity across the whole Pacific basin. The dipole feature occurs in eigenvector P2 (see Lau 1988, figure 2b) while the elongated, dual extrema feature is characteristic of eigenvector P3 (see Lau

1988, figure 2c). The correlation maps of 500 hPa geopotential height and SLP with the temporal coefficients associated with these higher eigenvectors resemble the PNA and the NPO/WP respectively (see Lau 1988, figs 4b, 4c, 15b and 15c).

While Lau links the WP with eigenvector P1 and we find the NPO/WP visually most similar to the teleconnection pattern associated with eigenvector P3, the similarities of the NPO/WP stormtrack response to all three leading eigenvectors suggests that the actual NPO/WP stormtrack response is aliased into all three 500 hPa geopotential maps and three SLP correlation maps. The dynamics of the NPO/WP are physically consistent with both a northward displacement of the stormtrack due to a latitudinally shifted jet and an increase in stormtrack activity due to an acceleration of the ambient westerly flow.

The impact of data period, variable-choice, and analysis pressure-level differences in the two studies is currently being assessed through additional analyses. It is also conceivable that NPO/WP variability undergoes significant submonthly evolution, with different stormtrack links in different evolution phases; this possibility is addressed in the following chapter.

2.3 – Climate Impact

The NPO/WP influence on North American climate is presented in this section through regressions on precipitation and SAT, as well as SST and sea ice. To put the influence in perspective, the winter precipitation and SAT climatology from the UEA data sets are displayed first (Fig. 2.9*a&b*). The Pacific Northwest gets most of its rain in winter, with coastal regions receiving as much 14 mm/day in this high-resolution data set. The southeast, with no preferred rainy season, on the other hand, gets 2-4 mm/day.

2.3.1 – Precipitation

The NPO/WP enhances precipitation in coastal regions of Canada and Alaska, reduces precipitation over the US Pacific Northwest and western Canadian provinces, and enhances the same over the south-central Great Plains and western Mexico (Fig. 2.9c). The signal is 0.3-0.5 mm/day outside coastal regions, where it is even stronger. A comparison with climatology indicates the NPO/WP signal corresponding to one PC unit to be, often, more than 15% of the climatology; as over south-central Great Plains and the western Canadian provinces.

The precipitation anomalies along the Alaskan/Canadian coast are also statistically significant (NPO/WP PC precipitation correlations here are ~0.4), and must be due to enhanced southerly flow impinging on coastal topography (figure 2.11c), and related uplift; and large-scale dynamical controls (figure 2.11a) on vertical velocity.[4] The southerly flow is enhanced along the eastern arm of the NPO/WP trough in the Aleutians (cf. Fig. 2.2a), leading to this dynamical influence. The precipitation decrease to the south, along the US Pacific Northwest coast, on the other hand, likely results from both northward displacement of the Aleutian low and from stormtrack displacements. The precipitation anomaly structure over the southern Plains is suggestive of links to the Gulf of Mexico; however, no significant circulation anomalies can be discerned in this area.

Climatologically, winter snow cover over the North American continent exceeds 20% north of the 40th parallel and surpasses 80% in most of Canada and Alaska (figure

---

[4] The operative vorticity balance on large scales is the Sverdrup balance ($\beta v \approx -f \vec{\nabla}_h \bullet \vec{V}$), when northward advection of planetary vorticity is balanced by horizontal convergence and upward motion. Such advection occurs along the eastern flank of the Aleutian low, leading to ascending motions and winter rainy season in the Pacific Northwest and Alaskan/Canadian coastal regions (e.g., Nigam and Ruiz-Barradas 2006). The dynamical control on vertical velocity operative in winter climatology must remain relevant during NPO/WP variability.

2.10*a*). Regressions of the NPO/WP PC onto monthly winter snow cover between 1971=

and 1994 reveal that the NPO/WP is related to a dipole in snow cover anomalies;

decreased snow cover occurs over central Canada, the northern Great Plains and New

England, while increased snow cover occurs over the American Rocky Mountains. A

comparison of the precipitation regressions and snow cover regressions suggests there is

not a direct relationship between precipitation amount and anomalous snow cover. No

precipitation perturbations occur in central Canada and New England, and in the northern

Great Plains, precipitation increases, while snow cover extent decreases. Over the Rocky

Mountains and Pacific Northwest, suppressed precipitation coincides with regions of

increased snow cover. The snow cover anomalies are instead related to SAT anomalies,

discussed in the following subsection. Negative SAT anomalies are collocated with

increased snow cover; positive SAT anomalies, increased solar radiation and warm

temperature advection all occur in the vicinity of decreased snow cover.

2.3.2 Surface air temperature

The SAT anomalies (Fig. 2.9*d*) result from the same circulation features discussed

above. Warmer temperatures over Alaska and the Pacific Northwest, and interior central

Canada, by as much as 2K, are from thermal advection. The NPO/WP cyclonic

circulation over the North Pacific positions southerly flow onto the Alaskan coast,

bringing in warmer maritime air. Similarly, the ridge over North America, albeit weaker,

leads to southeasterlies over much of central and western Canada, and northeasterlies to

the right of the ridge bring maritime air and warmth to the eastern seaboard, especially

the mid-Atlantic region. The flow becomes southeasterly moving into the Great Plains,

producing the 0.4-1.2K warming over the eastern and central United States. The

temperature change resulting from thermal advection by the NPO/WP circulation is plotted at 925 hPa in Fig. 2.9*e*. Its broad similarity with the NPO/WP temperature signal (panel *d*) supports the assessment regarding the advective origin of the temperature anomaly. Advection apparently explains about one-third of the amplitude, with the rest accounted for by increased surface shortwave radiation (2.12*a*).[5] Warm advection occurs not only at the surface but also aloft (2.12*b*), stabilizing the troposphere and decreasing cloud cover, thereby allowing more solar radiation to reach the land surface.

In the opposite phase (weakened Aleutian Low), NPO/WP is associated with colder temperatures to the east of the Rockies, consistent with the propensity for cold air outbreaks in this NPO/WP phase (Walker and Bliss 1932, Rogers 1981, Hsu and Wallace 1985).

2.3.3 – Sea Surface Temperature

The NPO/WP influence on SST is weak but noted here in view of the spatially coherent structure of correlations, which are displayed in Figure 2.13 atop the 1000 hPa wind regressions; maximum correlations are ~0.3. The SST signal is apparently wind driven: In the Tropics, the NPO/WP wind anomalies, especially, anticyclonic flow around the southern cell intensifies the Trades in the central/eastern basin and weakens westerlies in the subtropical western basin, while cyclonic flow about the northern cell strengthens the midlatitude westerlies. The resulting wind speed and surface fluxes – stronger in the trade wind zone and midlatitudes and weaker in the subtropics – lead to SST changes; a tri-band anomaly structure similar to the pattern of surface heat flux anomalies linked

---

[5] Contribution of the nonlinear ($-\vec{V}_{NPO} \bullet \vec{\nabla} T_{NPO}$) and the other linear advection term ($-\vec{V}_C \bullet \vec{\nabla} T_{NPO}$) has been ascertained to be small.

with sea-level pressure variability in the Bering Sea (Cayan 1992). Ekman pumping is

potentially contributing to the SST anomalies at 30ºN; the surface winds along this

latitude are conducive to downwelling, a process which would increase SST. SST

correlations in the equatorial Pacific and Indian Ocean are weaker, but not by much.

Note, only the contemporaneous SST correlations are displayed.

The lagged SSTs in the Pacific – the ones leading to the 'seasonal footprinting'

effect (Vimont et al. 2003) – are shown in 2.14, plotted for the negative phase

(anomalous subtropical cyclonic circulation) of the NPO/WP. Tropical and subtropical

Pacific SST regressions are plotted when the NPO/WP leads the SST field up to 12

months. SST anomalies persist in the northern tropics and subtropics (~15ºN-40ºN);

surface wind anomalies (not shown), are westerly for 4 to 6 months after the winter

NPO/WP. Six months after the peak NPO/WP, warm ENSO-like SST anomalies appear

along the equator and persist until a full year after the NPO/WP. The propagation

characteristics and amplitude are structurally consistent with an El Niño episode;

implicating the NPO/WP as a source of stochastic forcing for ENSO-like variability the

following winter (Vimont et al. 2003).

2.3.4 – Sea Ice Impacts

Our sea-ice signal (figure 2.15) is not in accord with that described in some earlier

studies, notably Rogers (1981) and Cavalieri and Parkinson (1987): Cavalieri and

Parkinson found no direct link between the Sea of Okhotsk MIZ and NPO/WP

variability, but found the NPO/WP negative phase (i.e., a westward shifted Aleutian

Low) linked with MIZ retreat in the Bering Sea. Likewise, Rogers (1981) did not firmly

link NPO/WP and MIZ position in the Sea of Okhotsk, only suggesting that sea ice

concentration decreased during the positive NPO/WP phase (eastward shifted, intensified Aleutian Low), i.e., opposite of our finding.

Although the strategy is similar, our analysis of a longer period, more consistent sea-ice record leads to contradictory findings: The MIZ does advance southward in the western Bering Sea during the NPO/WP positive phase, increasing ice concentration by as much as 10% (figure 2.15*a*). The MIZ response is non-uniform; there is a decrease in the eastern Bering Sea. A robust signal is, additionally, found in the Sea of Okhotsk where ice concentration increases by as much as 8% during the positive NPO/WP phase. Regressions of the WG WP index on sea ice concentration are higher in amplitude, but spatially similar to the regressions obtained from PC2 (figure 2.15*b*). These increments are twice as large as the PNA-related sea ice increase in the Bering Sea and Sea of Okhotsk (not shown).

Given that NPO/WP's influence on sea ice is quite different in our analysis, it is important to assess the dynamical and thermodynamical consistency of the sea ice variability pattern with the overlying circulation. The 1000 hPa NPO/WP circulation (SLP and wind vectors) and the resulting horizontal thermal advection are displayed in Figure 2.16. Westerly to west-northwesterly winds and cold air advection prevail over much of the Sea of Okhotsk and result in sea ice formation and ice drift away from the Russian coastline, thus increasing ice concentration in the Sea of Okhotsk. Similarly, northerly winds and cold air advection are linked with sea ice increase in the western Bering Sea. Anomalous flow in the eastern Bering Sea is however from the south-to-southeast direction, leading to warm air advection in that region. Interestingly, only a modest ice decrease is evident in that region (cf. Fig 2.15*a*).

Sea ice variability also arises from sea ice motion, which is influenced by a number of factors, including proximity of sea ice to the coast and the direction of prevailing winds relative to the coastline (Fissel and Tang 1991). Both Bering Sea and the Sea of Okhotsk are bordered by land on multiple sides which complicates the analysis of motion-induced sea ice variability. Internal ice dynamics introduces additional complexity, making the sea ice response to wind forcing dependent on local ice thickness: Thinner ice (lower internal stress) and lower sea ice concentration regions respond more strongly to atmospheric forcing (Shevchenko et al. 2004). These impacts, not considered here, could account for the pending inconsistency between the NPO sea ice signal and related atmospheric thermodynamic forcing (cf. Figs. 2.15a and 2.16).

2.4 – Intercomparison to other teleconnections

2.4.1 – Comparison to the PNA and ENSO

It is interesting and, perhaps, also important to differentiate the NPO/WP structure and impacts with those of PNA and ENSO variability, as the Pacific sector is home to all three variability modes. The SLP signature of PNA variability (EOF1, explaining 33.6% of the variance of winter Pacific SLP) is displayed in Figure 2.17a while that of ENSO variability is shown in panel b; the ENSO signature is obtained from Nino3.4 SST index regressions. Clearly, via constraints imposed by EOF analysis, the PNA and NPO/WP variability are uncorrelated, both temporally and spatially. Close inspection of the SLP patterns (cf. Figs. 2.2a and 2.17a) shows the PNA signal to be maximal near the nodal line of the NPO/WP signal, indicating that these patterns are in quadriture. The ENSO SLP has more overlap with the PNA pattern than NPO/WP. But the ENSO and PNA signals are still quite distinct, with the ENSO one focused in the Gulf of Alaska while the

PNA signal is in the shadow of the Aleutians. (See Nigam 2003 for a more in-depth

intercomparison.) The PNA and NPO/WP impact on the Asian-Pacific jet has been noted

before (cf. Fig. 2.6).

The PNA's influence on North American hydroclimate is shown in the left

column of Figure 2.16. In contrast with the NPO/WP signal, precipitation is diminished

everywhere from the Aleutians to the Pacific Northwest except for a very narrow zone

along the Alaskan Gulf. The impact on US is very different as well: Precipitation is

strongly suppressed in the eastern part with the exception of Florida, while there is no

impact on the southwest region and the central Great Plains, two areas significantly

influenced by NPO/WP variability.

The ENSO precipitation impact is well documented and discussed in the literature

(e.g., Ropelewski and Halpert 1986; Green et al. 1997) and is displayed here, only for

contextual reference. The broad similarity with the NPO/WP impact, especially over

southern United States, is noteworthy, notwithstanding the extensive enhancement of

precipitation over the southeastern states, including Florida, during El Nino winters.

The PNA's SAT impact on Alaska, Canada and the Pacific Northwest bears

striking resemblance to the NPO/WP warming signal (cf. Fig. 2.9*b*) in view of southerly

flow in both cases: south/southeasterly in case of the PNA and southwesterly in NPO/WP

variability. The PNA trough is more expansive, skirting the American coast and leading

to warmer temperature over the western states as well.[6] The PNA warming however does

not extend to the eastern seaboard, as in case of NPO/WP variability; a result that can

again be understood from consideration of anomalous thermal advection. Although

---

[6] Note, warmer SATs may also result from zonal advection, since southerly flow along the coast will lead
to Ekman downwelling, and warmer coastal SSTs. Climatological westerlies can then produce warm
advection.

bearing some structural similarity, the ENSO SAT signal is rather muted in comparison

with the other two, on account of weaker circulation impact over the American continent

(see Nigam 2003).

The above intercomparison reveals that NPO/WP variability exerts profound

influence on the Alaskan, Pacific Northwest, Canadian and US winter surface air

temperatures; more so than PNA or ENSO. The NPO/WP variability is likewise more

influential on the Pacific Northwest, western Mexico and south-central Great Plains

winter precipitation. Although, NPO/WP variability has not been extensively analyzed, it

is, evidently, as, if not more, consequential for the North American winter climate.

2.4.2 – Comparisons to the NAO

The NAO and NPO/WP share many structural similarities, leading to the notion

of dynamical analog (Nigam 2003; see figure 17 and attendant discussion). A somewhat

more extensive intercomparison of the two modes of winter variability is undertaken

here, in the interest of furthering insight into NPO/WP origin and evolution.

The NAO is diagnosed here just as the NPO/WP was: Unrotated, covariance-

based EOF analysis of area-weighted winter monthly SLP anomalies over the Atlantic

basin (80W-0°; 20ºN-85ºN). The first EOF closely resembles the NAO pattern: Its PC is

correlated with Hurrell's NAO index (Hurrell 1995) at 0.94.

Both SLP patterns exhibit a meridional dipole consisting of a zonally elongated

band in the subtropics and a center near 60°N (Figure 2.18; note, map rotation). A third

center having the same sign as the subtropical center is present ~180º of longitude away,

in both cases. The NAO pattern has almost twice the amplitude, though. The 500 hPa

regressions are strikingly similar, as well; with both patterns exhibiting vertical coherence; an equivalent barotropic vertical structure.

The NPO/WP and NAO patterns are located near the exit region of the Asian-Pacific and Atlantic jets, respectively (cf. Figure 2.19, left panels). The 300 hPa zonal wind anomalies are displayed atop the climatological jets in this figure, and the significance of the NAO anomaly is readily apparent: Not only is this anomaly twice as large, as noted earlier, it is superposed on a climatological jet that is 3 times weaker, making NAO perturbations very effective in jet modulation; perhaps, a factor of 6 more than the NPO/WP ones. The dipolar anomalies shift the jet poleward, and extend it eastwards as well; evidently, much more in the NAO case.

A troposphere wide view of jet variability is provided in the right panels, which show the climatological and anomalous zonal wind averages in the Pacific (120ºE-120ºW) and Atlantic (80ºW-0º) sectors. The sector-averaged wind anomalies straddle the climatological jet-core in both cases, rather precisely, in the NPO/WP case. But the anomalies are stronger and considerably more effective in the NAO case, for reasons stated earlier.

The NAO related stormtrack anomalies are displayed in figure 2.20. Like the NPO/WP, the positive phase of the NAO is linked to an intensified and focused stormtrack (figure 2.20*a,b*), with considerable poleward displacement observed in the diabatic heating anomalies (2.20*c*). The similarity in the response of the basin stormtracks to the two variabilities suggests similar mechanisms behind their development.

To be sure, there are some differences between these variability modes too. While both primarily involve poleward shift and eastward extension of the respective jets, the NAO zonal wind anomalies contain extra features in the Tropics and polar regions, albeit of weak amplitude. This difference not withstanding, the remarkable similarity in mature phase structure of the modes suggests similar genesis and spatio-temporal evolution. Analysis of weekly data is discussed later to address these issues.

Chapter 2 Figures
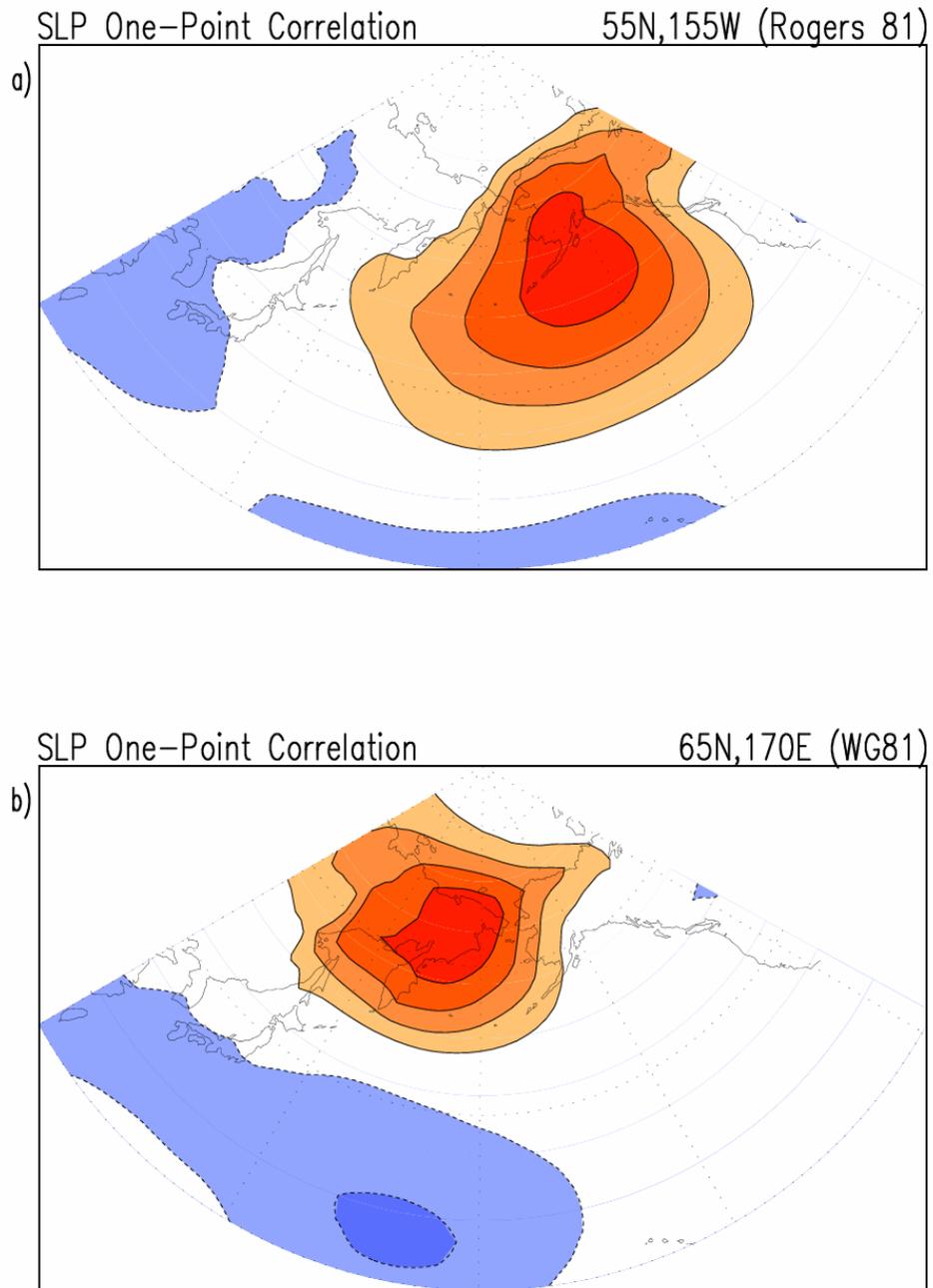
Figure 2.1: One-point correlations of monthly SLP anomalies during 1958-2001 winters in the ERA-40 data set: (a) with Rogers' (1981) NPO base point; (b) with Wallace and Gutzler's (1981) NPO base point. Base-point coordinates are noted in the upper right corner of each plot. The contour/shading interval is 0.2 and the zero-contour is suppressed. Solid (dashed) contours denote positive (negative) values.
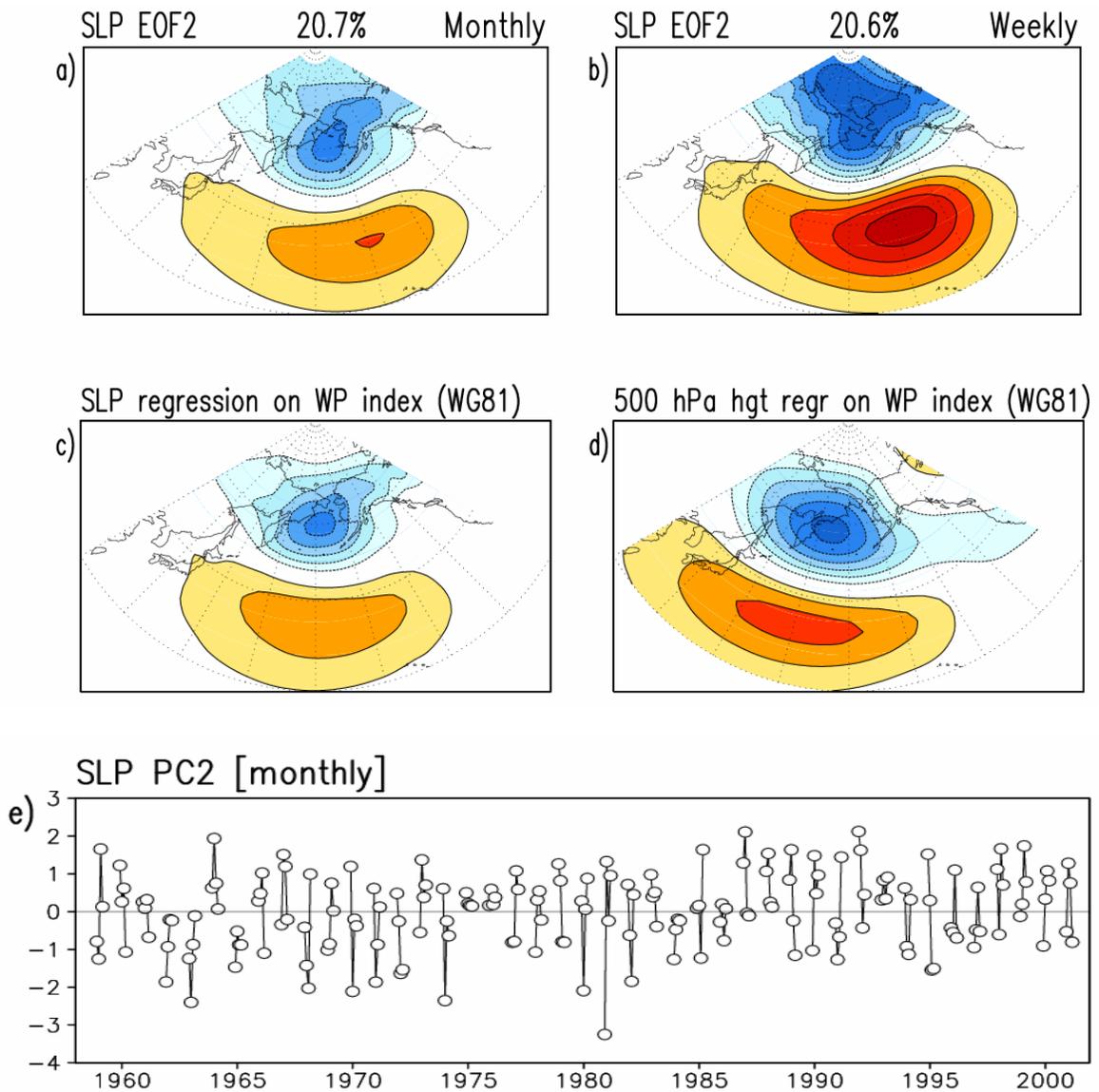
Figure 2.2: Winter sea-level pressure and height variability in the Pacific sector: (a) 2nd EOF from monthly (D,J,F,M) SLP analysis; (b) 2nd EOF from weekly SLP analysis (17 weeks per winter); Wallace and Gutzler's West Pacific teleconnection index regressions on (c) SLP and (d) 500 hPa geopotential height; (e) Principal component of 2nd EOF from monthly SLP analysis; defines our NPO/WP index. The 1958-2001 ERA-40 data is analyzed. Contour/shading interval is 1.0 hPa for SLP and 10 m for geopotential height. Solid (dashed) contours denote positive (negative) values; the zero-contour is suppressed.
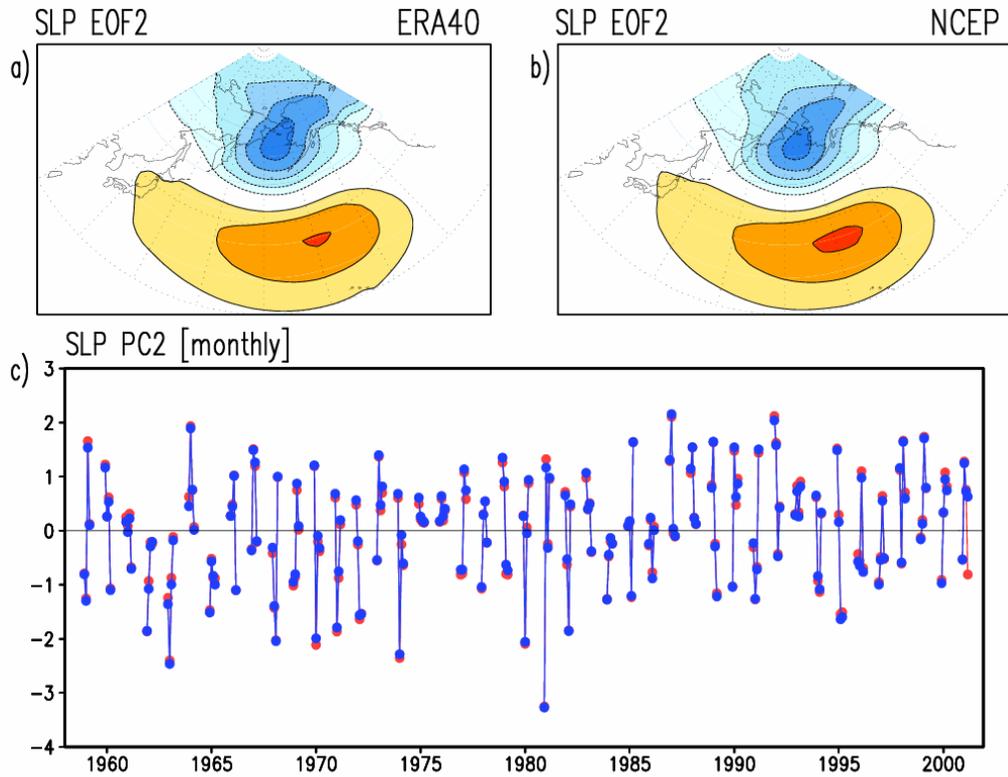
Figure 2.3: Comparison of winter sea-level pressure variability in the Pacific sector: (a) 2nd EOF from monthly (D,J,F,M) SLP ERA-40 analysis; (b) 2nd EOF from NCEP analysis; (c) Principal component of 2nd EOF from ERA-40(blue) and NCEP (red) monthly SLP analyses. Contouring/shading follows figure 2.2
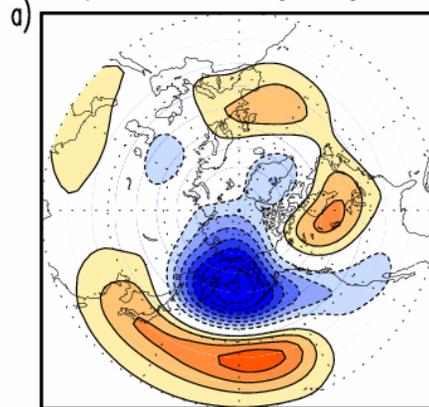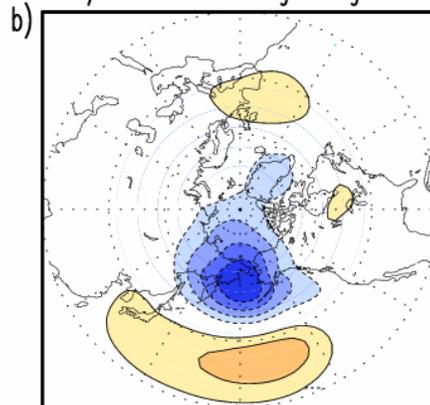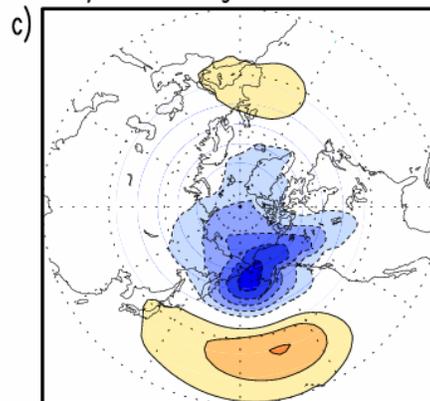
Figure 2.4: NPO/WP height and SLP regressions during 1958-2001 winter months (D,J,F,M): (a) 300 hPa,; (b) 700 hPa; and (c) SLP. Contour/shading interval is 10 m for height and 1hPa for SLP, and the remaining convention as before.
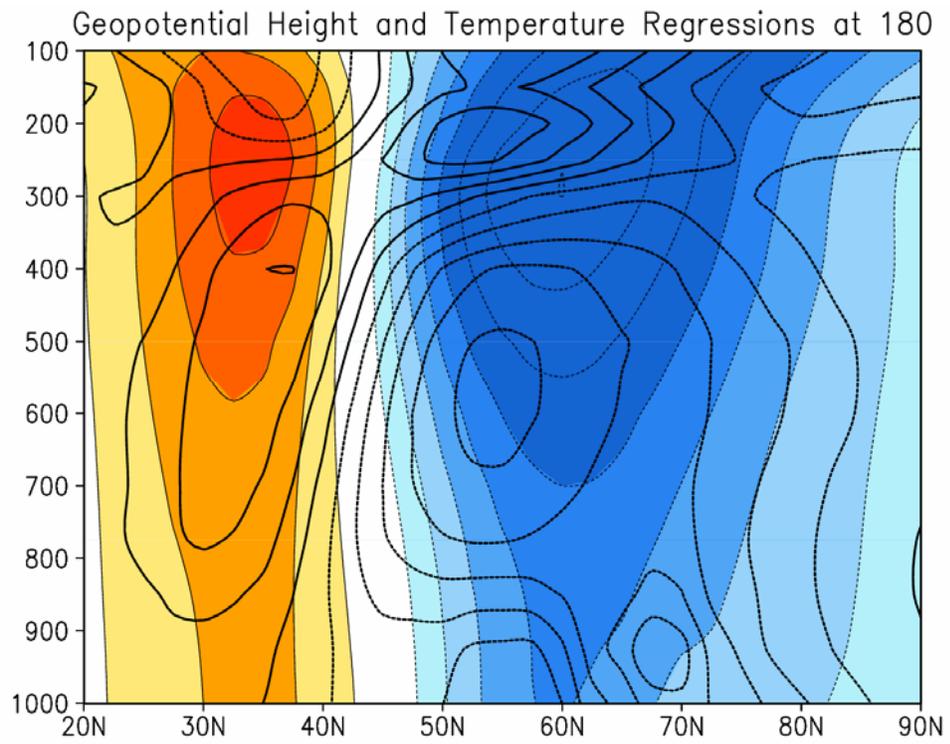
Figure 2.5: NPO/WP geopotential height (shading/thin contours) and temperature (thick contours) regressions along 180º during 1958-2001 winter months. Height is contoured at 10 m, while temperature at 1K interval. Contour/shading convention as in figure 2.4.
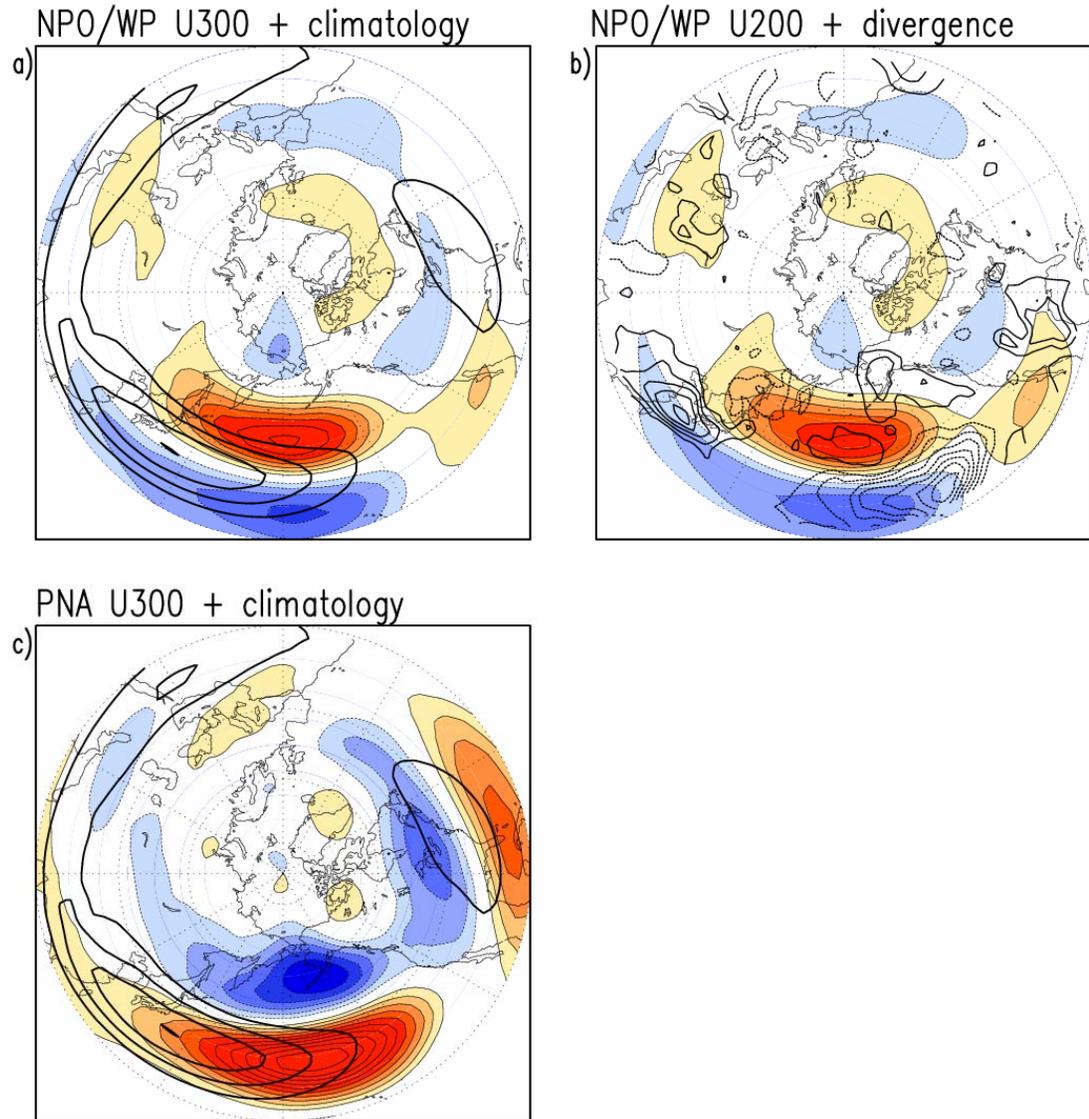
Figure 2.6: Zonal wind and divergence regressions during 1958-2001 winter months: (a) NPO/WP zonal wind superposed on the climatological field (thick contours) at 300 hPa; (b) NPO/WP horizontal divergence (thick contours) and zonal wind anomaly at 200 hPa; (c) As in panel a except for the PNA mode. Contour/shading interval for zonal wind anomaly is 1 m/s. Climatology contours begin at 30 m/s with an interval of 10 m/s. Divergence contour interval is 2 x 10^{-7}s^{-1}. The zero-contour is suppressed in all plots.
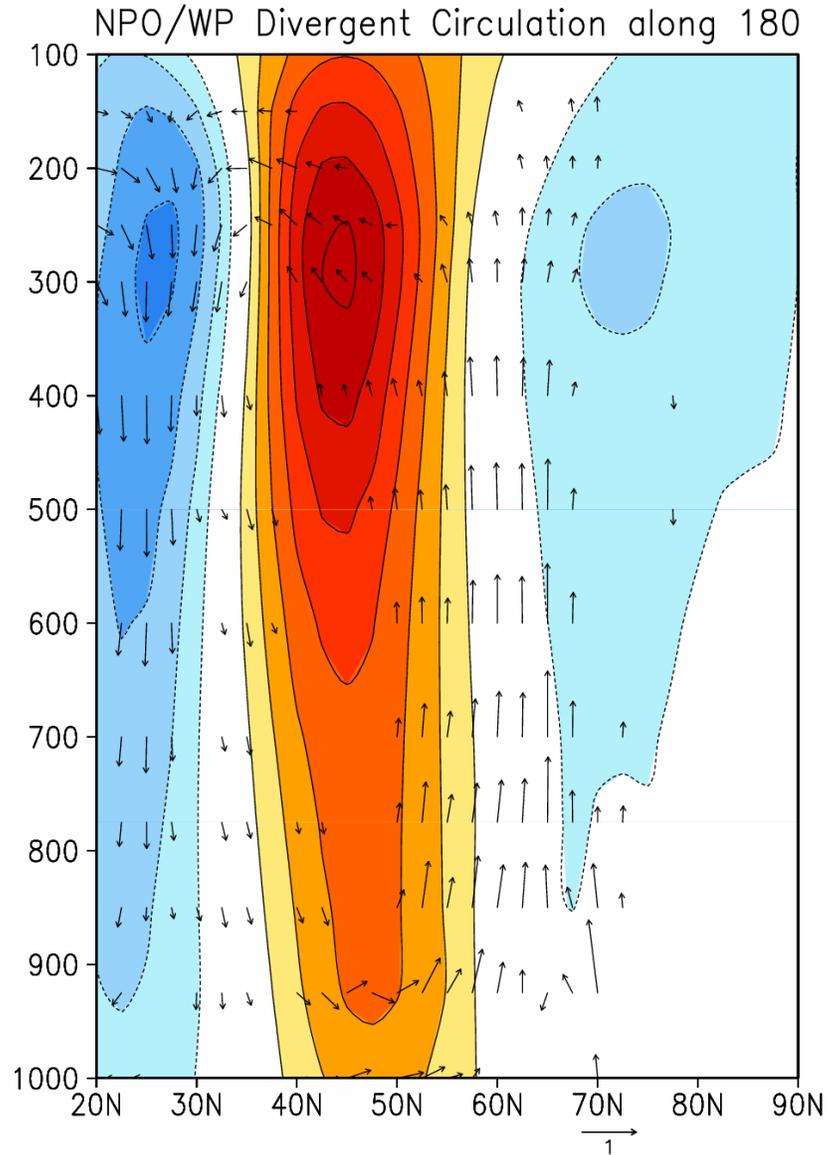
Figure 2.7: NPO/WP zonal wind (contoured/shaded) and divergent circulation (vectors) along 180º during 1958-2001 winter months in ERA-40 data. Contour/shading interval for zonal wind is 1.0 m/s. The divergent wind vector (V_χ, $-\omega$) is plotted after multiplying the pressure vertical velocity by -100; using the indicated scale and when the vector magnitude exceeds 0.1. V_χ is the divergent component of the meridional wind.
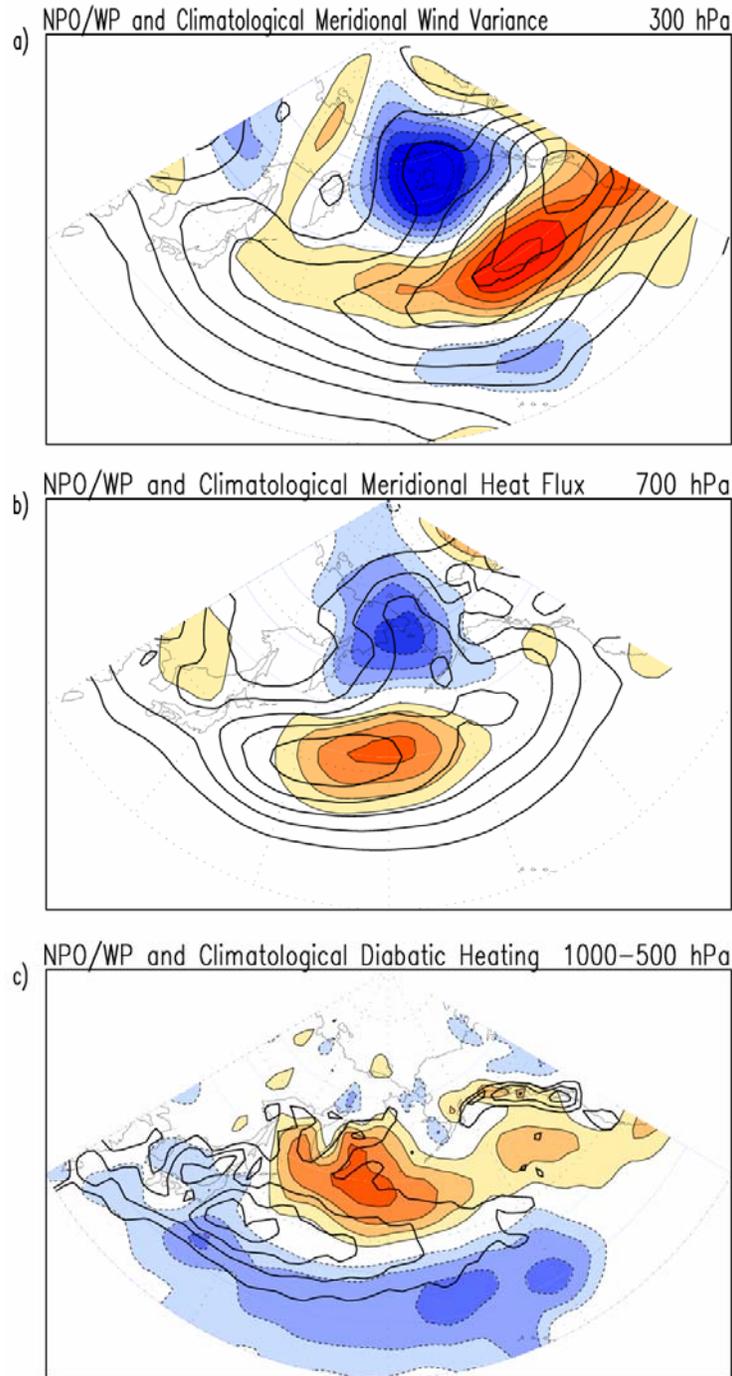
Figure 2.8: NPO/WP links with Pacific stormtracks during 1958-2001 winter months in ERA-40 data: (a) Regressions on 300 hPa submonthly meridional wind variance (contoured/shaded at 10 m^2/s^2) superposed on the corresponding climatology (thick contours at 50 m^2/s^2 interval); (b) Regressions on submonthly meridional heat flux (contoured/shaded at 1 K m/s) superimposed on the corresponding climatology (thick contours at 5 K m/s) at 700 hPa; (c) Regressions on vertically integrated (1000-500 hPa) diabatic heating (contoured/shaded at 0.1 K/day) superposed on the corresponding climatology (thick contours at 1 K/day interval; only positive values contoured to avoid confusion).
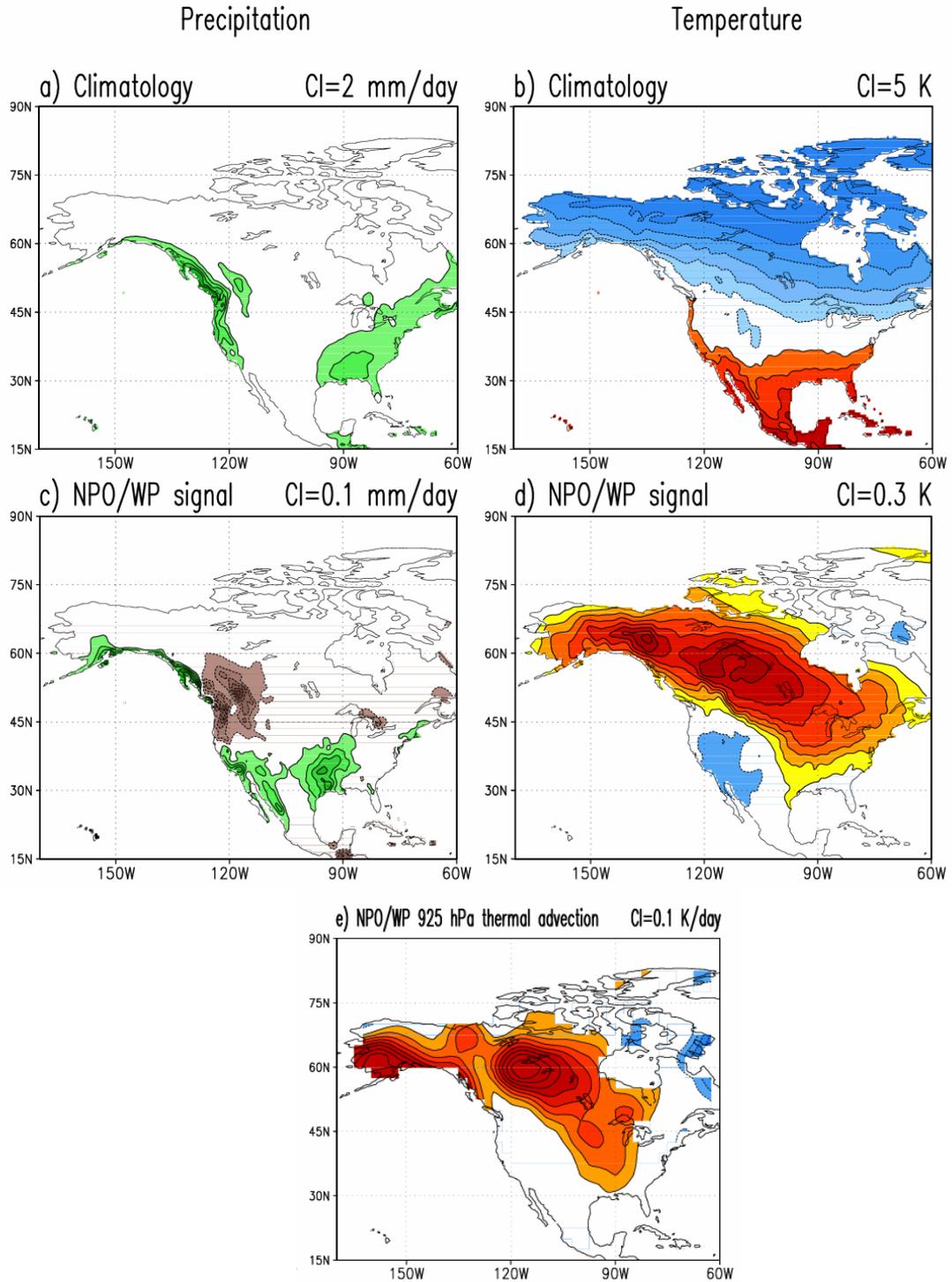
Figure 2.9: Climatological winter (DJFM) precipitation and surface air temperature over North America from University of East Anglia's CRU data is in the top panels (a-b); the 1958-2001 period climatology is displayed using indicated intervals. The NPO/WP regressions on the same winter month fields are in the middle panels (c-d), while the advective temperature change arising from the 925 hPa NPO circulation ($-\vec{V}_{NPO} \bullet \vec{\nabla}T_C$) is displayed in the bottom panel (e). Solid (dashed) contours denote positive (negative) values in all panels, and the zero-contour is suppressed.
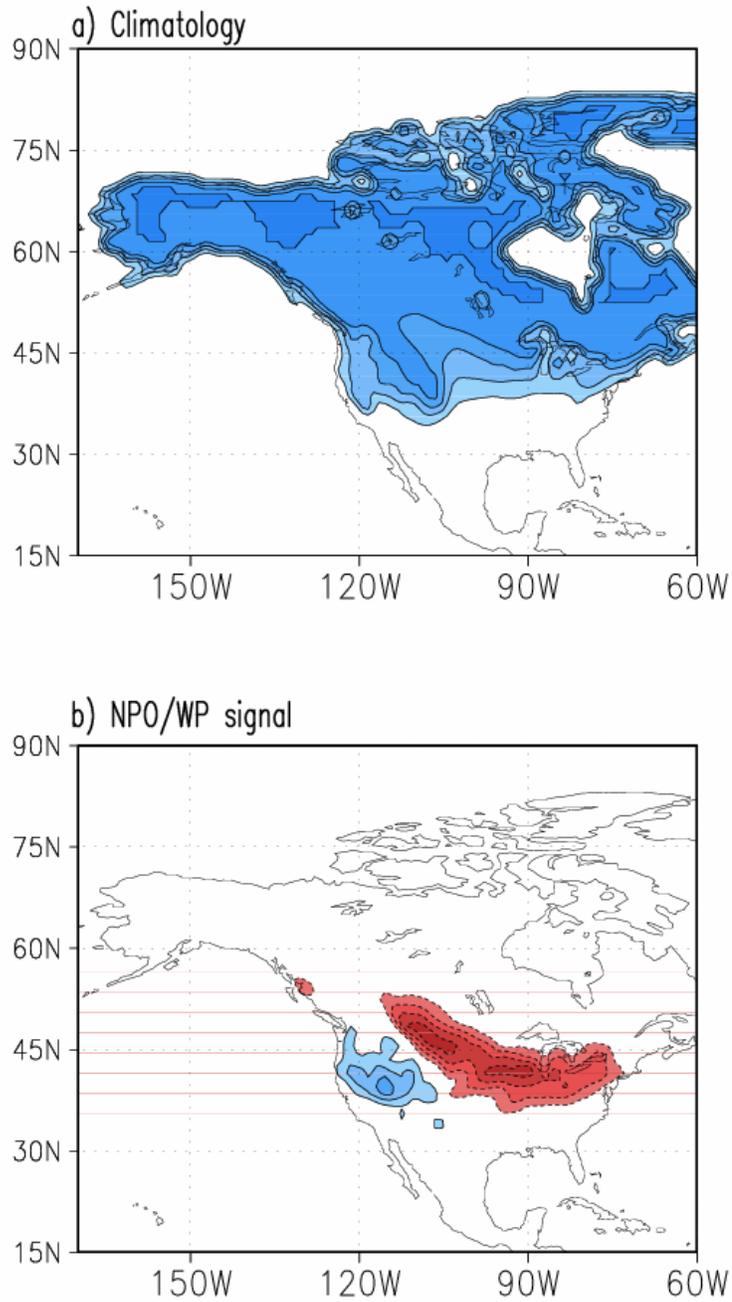
Figure 2.10: Climatological North America snow cover during December-January-February-March 1971-1994 from the Northern Hemisphere EASE-Grid weekly snow cover and sea ice extent (panel a). The NPO/WP regressions on the same winter month field are displayed in panel b. Climatological snowfall is contoured/shaded at an interval of 20%; regressions are contoured/shaded at an interval of 2%. Blue (rose) shading and solid (dashed) contours denote positive (negative) values and the zero contour is suppressed in both plots.
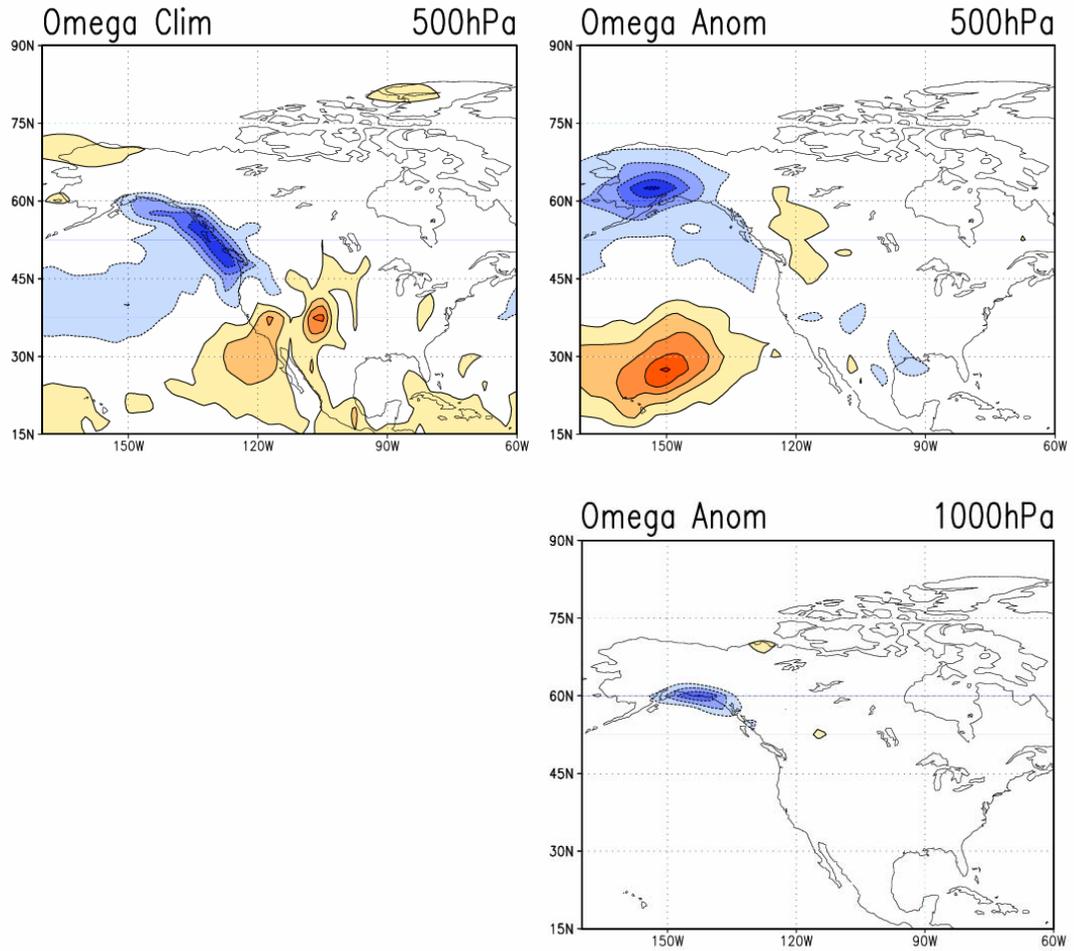
Figure 2.11: Climatological and NPO/WP vertical velocity regressions at 500 hPa (top) and 1000 hPa (bottom). Negative values indicate upward vertical motion; units are hPa/day. Solid (dashed) contours denote positive (negative) values and the zero-contour is suppressed.
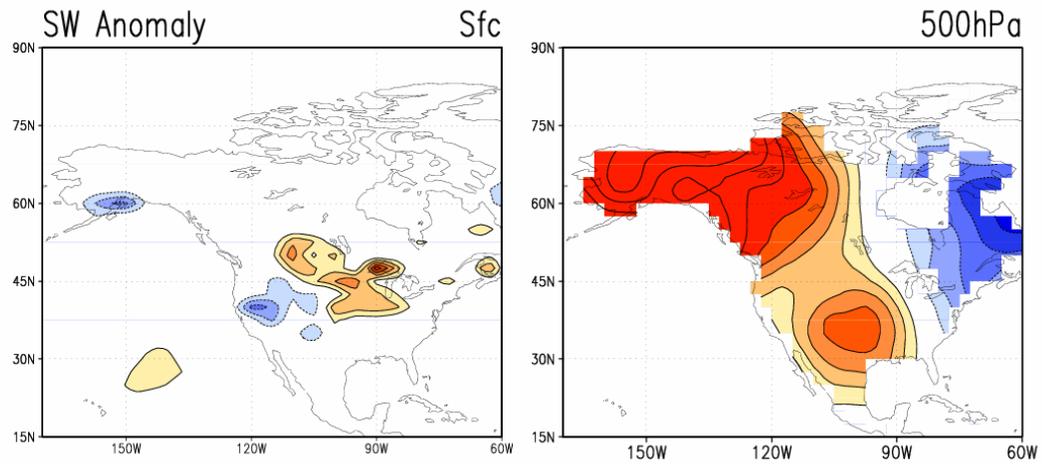
Figure 2.12: NPO/WP net surface shortwave radiation regressions (left) and 500 hPa horizontal temperature advection (($-\vec{V}_{NPO} \bullet \vec{\nabla} T_C$); right). SW radiation is contoured/shaded at 10 W/m^2 and 500 hPa temperature advection is contoured/shaded at 0.1 K/day. The zero contour is suppressed in both plots.
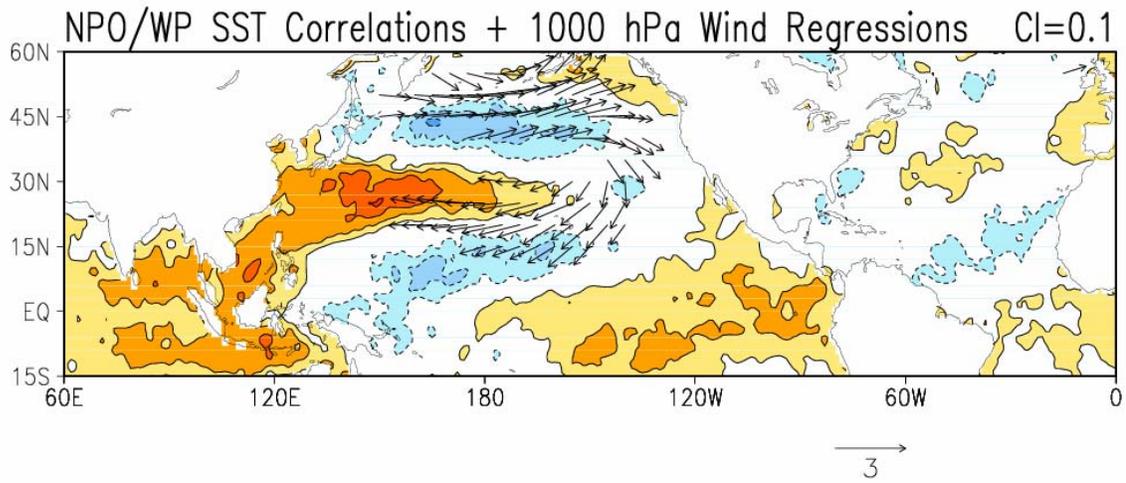
Figure 2.13: NPO/WP SST correlations and 1000 hPa wind regressions during 1958-2001 winter months. SST is from the HadISST1.1 dataset while winds are from ERA-40. Wind vectors are suppressed when the wind speed is less than 0.5 m/s. Solid (dashed) contours denote positive (negative) values and the zero-contour is suppressed.

Figure 2.14: NPO/WP lagged SST regressions using the PC from the DJFM monthly analysis. The regressions are plotted for lead times up to 12 months. Contouring interval is 1K, and solid (dashed) contours denote positive (negative) values and the zero-contour is suppressed.
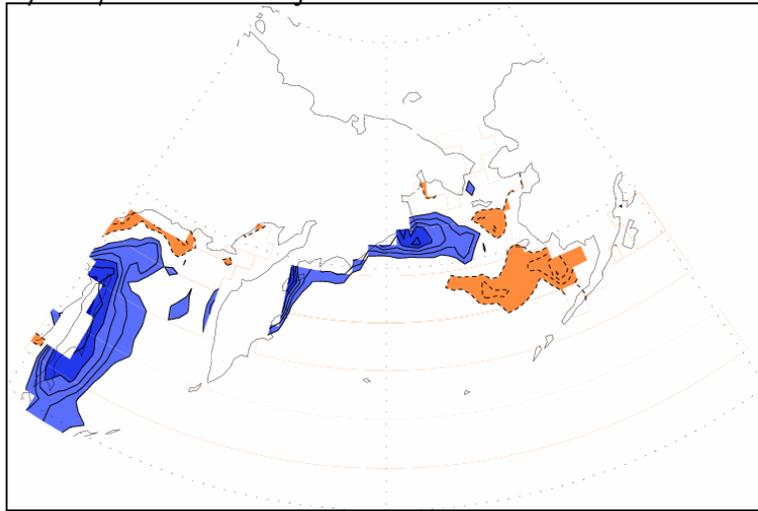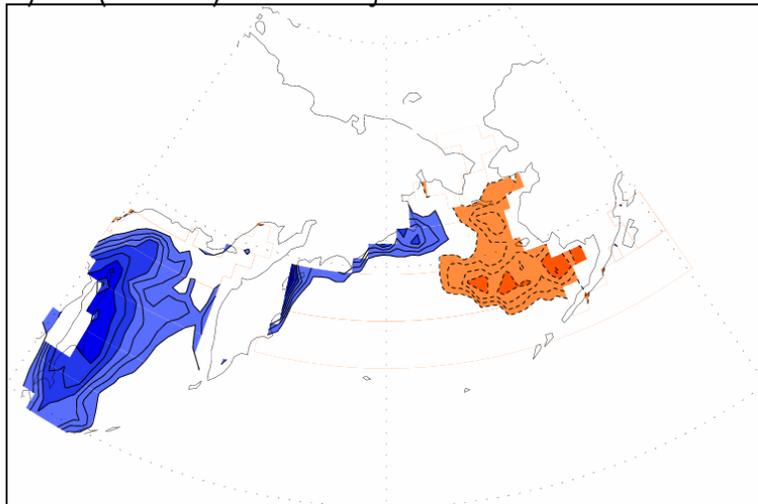
Figure 2.15: Regressions on Sea of Okhotsk and Bering Sea ice concentration during the 1979-2001 winter months (D,J,F,M): (a) NPO/WP regressions; (b) Wallace and Gutzler's WP index regressions. Contour/shading interval for ice concentration is 1%. Solid (dashed) contours denote positive (negative) values and the zero-contour is suppressed.
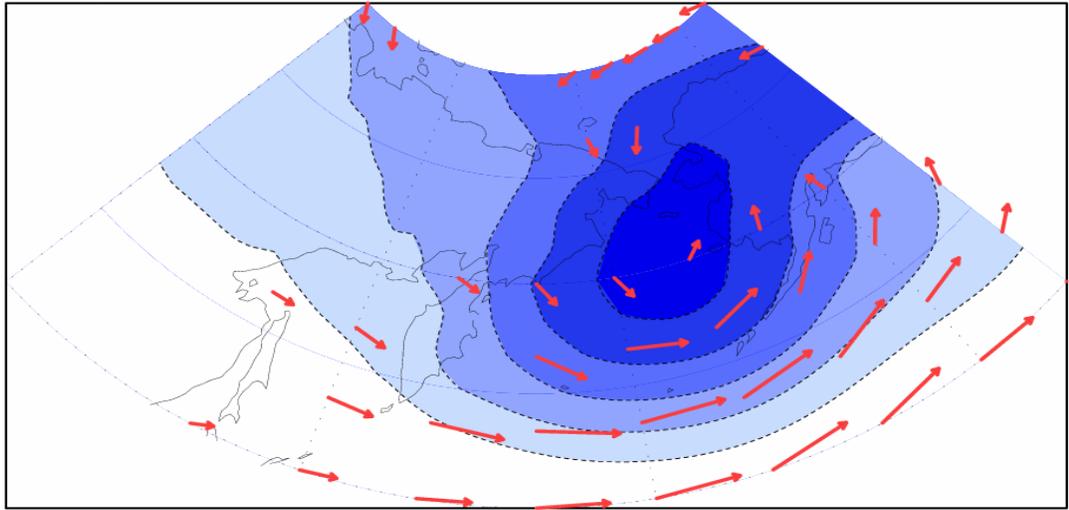
$$-\vec{V}_{NPO} \bullet \vec{\nabla} T_c$$
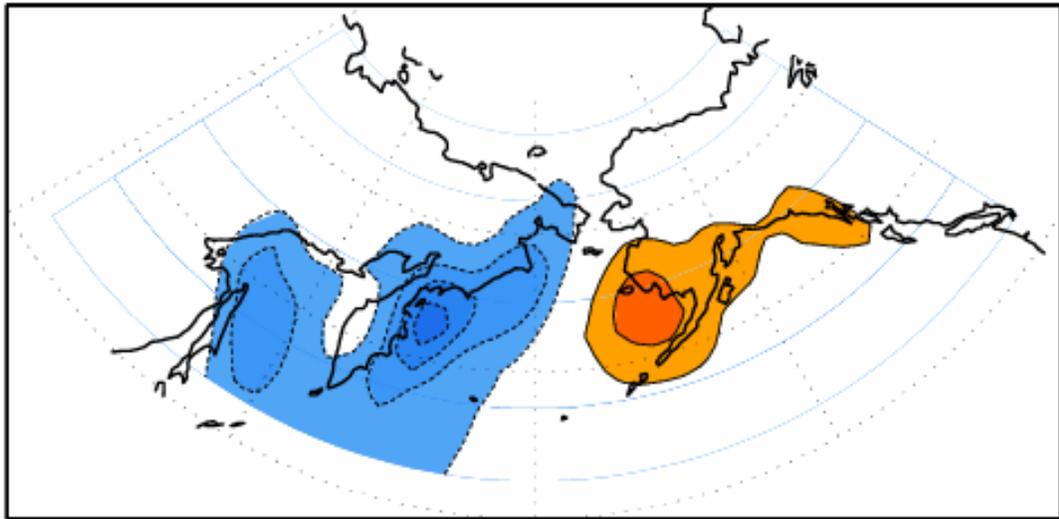
Figure 2.16: NPO/WP SLP and 1000 hPa wind regressions during 1958-2001 winter months (top) and 1000 hPa horizontal temperature advection by the NPO/WP circulation (bottom). Wind vectors are suppressed when the wind speed is less than 1 m/s. SLP is contoured at 1 hPa and thermal advection at 0.4 K/day interval. Solid (dashed) contours denote positive (negative) values and the zero-contour is suppressed in all panels.
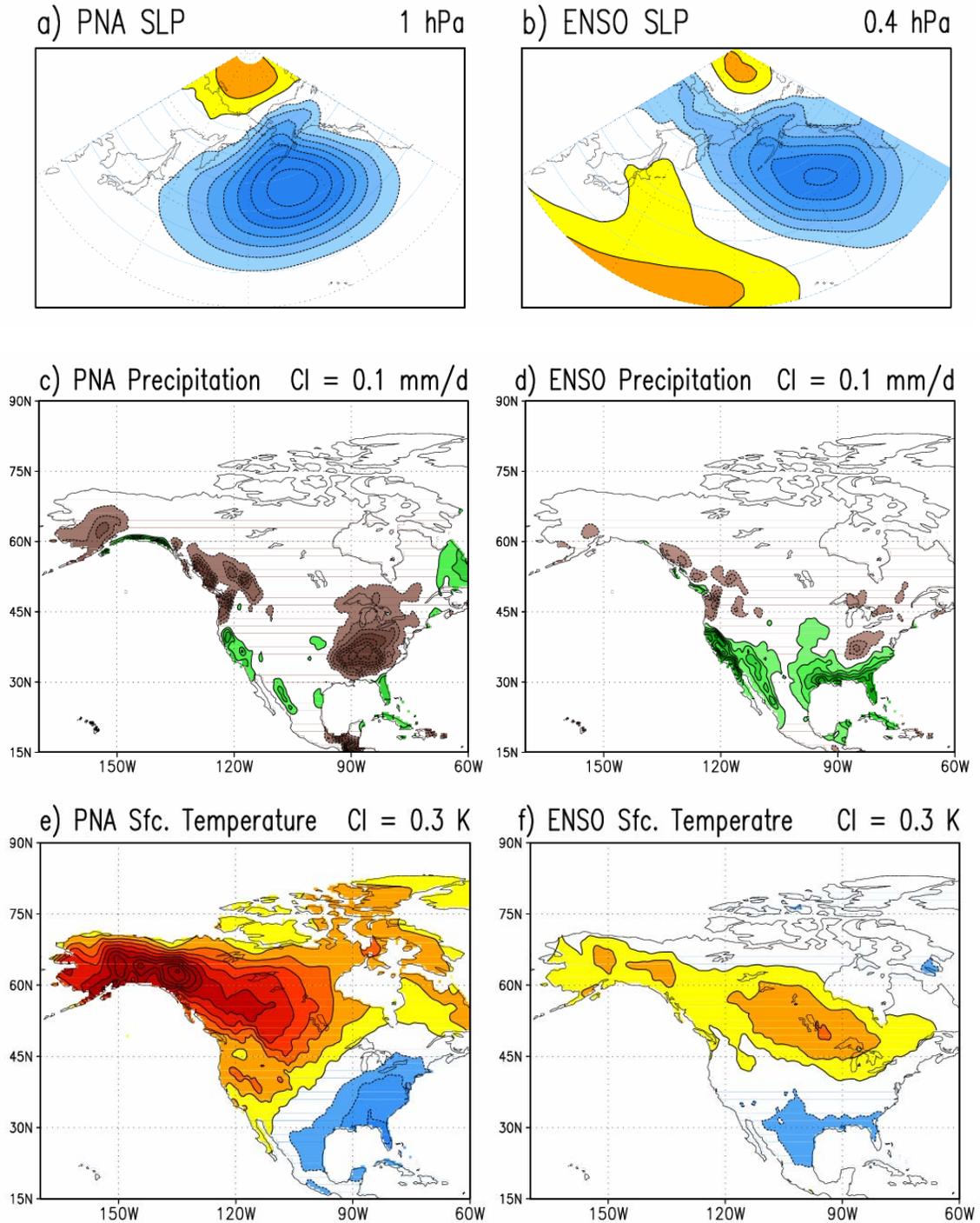
Figure 2.17: Winter sea-level pressure (top), precipitation (middle), and surface air temperature (bottom) patterns associated with PNA and ENSO variability: PNA anomalies are diagnosed from regressions of the leading PC of monthly SLP analysis (the 2nd mode of which is NPO/WP); ENSO ones are obtained from Nino3.4 SST index regressions; all are for the 1958-2001 winter months. Contour/shading interval is 1.0 hPa for the PNA SLP, 0.4 hPa for ENSO SLP, 0.1 mm/day for precipitation, and 0.3 K for temperature. Solid (dashed) contours denote positive (negative) values and the zero-contour is suppressed.

81
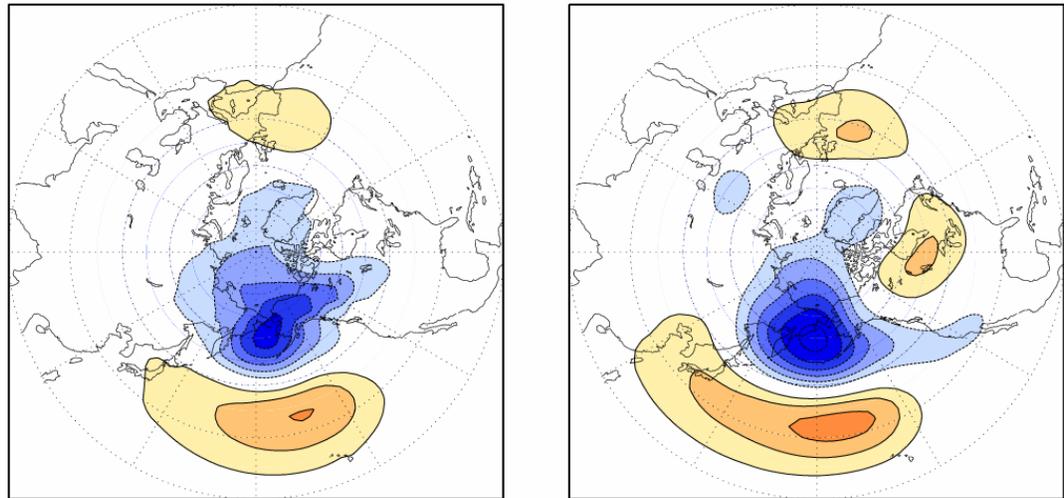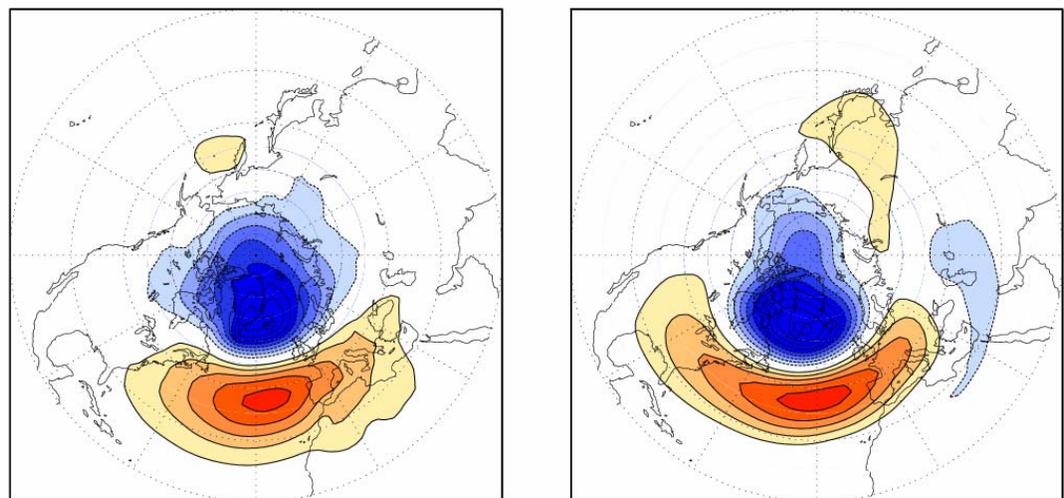
Figure 2.18: Winter sea-level pressure and 500 hPa height patterns associated with NPO/WP (top) and NAO (bottom) variability in the 1958-2001 winter months in the ERA-40 data set. Contour/shading interval is 1.0 hPa for SLP and 10 m for geopotential height. Solid (dashed) contours denote positive (negative) values and the zero-contour is suppressed. Note the map rotation between top and bottom panels.
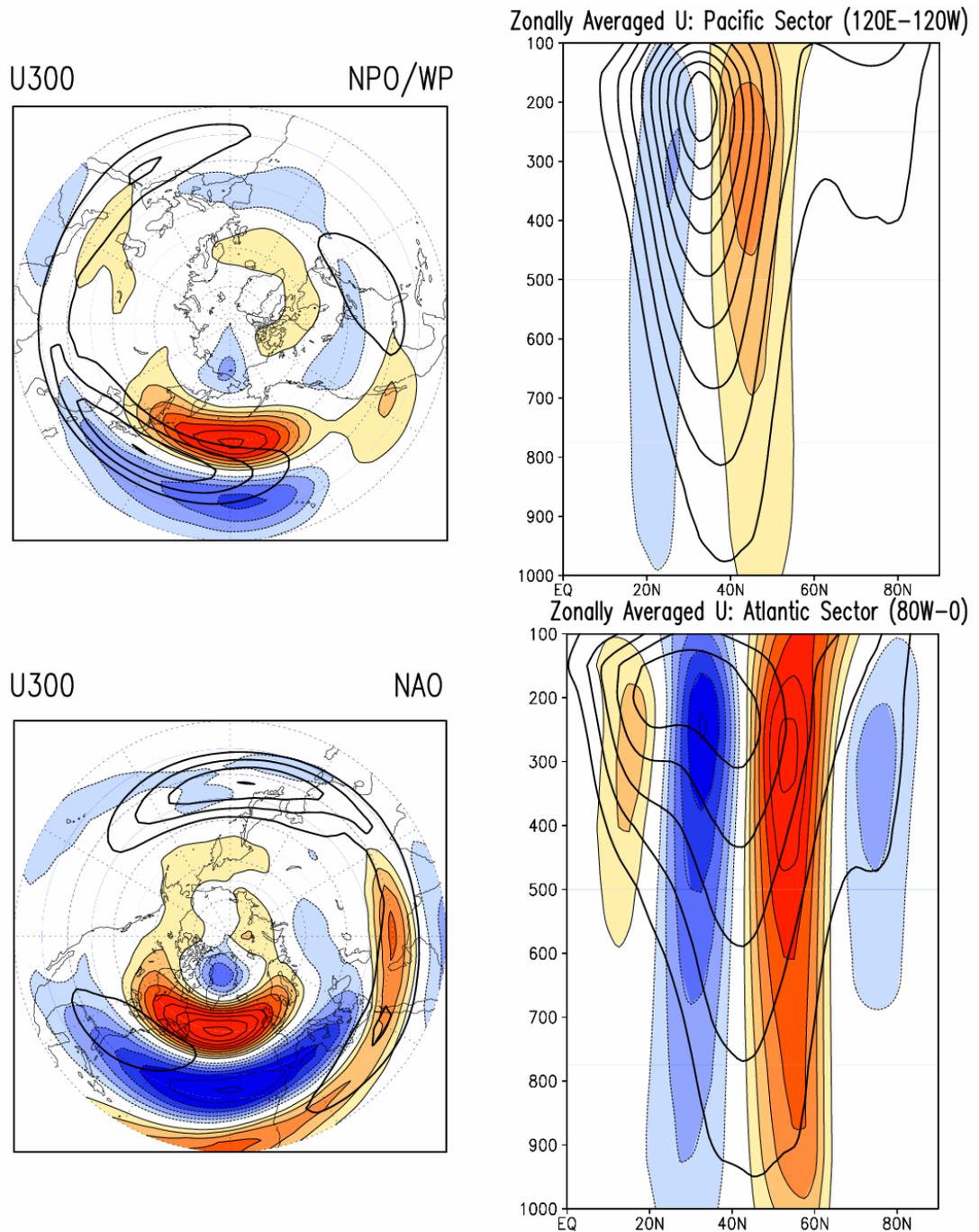
Figure 2.19: Zonal wind patterns associated with NPO/WP (top) and NAO (bottom) variability in the 1958-2001 winter months (D,J,F,M) in the ERA-40 data set. The corresponding period zonal wind climatology is superposed using thick contours. The 300 hPa regressions (contoured/shaded at 1 m/s interval) and climatology (starting at 30 m/s with an interval of 10 m/s) are shown in the left panels. The right panels show latitude-height cross-sections of the Pacific and Atlantic sector averaged flow: Pacific sector (120E-120W), Atlantic sector (80W-0). Cross-section regressions are contoured/shaded with a 1 m/s interval, while sector climatology is contoured with a 5 m/s interval. Note the map rotation between upper and lower left panels.
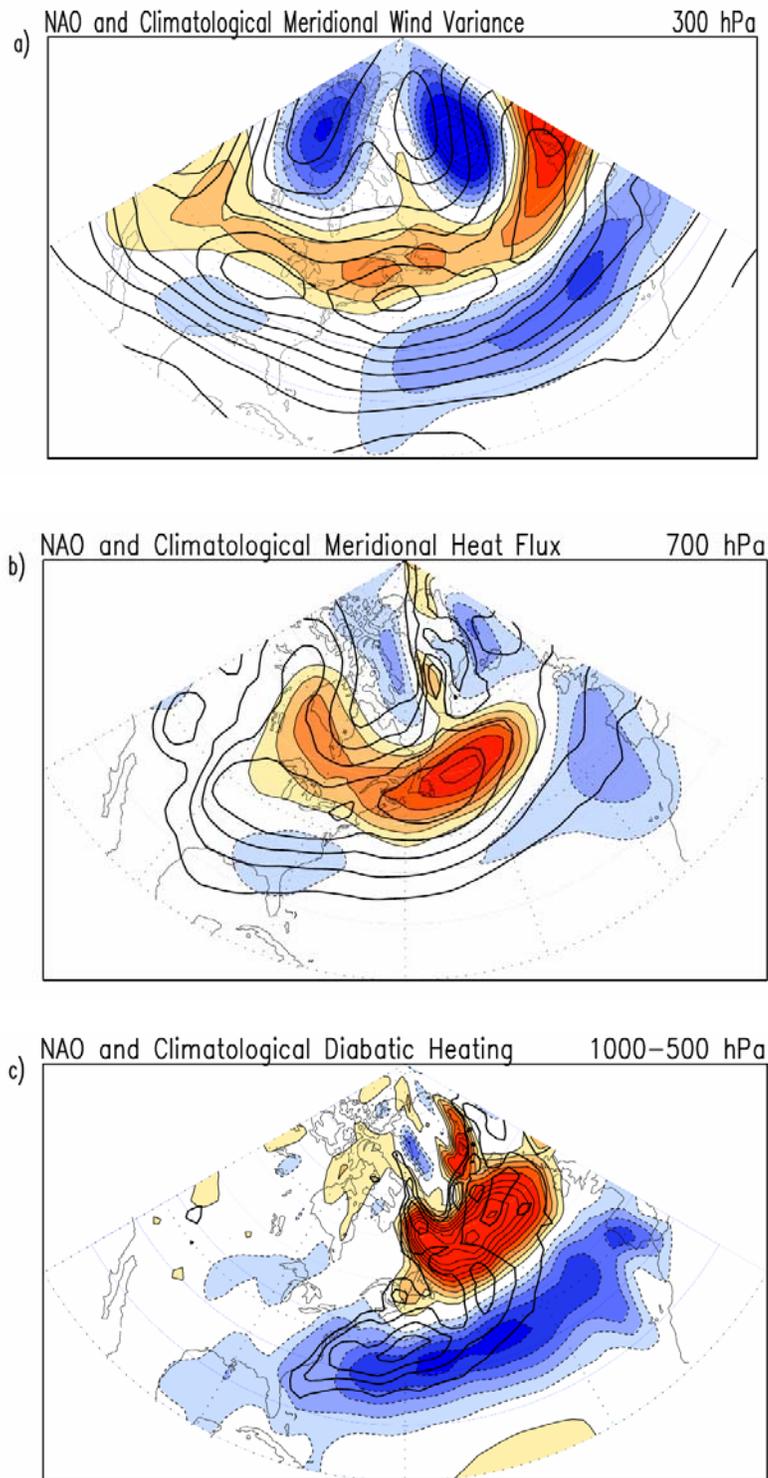
Figure 2.20: As in figure 2.7, except for the NAO.

Chapter 3: The North Pacific Oscillation/West Pacific Pattern: Submonthly evolution and weekly impacts

This chapter investigates the NPO/WP submonthly evolution and structure. The characteristics of the nascent and decay phases are identified and lag-lead connections to the NAO and PNA are sought. The evolution of the response of the hydroclimate, SST and the MIZ to an NPO/WP episode is also quantified. The analysis relies heavily on extended empirical orthogonal function (EEOF) analysis, which extracts various modes of spatio-temporal variability from the desired geophysical field.

3.1 – Statistical analysis of the weekly NPO/WP

3.1.1 – NPO/WP evolution from EOF analysis

The most common and simple method of determining the antecedent and latter phases of a teleconnection pattern is to compute lag lead regression coefficients using the principle component generated from a standard EOF analysis. The PC is regressed on data points which lag or lead the PC by one or two time steps. To determine the structure of the NPO/WP prior to and subsequent to the peak phase, the PC from an EOF analysis performed on weekly winter SLP anomalies is regressed on the weekly SLP field from two weeks in advance of and two weeks following the mature phase (Figure 3.1).

Evident in the lag-lead regressions is the lack of any precursor phase two weeks before maximum amplitude is attained. Only weak anomalies, on the order of 1 hPa, in the subtropical Pacific (~35ºN) and polar cap (~80ºN) are present. One week prior to maximum amplitude, the suggestion of a Pacific dipole appears. The ridge in subtropical Pacific intensifies to 2 hPa, approximately 1 hPa less than the magnitude of the southern

node in the monthly analysis, while the polar SLP anomalies are asymmetric about the pole, deepening to -2 hPa over a large area of the Arctic Circle. Obviously, at zero lag, the familiar dipole returns and the SLP anomalies are at their maximum amplitude. A large area of low pressure is centered off the northern Alaskan coast, reaching a minimum pressure of -7 hPa. Much of the subtropical Pacific is under the influence of broad high pressure, with a center of 5 hPa located north of Hawaii. A similarly signed, tertiary center is present in the Atlantic, attaining an amplitude of 1 hPa.

The low pressure perturbation in the North Pacific dissipates rapidly, with a weak -2 hPa center positioned over the Siberian coast. The anomalous high is displaced poleward from its original position, now centered on 40ºN with an amplitude of 4 hPa. The tertiary center over the Atlantic is all but disappeared. Two weeks after the mature phase structure, there is almost no indication of any persistent pressure anomalies. Two centers are present; a high pressure perturbation around 40ºN and a low pressure center over Greenland.

Lag-lead regressions of the PC with 200 hPa geopotential height anomalies are also calculated, to ascertain tropical connections (figure 3.2). Two weeks prior to the mature phase dipole, moderate height anomalies are dispersed throughout the Northern Hemisphere north of 30ºN. No height perturbations in the tropics, at least between 20ºN and 25ºN, are present, suggesting the NPO/WP is not a response to shifts in tropical convection and diabatic heating anomalies (á la the ENSO midlatitude response).

The development of the NPO/WP aloft is similar to the surface, except that the amplitude of the anomalies is much larger, indicative of a cold core structure. The height anomalies develop and decay very rapidly and the height anomaly pattern at zero lag is

suggestive of low frequency Rossby wave dispersion. The baroclinic structure described in Hsu and Wallace (1985) is also prevalent at zero lag, with a ridge at 200 hPa atop lower SLP.

The absence of any signal two weeks prior to the mature phase of the NPO/WP demonstrates the disadvantages of lag-lead regressions when seeking the nascent and decay phases of teleconnections. The PC, or whichever index is used, is keyed to search for similar spatial patterns during the weeks prior to and after the peak phase. If the characteristics of the early and latter stages are not similar to the mature phase, the modal development is misrepresented and the underlying dynamic and thermodynamic mechanisms behind teleconnection development are not able to be determined. Thus, a more powerful statistical tool is necessary; for our purposes, we employ EEOF analysis.

3.1.2 – NPO/WP from weekly EEOF analysis

The NPO/WP is the second EEOF of winter (DJFM) 1958-2001 weekly SLP; as with the monthly analysis, the PNA is the leading mode. Figure 3.3 reveals substantially different evolutionary characteristics than the regression analysis in the previous section. A strong low pressure anomaly of -12 hPa is centered over the Aleutian Islands, and only a minor perturbation (2 hPa) in subtropical SLP is present at a lag of -2 weeks. The monopole structure of the pre-peak phase NPO/WP explains why the regressions of the 2nd PC from the traditional EOF analysis did not return a similar pattern; almost no hint of the mature phase dipole is present. At a lag of
-1 week, both centers amplify, and the first indication of an oscillation occurs. The southern node, still centered north of Hawaii, amplifies to 4 hPa. The northern node deepens to -16 hPa and is shifted slightly northwestward, now centered just north of the

Aleutians. At zero lag, the familiar mature phase dipole returns, and is structurally similar but larger in magnitude to the mature phase extracted in the monthly analysis. A broad area of anomalously high pressure covers much of the subtropical Pacific Basin, with a center of 6 hPa at 35ºN. The northern center has weakened slightly, to -14 hPa, and continues to propagate to the northwest, now located over the Bering Sea.

During the decay phase, the NPO/WP once again displays a monopole structure, except the lone center is an expansive high pressure anomaly over the subtropical and midlatitude Pacific Ocean. The high anomaly is centered just south of 40ºN, and attains its maximum amplitude of 10 hPa. The low pressure center continues to retrograde to the northwest, now centered over Eastern Siberian and weakened to -8 hPa, which is 60% of its original magnitude. At +2 weeks lag, the low pressure anomaly has substantially weakened, with a weak perturbation of 4 hPa over the Eastern Siberian Sea. The midlatitude Pacific remains under the influence of the anticyclonic anomaly, with a center of 8 hPa positioned on 40ºN.

The presence of the initial pressure perturbation in the vicinity of the Aleutian Low implies internal atmospheric dynamics, possibly stormtrack variability, are responsible for the initiation of an NPO/WP event. Lag-lead regressions of the PC from the EEOF analysis are presented in the following section, looking for antecedent geopotential height and stormtrack connections to the NPO/WP.

3.1.3 – Persistence of an NPO/WP episode

The autocorrelation of the NPO/WP PC provides insight into the duration of an NPO/WP episode (figure 3.4). Using either 0.5 or $1/e$ as the decorrelation timescale, an NPO/WP episode lasts for 2-3 weeks. The autocorrelation increases rapidly from -2

week lag to -1 week lag; the quick increase in the autocorrelation in the two weeks prior to the peak further indicates that the NPO/WP is the product of internal atmospheric variability, as opposed to forced by a slowly varying component of the climate system (i.e. SST).

3.2 – The NPO/WP: Submonthly Evolution and Structure

3.2.1 – Evolution of SLP

A hemispheric view of the NPO/WP SLP anomalies is shown in figure 3.5. At -2 weeks, the prominent feature is an intensified Aleutian Low, positioned over Alaska and the Aleutian Islands. SLP anomalies associated with this center extend across the Arctic Ocean to Greenland, and extend southeastward along the Canadian Rockies. Minor pressure perturbations are in the subtropical Pacific (1 hPa) and northern Atlantic (2 hPa). An intensified Aleutian Low is present at -1 week as well, influencing the Arctic Basin and Greenland. Over the United States, low pressure traverses a route parallel to the contours of elevation in the western US. The subtropical node, centered at 30ºN, amplifies to 2 hPa, and the tertiary center in the North Atlantic remains, with an equivalent magnitude. At zero lag, the NPO/WP is nearly identical to the mature phase structure from the monthly analysis (cf. Figure 2.4). Low pressure extends over the Arctic Circle and expands southeast towards the Great Lakes. The center is now positioned off Alaska, with a central pressure anomaly of -6 hPa. The southern lobe is centered on 35ºN, with a pressure perturbation of 3 hPa and expands westward to Japan. Over the Atlantic, the tertiary center is still present, weakened to 1 hPa. The dipole is still present one week after the peak phase, but the poleward center has weakened

considerably, to -3 hPa. The anomaly is still expansive, influencing much of Russia. The anticyclonic circulation is amplified, to 5 hPa, and covers nearly the entire midlatitude and subtropical Pacific Ocean. At a lag of +2 weeks, all initial developmental and mature phase characteristics have vanished, with only a monopole in the Pacific Basin.

3.2.2 – Evolution of upper tropospheric features

The upper tropospheric evolution is presented in figure 3.6, with a wave train emanating from the subtropical Pacific two weeks before the peak. The most notable feature is a deep trough at 300 hPa, with geopotential height anomalies exceeding 100 m at the center. Due east of the trough is a dual centered ridge, with centers over interior Canada and the eastern Atlantic. To the south, a broad low-latitude anomalous ridge of 30 m encompasses much of the subtropical Pacific. Considerable circulation anomalies are present one week before the peak SLP anomalies. A broad ridge occupies the subtropics and southern Asian continent, and the trough has deepened further. The pattern over the Pacific is distinctly equivalent barotropic; the anomalies amplify with height (not shown). Over the North American continent, the ridge present in the upper troposphere is atop lower pressure anomalies, rendering the NPO/WP baroclinic over the United States and Canada. At a time lag of zero, the wave train is slightly less defined; the dipole is present over the Pacific Basin, but the additional centers are slightly less defined. Evident, though, is a trough positioned over the southwest United States, originally identified in Barnston and Livezey (1987). During the decay phase, the trough propagates to the northwest at a lag of +2 weeks. The subtropical ridge is positioned slightly poleward of its original position, as is the trough over the western United States.

Zonal wind anomalies occur in conjunction with the circulation anomalies in the upper troposphere. The monthly analysis links the NPO/WP to a northeastward displacement of the Asian-Pacific jet stream, and the divergence anomalies are thermal wind restoring, implicating other dynamical processes in development of zonal wind anomalies. Closer inspection of the evolution of the zonal wind anomalies on weekly timescales (figure 3.7) reveals that initially, an eastward extension of the jet exit region of the Asian Pacific jet occurs. The left front quadrant, located in the jet exit region, is conducive to the development of synoptic scale transients, further alluding to fluctuations of the stormtrack being a primary driver of NPO/WP variability. As an NPO/WP episode continues to evolve, the zonal wind anomaly develops a dipole structure, with the anomalies straddling the climatological jet axis and nudging the jet northward. The effects of the NPO/WP are not only confined to the Asian Pacific jet; the Atlantic jet stream weakens slightly, reducing the already diffuse jet.

An alternative view of the jet anomalies is depicted in figure 3.8. Zonally averaged zonal wind anomalies between 120ºE-120ºW are plotted, and the climatological zonal wind bounded by the same longitudes is presented to place the anomalies in context. At the outset, the maximum zonal wind perturbation is situated around 400 hPa and is centered near the climatological jet core. Only a minor perturbation is equatorward of the jet. The original zonal wind perturbation moves northward and coincides with the development of a dipole, implying a poleward shift in the Asian Pacific jet.

Stormtrack variations excite certain North Pacific circulation variabilities which, while not named the NPO/WP, contain the salient features of the NPO/WP. The Aleutian

Block (ALB) pattern described by Nakamura and Wallace (1990) is spatially similar to the negative phase NPO/WP (their figure 5). In the SLP field, the ALB pattern is characterized by a westward shifted Aleutian Low, comparable to the AA pattern described by Rogers (1981). The negative phase ALB, associated with an eastward shifted Aleutian Low, features intensified zonal flow in the eastern Pacific, found in the Pacific pattern (Hsu and Wallace 1985) and the positive phase NPO/WP (c.f. figure 2.8).

Two to five days prior to the onset of the positive ALB phase, enhanced baroclinic activity occurs upstream in the Pacific basin, protracting the developing block by depositing anticyclonic vorticity in the vicinity of the low-frequency circulation. As the blocking circulation intensifies, the stormtrack in the western Pacific basin splits, with one branch deflected poleward and the other deflected equatorward. The equatorward flank of the stormtrack is related to the development of a cyclonic circulation immediately south of the block. The fully developed stage of the ALB pattern, then, is a modon-like structure, with the development of the northern node preceding the development of the southern node. As the ALB decays, the upper level height feature retrogrades to the northwest, traversing a pattern similar to the northern node of the NPO/WP.

The negative phase of the ALB teleconnection is preceded by suppressed baroclinic activity. This suppressed baroclinic activity propagates upstream and is deflected around the developing cyclonic circulation. Along the dipole node, an intensified stormtrack and meridionally tightened, eastward extended jet stream are present. At the surface, an enhanced, eastward Aleutian Low occurs in conjunction with the features aloft. The circulation anomalies associated with the negative phase of the

ALB are returned in our analysis of both monthly and weekly SLP anomalies, linking the NPO/WP to the ALB and thus, stormtrack fluctuations.

The NPO/WP also contains some of the salient features of the persistent height anomaly over the North Pacific Ocean described by Dole and Gordon (1983) and Dole (1986). The composite anomalies associated with the negative Pacific (PAC) cases feature an intensified Aleutian Low and tropospheric temperature anomalies in phase with the height anomalies (Dole figs. 8 & 9). The stormtrack during the negative PAC cases is a zonally intensified one, physically consistent with an enhancement of the climatological westerlies.

Dole and Black (1990) and Black and Dole (1993) delved into the genesis mechanisms of the PAC anomaly and found a substantial contribution from baroclinic energy connected to synoptic scale cyclogenesis. As the disturbance propagates downstream, energy conversions broaden the circulation; attaining a barotropic structure and developing into a persistent anomaly over the North Pacific. Typically, the initial cyclogenesis is "bomb cyclogenesis," defined as a rapidly intensifying extratropical cyclone whose pressure decreases 24 hPa in 24 hours. The use of weekly quantities filters out synoptic scale variability, preventing isolation of individual bomb cyclogenesis events. However, the authors note that Pacific bomb cyclogenesis is typically preceded by an outbreak of cold air over the Tibetan Plateau and Siberia. Regression of the NPO/WP PC on global temperature reveals a broad area of cold temperatures over the Asian continent in the weeks preceding an NPO/WP episode (not shown).

Furthermore, using weekly data to investigate the impact of the NPO/WP on the jet, and consequentially, the stormtrack, provides some resolution regarding the

discrepancies between Lau's (1988) analysis and our analysis. The leading three

eigenvectors from Lau's analysis of stormtrack variability contain NPO/WP features.

Lau links the first EOF, a monopolar intensification of the stormtrack, to the WP, and the

third EOF, decreased eastern Pacific eddy activity, to the negative phase of the NPO. We

know from our earlier analysis that the NPO and WP are inseparable, and that analysis of

a variety of variables linked the NPO/WP to both an enhanced focused stormtrack (due to

an acceleration of the ambient westerly flow) and a latitudinally shifted stormtrack (due

to a poleward shifted Asian Pacific jet).

     The constantly varying NPO/WP jet anomalies do provide insight into the

discrepancies between the conclusions drawn by Lau and us, presented in the earlier

section. Initially, a single zonal wind anomaly is present, near the axis of the

climatological jet stream, accelerating the background westerly flow and leading to a

latitudinally inert intensification of the stormtrack. As the NPO/WP develops, the zonal

wind anomaly shifts poleward, and, due to the close relationship between the jet stream

and stormtrack, the stormtrack follows accordingly. A poleward shift in the stormtrack

causes a dipole in eddy activity as synoptic transients traverse a northward path.

     The findings in earlier studies, coupled with the insight gleaned from our analysis,

suggest that the NPO/WP is an internal mode of variability, driven primarily by

variations in stormtrack activity.

3.3 – Implications for winter weather, SST and sea ice

3.3.1 – Precipitation

Regressions of the EEOF PC2 on weekly precipitation field, created from the daily US-Mexico station precipitation, are used to quantify the impact of the NPO/WP on subseasonal precipitation (figure 3.9). Two weeks prior to the mature phase, both the eastern third of the United States and the Pacific Northwest experience a decline in precipitation, on the order of 0.3 to 0.4 mm/day. The decrease in Pacific Northwest precipitation is likely tied to a disruption of the Sverdrup balance; the reason behind the precipitation decline in the eastern United States is not immediately evident. One possible explanation is the presence of an anticyclonic circulation situated over Canada; anomalous easterly flow opposes the westerly flow impinging on the Rocky Mountains, stunting lee cyclogenesis. Another possible explanation is the weakening of the Atlantic jet (cf. figure 3.7). The southeastern United States is a source region for lows which eventually evolve into powerful winter nor'easters, however, in the presence of a weaker jet, the necessary upper air dynamics for baroclinic cyclogenesis disappears.

One week prior to the mature phase, the negative precipitation anomalies in the eastern United States and Pacific Northwest persist, with each anomaly exceeding 0.4 mm/day over much of the two regions. The circulation features at this stage are similar to the week before, explaining the persistence of the anomalies. At this time, the first hint of increased precipitation over the Great Plains region and central United States is present, with a small positive anomaly of 0.1 mm/day extending from the Gulf Coast to the Ozarks.

At a time lag of zero, the precipitation anomalies bear a resemblance to those associated with the mature phase. The anomaly structure is not identical, but broad similarities are present; a large decline associated with a displaced Aleutian Low occurs

over the Pacific Northwest, exceeding 0.8 mm/day in some regions, and enhanced precipitation happens over much of the southern United States, with a large region experiencing a 0.1-0.2 mm/day increase in precipitation. The original negative precipitation perturbation in the eastern United States has disappeared.

One week after the peak phase, positive precipitation anomalies cover the southern United States and Great Plains, with some regions exceeding over 0.4 mm/day, while the Pacific Northwest continues to be dominated by decreased precipitation. A positive precipitation perturbation is also present in southern California, similar to the area affected by a warm ENSO event. Two weeks after the peak phase, the only precipitation anomaly present is a large area of enhanced precipitation, surpassing 0.5 mm/day over the southern Great Plains. Westerly wind anomalies are present over this region one to two weeks after the peak of the NPO/WP, providing the necessary upper level dynamics to promote convergence and rising motion. Precipitation in the Pacific Northwest is no longer affected, likely related to the return of the Aleutian Low to its climatological position.

3.3.2 – Temperature

1000 hPa temperature is used to quantify the impact of NPO/WP variability on temperature on weekly timescales (figure 3.10). Two weeks before the mature phase, a broad area of positive temperature anomalies are spread across Canada and the northern United States; this pattern is similar to the regression pattern obtained from regressing the monthly NPO/WP time series on station based surface air temperature. These anomalies are largely of advective origin, arising from the enhanced southerly flow over much of the continent. One week later, the warm anomalies continue to plunge southward,

extending from Alaska eastward to the eastern seaboard. At lag zero, the warm

anomalies extend equatorward to the Gulf of Mexico and negative temperature anomalies

cover much of the western United States. The development of negative temperature

anomalies coincides with the appearance of a trough (c.f. figure 3.6) centered over the

southwestern United States, similar to the center found in Barnston and Livezey (1987).

During the decay phase, the positive temperature anomalies disappear as the northern

center dissipates, while the negative temperature anomalies broaden as the trough moves

northward.

3.3.3 – Sea surface temperature response

As with the monthly correlations, the magnitude of the weekly SST regressions is

small, but the coherence of the pattern necessitates commenting. Little to no SST

perturbation is present prior to the onset of NPO/WP variability; small anomalies occur in

the midlatitude and equatorial Pacific and in the Indian Ocean as well (figure 3.11). The

lack of any precursor signal furthers the belief that the NPO/WP is not a midlatitude

response to tropical SST forcing. One week prior to the mature phase, a slight hint of a

warming around 30ºN occurs, where anomalous easterlies act to oppose climatological

westerlies in that region. At lag zero, the midlatitude Pacific cools and the region of

warming expands. One week after the mature phase, the amplitude of the SST anomaly

around 30ºN increases and cold anomalies begin to appear along the west coast of the

United States. Two weeks after the mature phase, the SST anomalies peak, with a

horseshoe of negative anomalies in the eastern Pacific and a vast region of positive

anomalies extending from the coast of China into the central Pacific Basin.

The coupling is achieved by the exchange of turbulent latent and sensible heat fluxes at the air-sea interface. Around 30ºN, where warm anomalies are present, the NPO/WP circulation opposes the climatological westerly flow. This decline in atmospheric circulation reduces the exchange of turbulent heat, via a reduction in processes such as evaporation. Conversely, both south and north of 30ºN, the circulation acts to enhance the ambient flow. In the midlatitudes, anomalous westerly flow imposed upon climatological westerlies exacerbates the transfer of turbulent heat from the oceanic mixed layer to the lower atmosphere, lowering the SST. Likewise, anomalous northeasterlies in the trade winds region also cool the ocean surface through similar processes. The closed horseshoe along the coast is a combination of two processes; increased upward heat flux due to colder, northerly winds, and upwelling related to Ekman motion off the coast.

Deser and Timlin (1997) demonstrated that weekly atmosphere-ocean coupling is strongest when the atmosphere leads the ocean by 2 weeks. Our results corroborate theirs, as the maximum SST anomalies are observed two weeks following the maximum circulation anomalies. The SST anomalies at a lag of +2 weeks are plotted with the wind regressions at lag zero in figure 3.12. Clearly, the SST pattern is in response to the strong atmospheric circulation observed two weeks prior.

3.3.4 – Sea Ice Response

The NPO/WP greatly impacts the MIZ in the Bering Sea and Sea of Okhotsk, as demonstrated in the monthly analysis. Since Arctic sea ice is such a delicate component of the climate system, understanding the variability of the MIZ on all timescales is paramount. Although much of the sea ice variability is on interannual to decadal

timescales, there is a subseasonal component to sea ice variability. The variability present on this timescale is forced strictly by the atmosphere, mainly by means of circulation changes which induce dynamic ice motion. Fang and Wallace (1994) first demonstrated the ability of the ice to respond to such high frequency forcing, linking a dipole in sea ice between the Bering Sea and Sea of Okhotsk to a geopotential height pattern similar to the NPO. Increased (decreased) sea ice concentration in the Sea of Okhotsk (Bering Sea) is preceded by north to northwesterly (southerly) winds and negative (positive) 1000-500 hPa thickness anomalies by one week. A similar relationship is present in the Atlantic, with the NAO forcing a decline (increase) in sea ice concentration in the Barents-Greenland Seas (Labrador Sea).

We find a similar structure to the dipole described in Fang and Wallace when lag-lead regressions of PC2 on weekly sea ice are calculated. During the evolutionary phase of the NPO/WP the Aleutian Low is situated to the northeast of its climatological position, resulting in northerly flow over the western Bering Sea. Figure 3.13 shows that two weeks prior to the peak of the NPO/WP, the MIZ is extended southeastward in the Bering Sea while negative sea ice concentration anomalies are present in the Sea of Okhotsk. One week later, the MIZ in the Bering Sea retreats slightly to the northwest; nearly no ice concentration anomalies are present in the Sea of Okhotsk. At lag zero, the MIZ in the Sea of Okhotsk is extended eastward, while the MIZ in the Bering Sea is continues its retreat, with a small decline in sea ice concentration north of the Aleutians. One week after the peak phase, the MIZ remains extended in the Sea of Okhotsk and western Bering Sea, but continues to retreat in the eastern Bering Sea. The pattern two

weeks later is similar; an increase in sea ice concentration in the Sea of Okhotsk and western Bering Sea and a decrease in sea ice concentration in the eastern Bering Sea.

Plotted in the bottom panel of the right column is the difference in sea ice anomalies between +2 weeks and -2 weeks. The difference plot reveals a dipole in sea ice anomalies, with a net decline in Bering Sea sea ice concentration and a net increase in sea ice in the Sea of Okhotsk. This dipole is in stark contrast to the dipole described in Rogers (1981), who finds an increase (decrease) in Bering Sea (Sea of Okhotsk) sea ice concentration. The minor differences in our definition of the NPO explain the discrepancies in the sea ice footprint, and this is clarified by the lag-lead regressions. Our definition is purely statistically based; the mature phase NPO/WP is defined as the peak of the SLP dipole. Rogers defines the NPO as an oscillation in surface temperatures between the Aleutians and Edmonton, Canada; these temperature anomalies are likely largest when the Aleutian Low is at its strongest and most eastward location. This occurs not during the peak dipole phase of the NPO/WP, but instead, two weeks before. The sea ice footprint at this time is, in fact, a dipole between the Bering Sea and Sea of Okhotsk, with more (less) sea ice in the Bering Sea (Sea of Okhotsk).

3.4 – Connections to the PNA

The analysis dictates that at lag zero the PNA and NPO/WP are uncorrelated; however, the possibility of linkages at lags and leads is present. The PNA is the first EEOF of weekly winter SLP, and the regressions of EEOF PC1 on the SLP field are plotted in figure 3.14. Compared to the NPO/WP, the PNA is a more slowly varying phenomenon, with a monopole SLP anomaly persisting over the North Pacific for the five week period. An opposite-signed, dual-centered SLP anomaly is present over the Arctic

Circle as well. Initially, the zonal expanse of the SLP anomaly in the North Pacific is large, covering 120º of longitude. As time moves forward, the SLP center becomes more symmetric, broadening its latitudinal extend and shrinking zonally. Two weeks after the peak phase of the PNA, the SLP anomaly in the North Pacific is situated just south of the Aleutian Islands and extending southeast along the Canadian Rocky Mountains. Visually, this structure is very similar to the antecedent phase of the NPO/WP.

Calculating the lagged correlation between the time series reveals that this is likely more coincidental than an indication that PNA variability excites NPO/WP variability (or vice versa). The correlation between the two PCs never exceeds ~0.3, below the level of statistical significance.

3.5 – NAO and NPO/WP: Interbasin linkages?

The concept of an "atmospheric bridge" has been put forth in multiple studies; the atmospheric bridge is the linkage between tropical SST anomalies related to either ENSO or tropical Atlantic variability to midlatitude SST anomalies in the both ocean basins (Lau and Nath 1996; Lau 1997; Alexander et al. 2002). The midlatitude SST anomalies are forced by anomalous atmospheric circulation associated with the initial tropical SST perturbation; the tropical and midlatitude SST anomalies are then correlated, but not contemporaneously. The atmosphere is not the only component of the Earth system which can behave as a bridge. The Eurasian continent communicates spring sea ice extent anomalies to the summer monsoon circulation via changes in early summer soil moisture content (Zhao et al. 2004).

The NPO/WP and NAO are contemporaneously uncorrelated; the correlation between the monthly PCs is 0.22. However, antecedent and subsequent correlations are

calculated to determine connections between the NPO/WP and NAO and ascertain drivers of interbasin connectivity

The NAO SLP anomalies (figure 3.16) evolve in a similar manner; initially, there is a strong northern center with a moderate SLP perturbation to the south. A weak tertiary center is also present in the opposite basin, here; it is centered over the Bering Sea. One week later, both centers have deepened, and the northern center is shifted eastward, closer to the coast of Greenland. At lag zero, the classic NAO pattern is observed; low pressure centered in between Iceland and Greenland, a broad area of high pressure stretching across the midlatitude Atlantic Basin and an additional faint center in the North Pacific. One week after the peak phase, the northern center weakens, only slightly, while the southern node strengthens and moves poleward. Two weeks after the peak phase, the northern node is considerably weakened, and much of the Atlantic Basin is dominated by positive pressure anomalies. The tertiary center in the North Pacific disappears.

While an analogous evolution of the NAO SLP anomalies (strong polar low to dipole to strong subtropical and midlatitude high) occurs, there are significant differences as well. First, the NAO is never monopolar; a meridional dipole is present over the five week period. Second, the centers are relatively stationary over the five week period, especially compared to the NPO/WP centers. Autocorrelation of the NAO PC is calculated (figure 3.17); although the NAO is primarily a subseasonal phenomenon, it is obviously more persistent. The autocorrelation falls to 0.5 at a lead/lag of 3 weeks, and falls just below $1/e$ at a lag/lead of 4 weeks. Conversely, the NPO/WP is not persistent, lasting only a few weeks. Furthermore, the correlation between the two PCs never

exceeds 0.1, which is a smaller correlation than that between the monthly PCs (figure 3.18). The longevity (5-6 weeks) of an NAO episode suggests that additional outside forcings, as well as internal atmospheric variability, can produce NAO episodes. Previous studies have suggested that Atlantic SST variability (Cassou et al. 2004a, Cassou et al. 2004b), Pacific SST variability (Nigam, personal communication) and Arctic sea ice anomalies (Francis, personal communication) can all force NAO-like variability in the Atlantic. No comparable relationship between the NPO/WP and these slowly varying constituents of the climate system is found in this study. While the possibility that similar internal dynamics excite both an NAO episode and NPO/WP episode, the evidence presented here suggests that neither is a forcing of the other and that the NAO is the atmospheric response to a variety of forcings.

Chapter 3 Figures
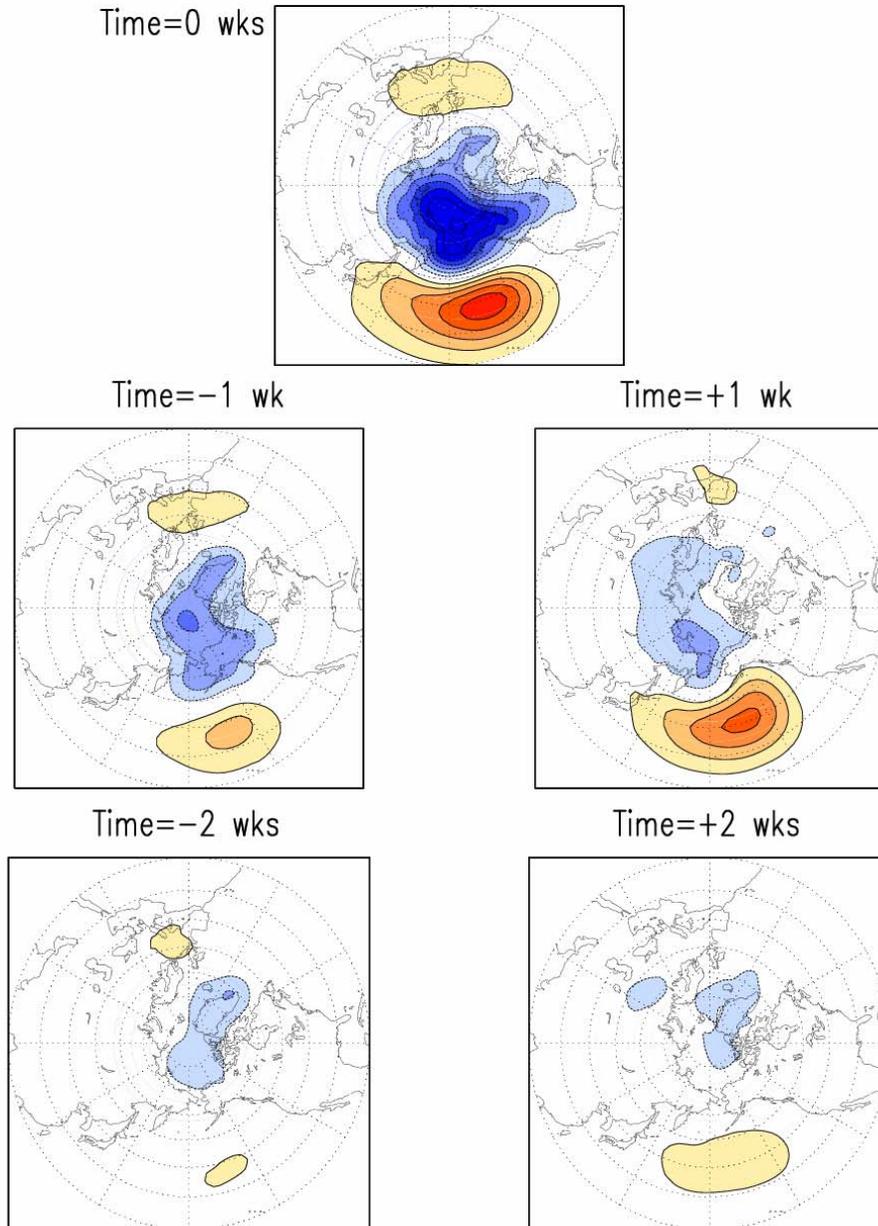
Figure 3.1: Lagged regressions from -2 weeks to +2 weeks of the weekly PC2 from EOF analysis on weekly winter SLP between 1958 and 2001 from the ERA-40 Reanalysis. Winter is defined as the 18 weeks starting on the Wednesday closest to December 1st. SLP shading/contouring follows SLP shading/contouring of figure 2.2.
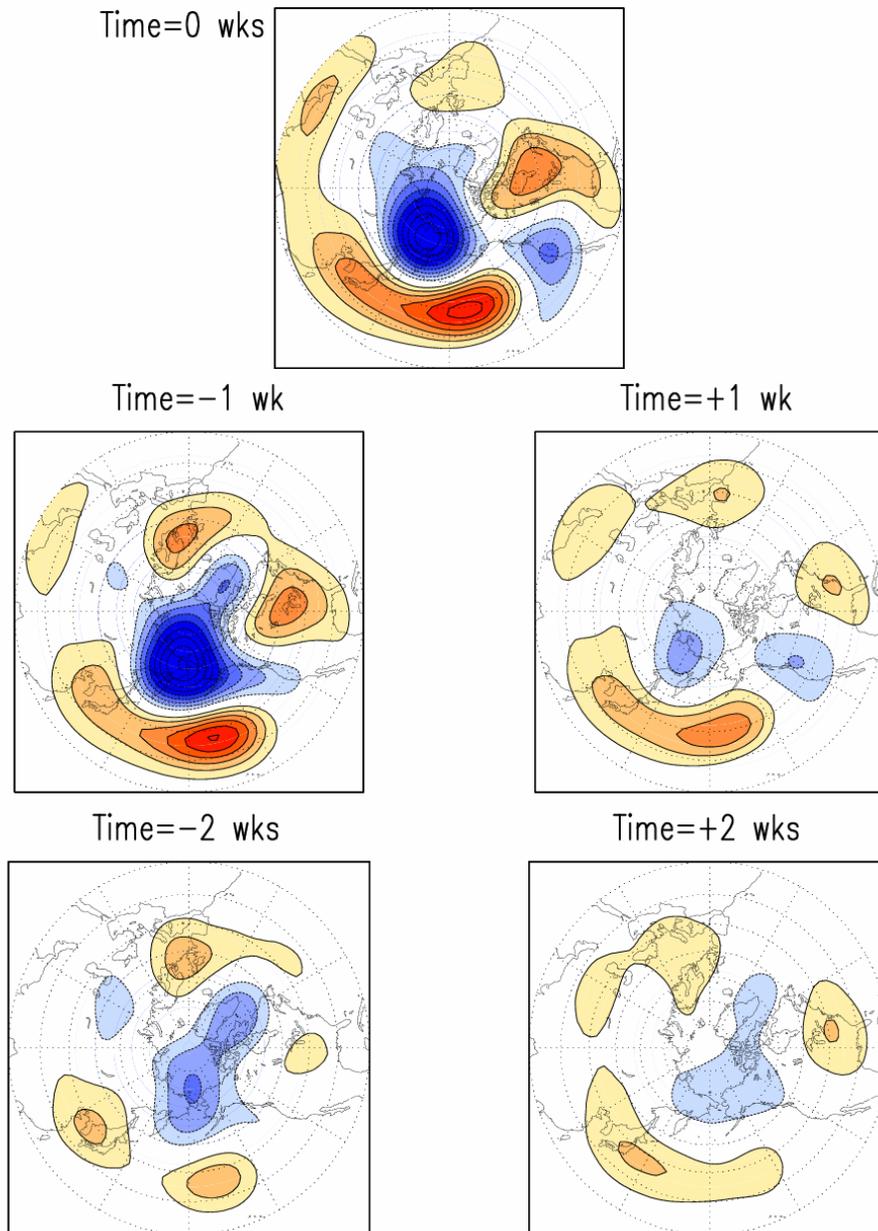
Figure 3.2: Lagged regressions from -2 weeks to +2 weeks of the weekly PC2 from EOF analysis on weekly winter 200 hPa geopotential height between 1958 and 2001 from the ERA-40 Reanalysis. Winter is defined as the 18 weeks starting on the Wednesday closest to December 1st. Figure shading/contouring follows height shading/contouring of figure 2.4.
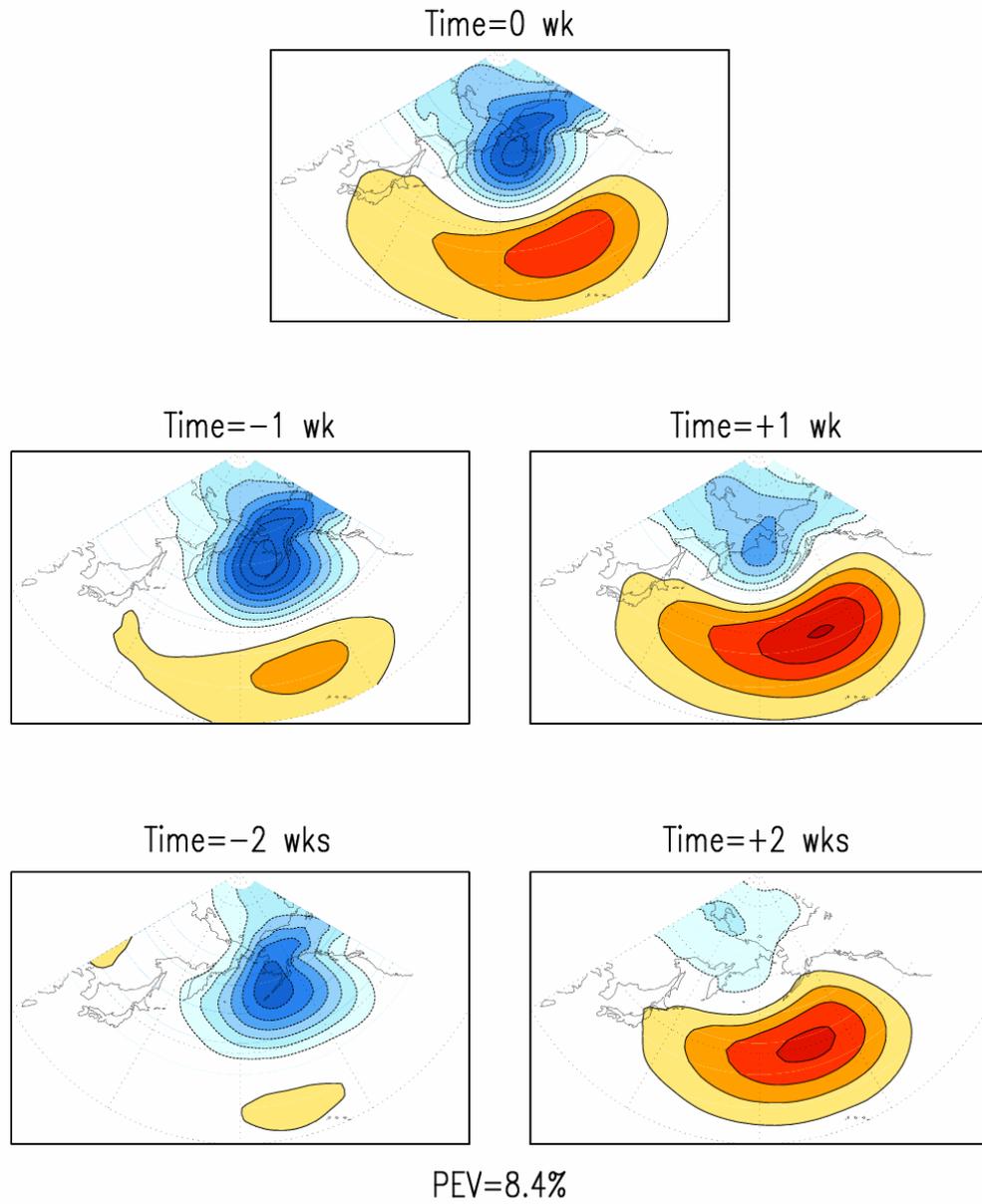
Figure 3.3: The second extended empirical orthogonal function of weekly DJFM 1958-2001 SLP anomalies from the ERA-40 reanalysis. Time lag is specified to be +/- 2 weeks and the percentage of explained variance is 8.4%. Shading/contouring follows SLP shading/contouring in figure 2.2.
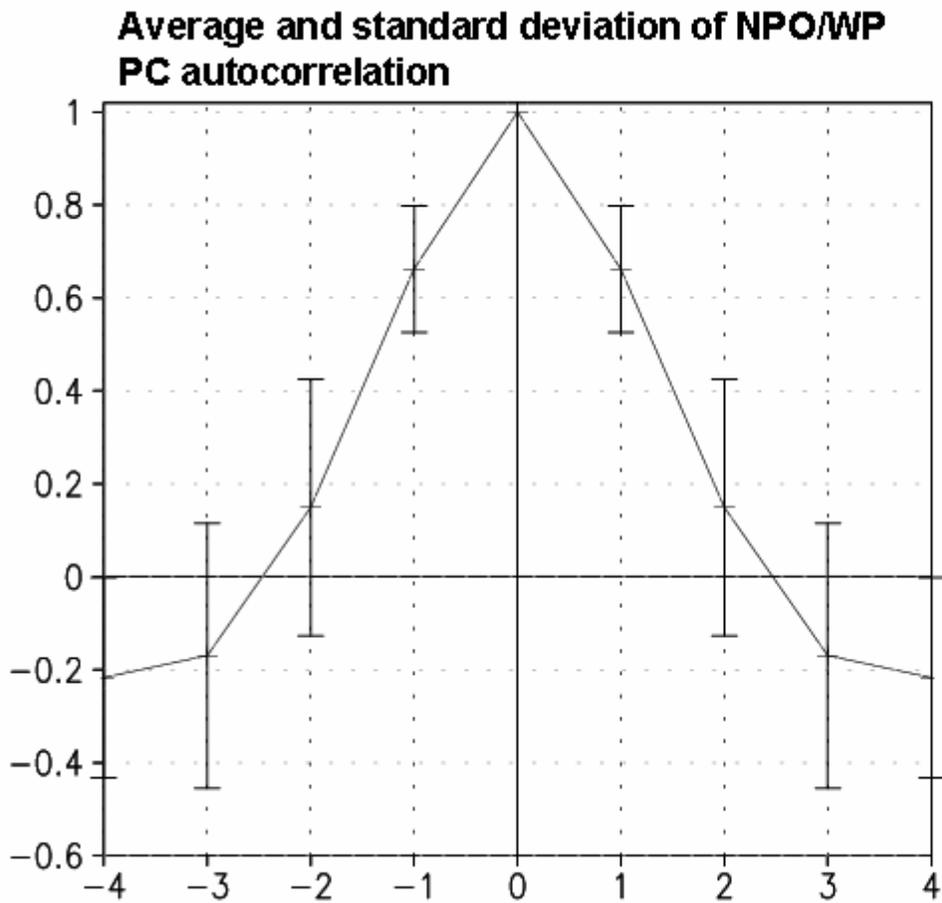
Figure 3.4: Autocorrelation of EEOF PC2, the PC which is associated with NPO/WP variability. The curve displays the average autocorrelation of the PC for 1958-2001 winters and the bars indicate the standard deviation over the 44-year analysis period. The duration of an NPO/WP episode based on the autocorrelation is approximately 2-3 weeks.

Evolution of the NPO/WP SLP Anomalies

Time=0 wks

Time=−1 wk

Time=+1 wk

Time=−2 wks

Time=+2 wks
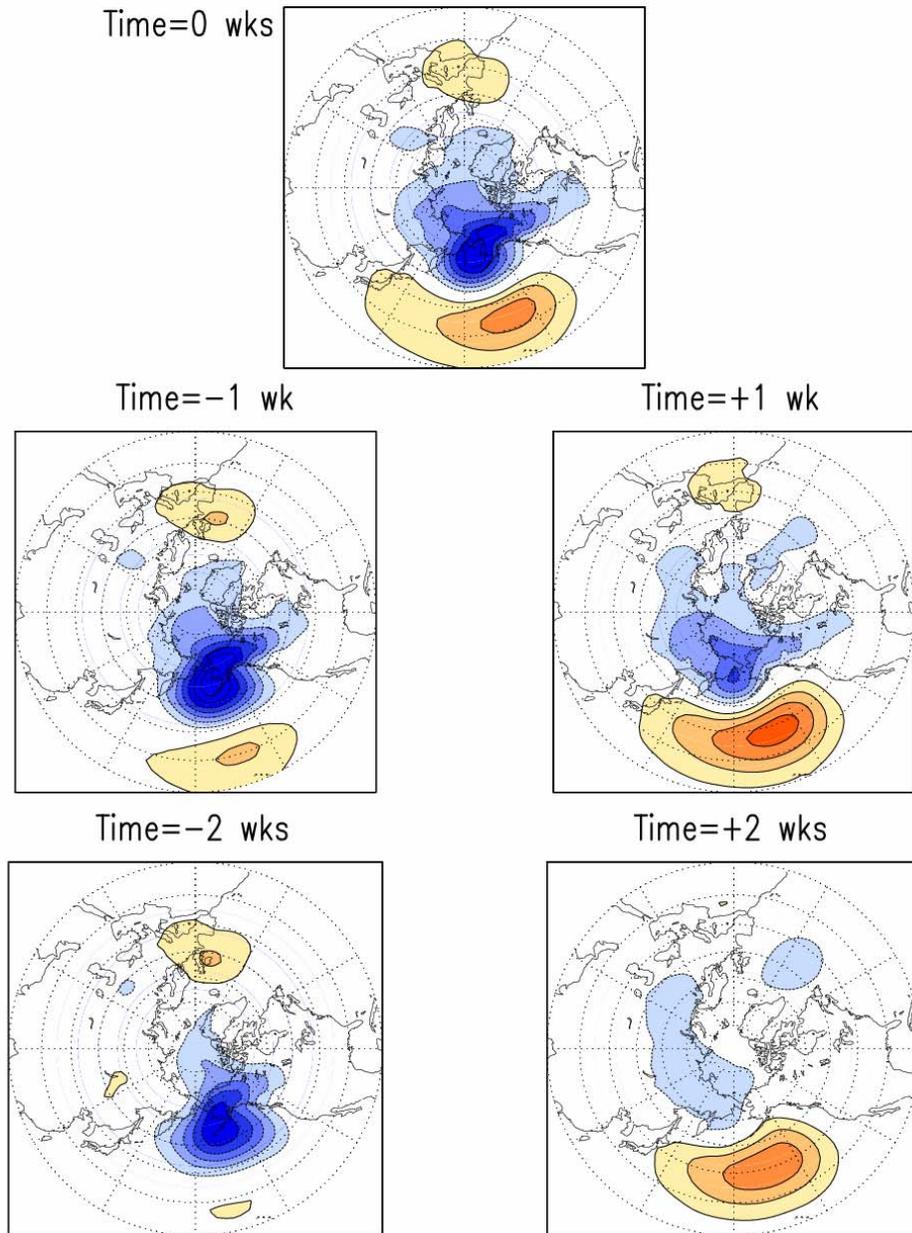
Figure 3.5: Lag-lead regressions of EEOF PC2 on weekly DJFM SLP for winters 1958-2001. SLP contouring shading follows figure 3.2.

Figure 3.6: Lag-lead regressions of EEOF PC2 on weekly DJFM 300 hPa geopotential height for winters 1958-2001. Geopotential height contouring/shading follows figure 3.3.

Evolution of the NPO/WP 300 hPa Zonal Wind Anomalies

Time=0 wks

Time=−1 wk

Time=+1 wk

Time=−2 wks

Time=+2 wks
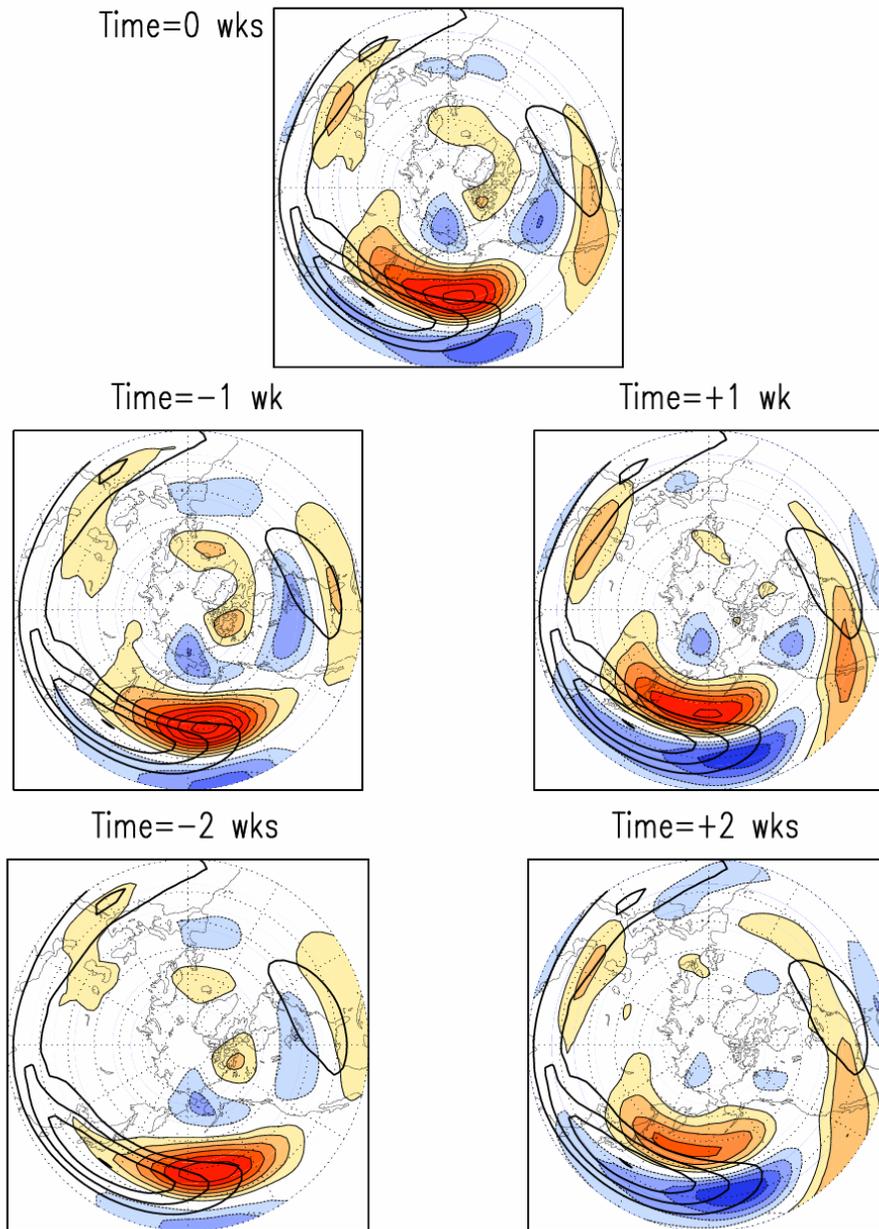
Figure 3.7: Lag-lead regressions of EEOF PC2 on weekly DJFM 200 hPa zonal wind and DJFM climatology for winters 1958-2001. Zonal wind contouring/shading follows figure 2.6.
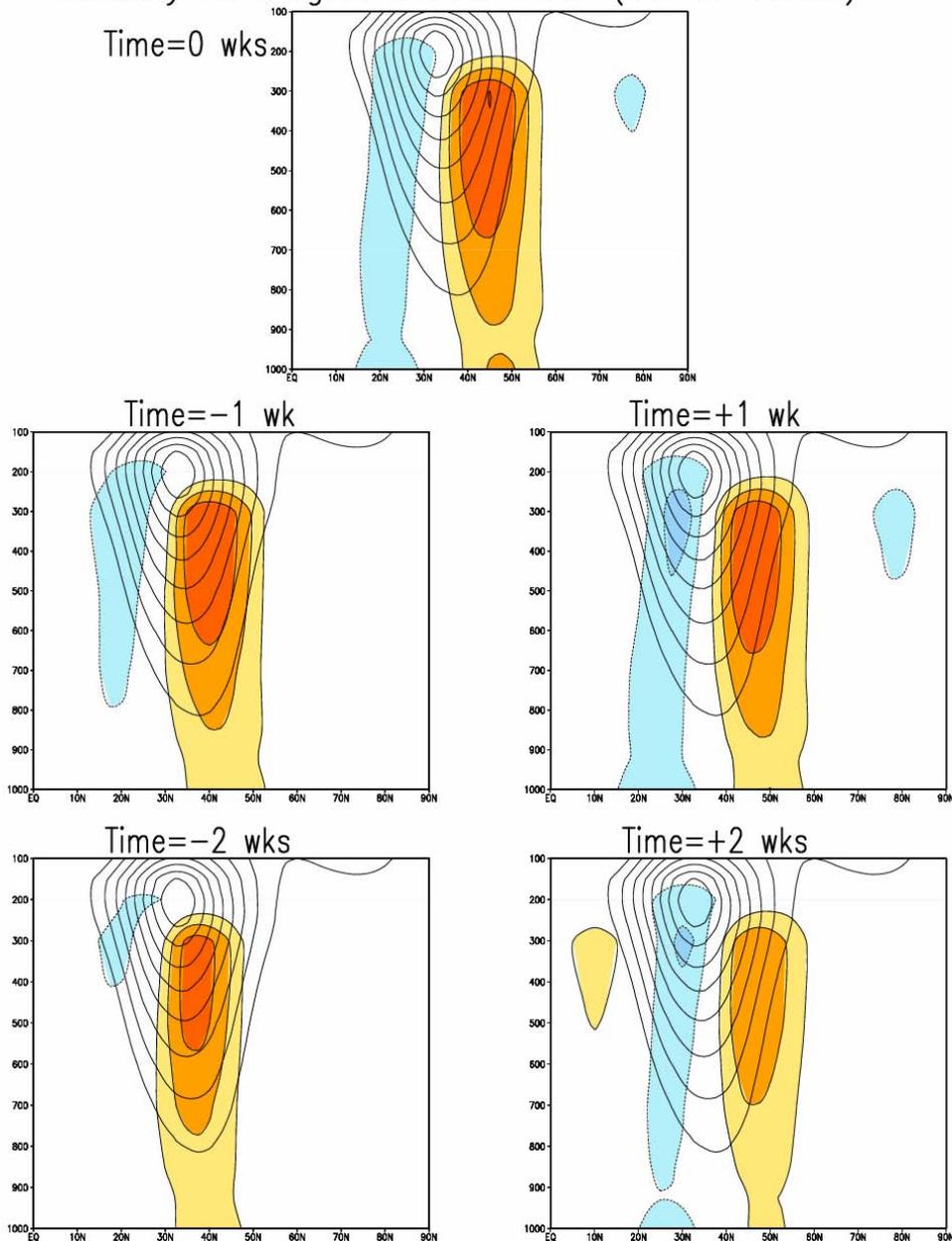
Figure 3.8: Lag-lead regressions of EEOF PC2 on weekly DJFM zonally averaged zonal wind for winters 1958-2001 and DJFM climatology in the Pacific sector (120ºE-120ºW). Regressions are contoured/shaded every 1 m/s and climatology is contoured every 5 m/s beginning at 10 m/s. The zero contour is suppressed.
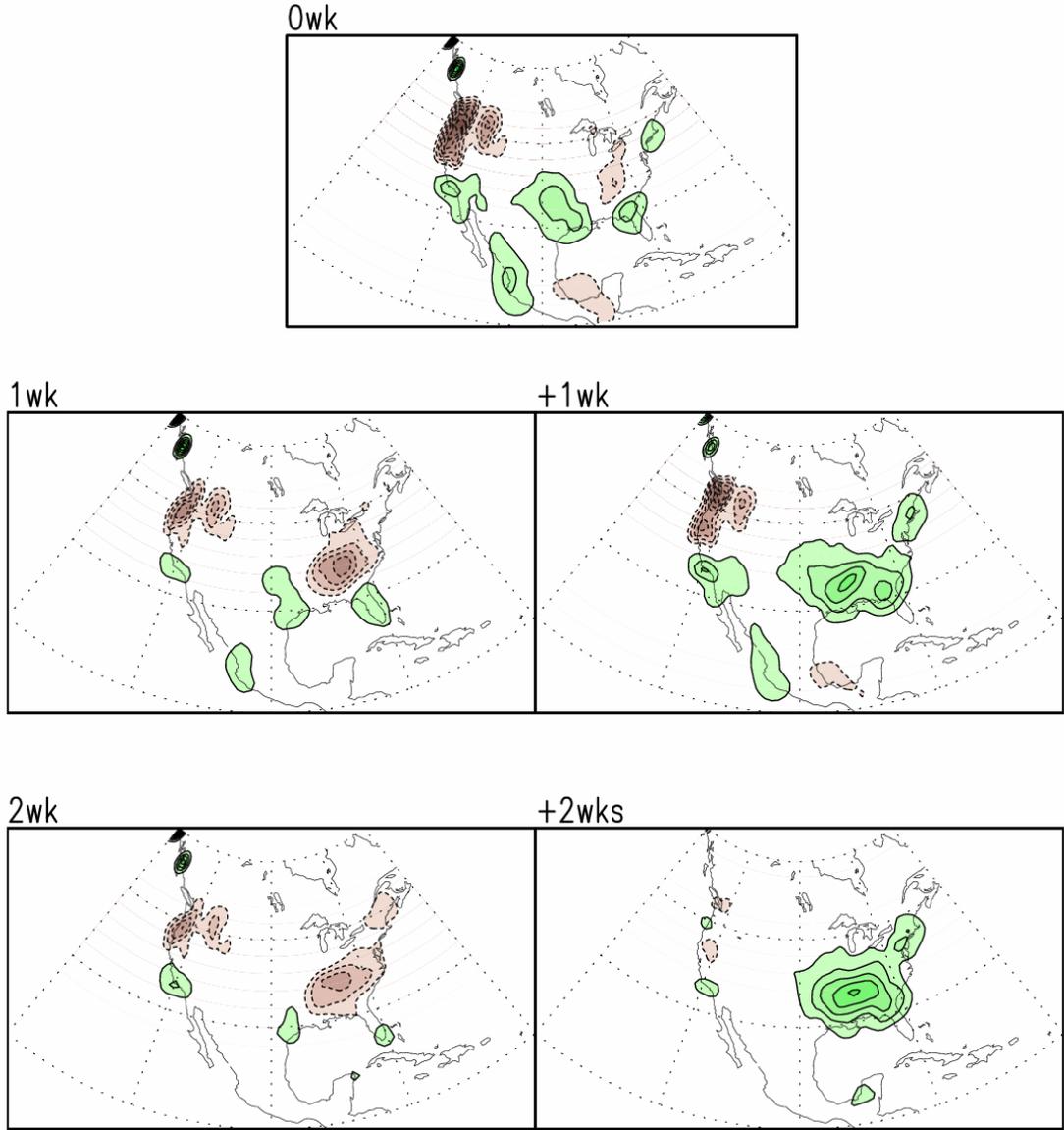
Figure 3.9: Lag-lead regressions of EEOF PC2 on weekly DJFM 1958-2001 precipitation. Weekly precipitation is developed from the daily US-Mexico station based precipitation observations, and winter is defined as the same 18 week period. Contouring/shading is 1 mm/day and the zero contour is suppressed.
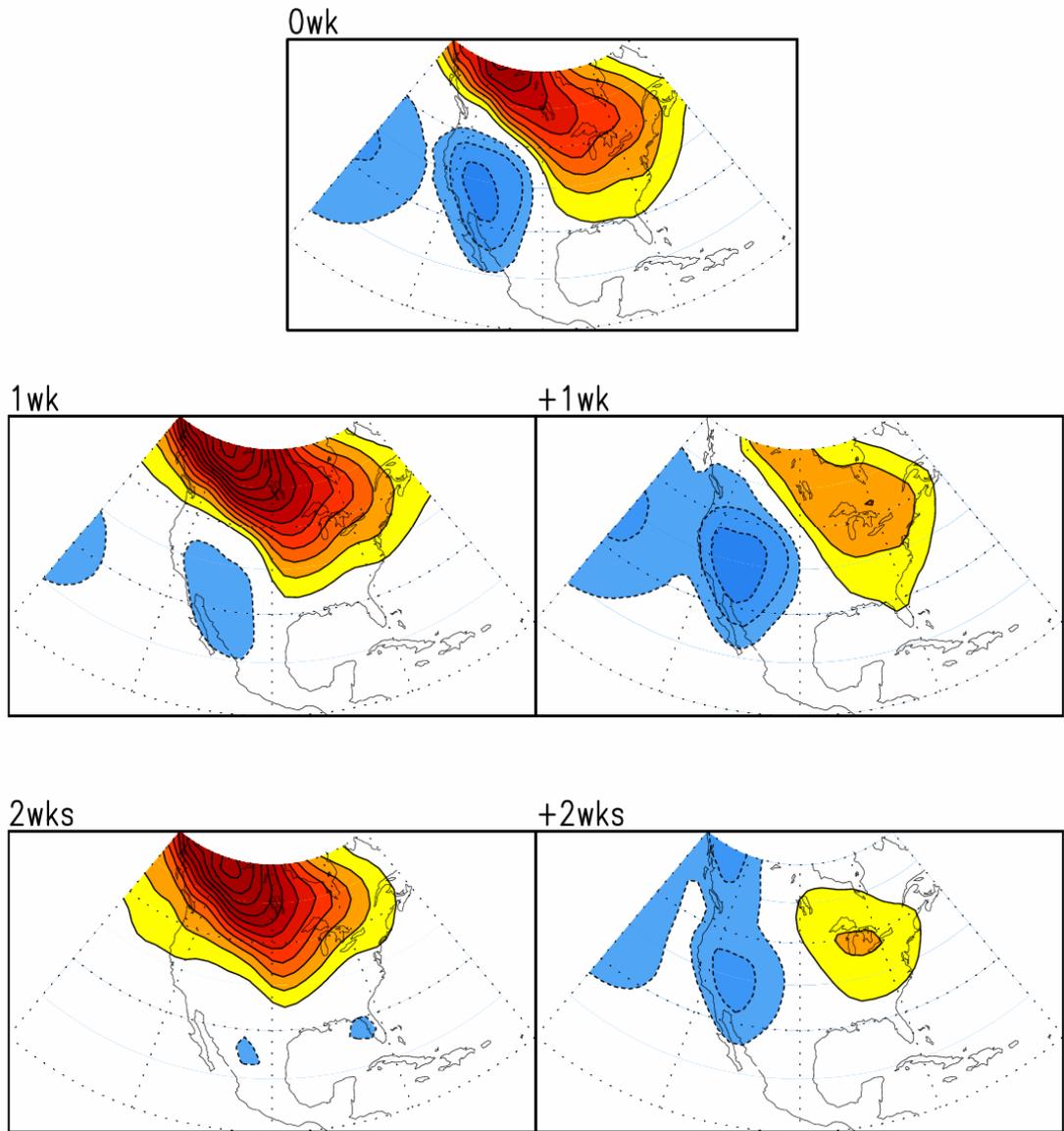
Figure 3.10: Lag-lead regressions of EEOF PC2 on weekly DJFM 1958-2001 1000 hPa temperature from the ERA-40 reanalysis. Contouring/shading is 0.3K and the zero contour is suppressed.
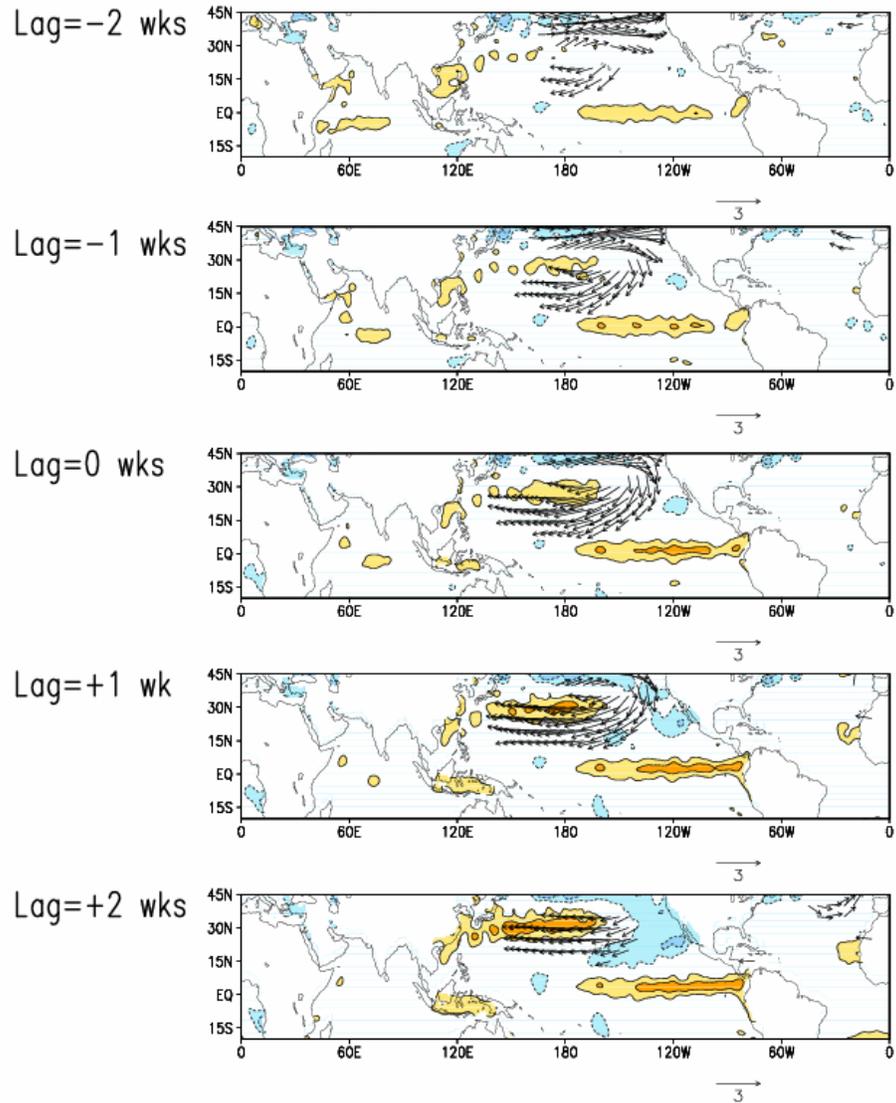
Figure 3.11: Lag-lead regressions of EEOF PC2 on weekly ERA-40 1000 hPa horizontal winds and weekly DJFM 1958-2001 SST from the Reynolds-Smith OI2. SST contouring/shading is 0.1K and the zero contour is suppressed. Wind vectors are suppressed when the anomalous wind is less than 0.5 m/s; reference vector provided below each plot.

114

SST Anomalies (lag=+2) and 1000 hPa wind (lag=0)
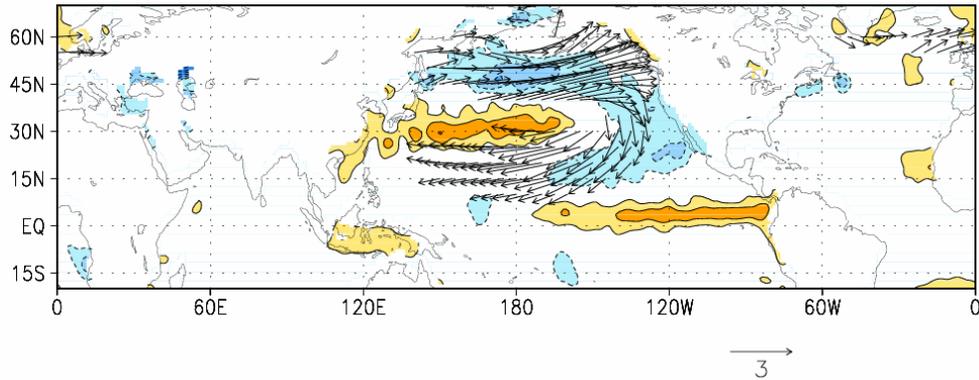
Figure 3.12: Regressions of EEOF PC2 on SST at lag = +2 weeks (shaded/contoured) and 1000 hPa horizontal winds at lag = 0 weeks (vector). SST shading/contouring follows figure 3.9 and vectors exceeding 1.0 m/s are plotted.

Lag–Lead Sea Ice Regressions

Lag 0

Lag +1

Lag −1

Lag +2

Lag −2

t=+2 minus t=−2
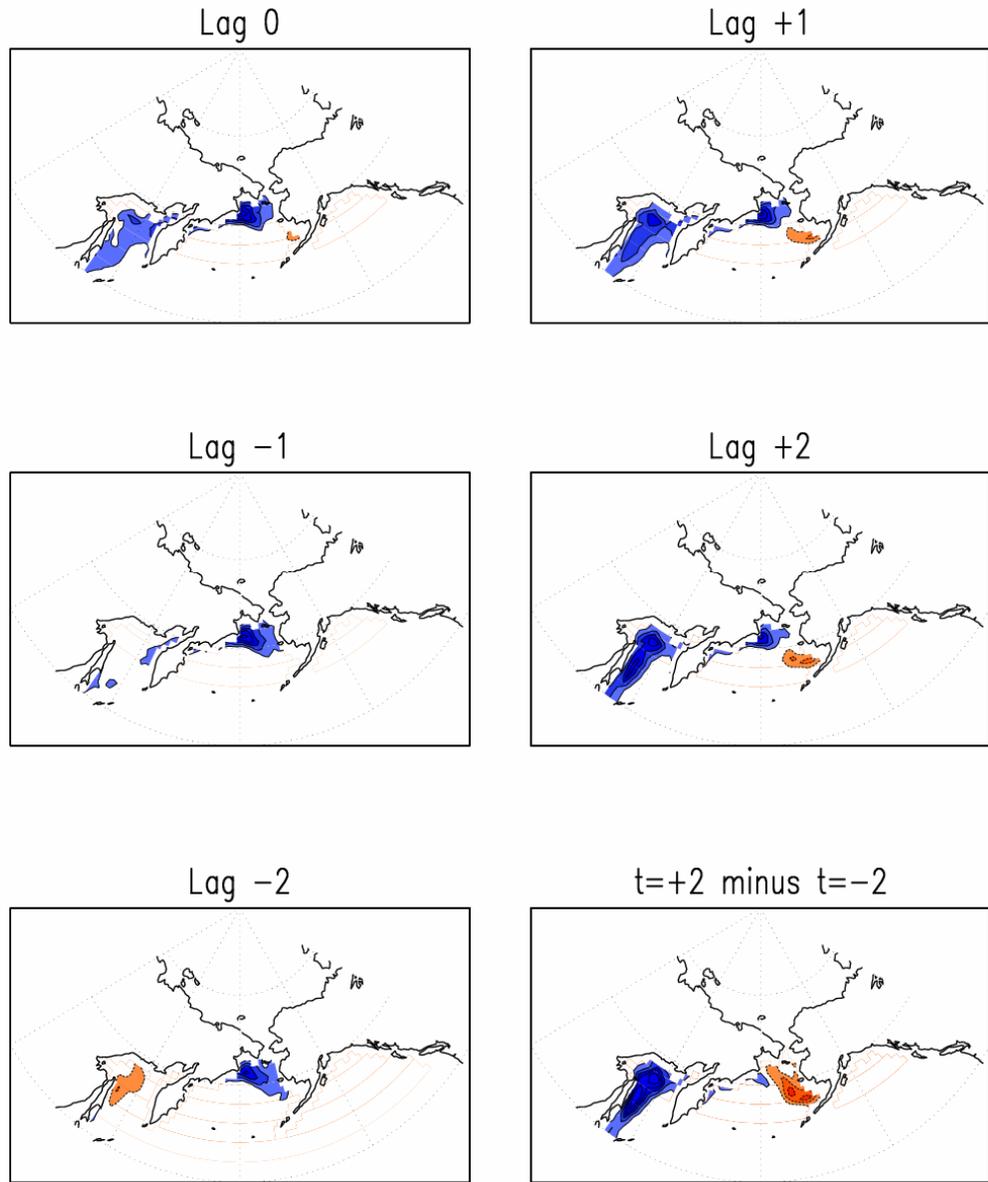
Figure 3.13: Lag-lead regressions of EEOF PC2 on weekly satellite-based sea ice concentration for DJFM 1979-2001 and the difference between lag = +2 weeks and lag = -2 weeks (bottom right panel). Shading/contouring is 2% and the zero contour is suppressed.

Evolution of the PNA SLP Anomalies
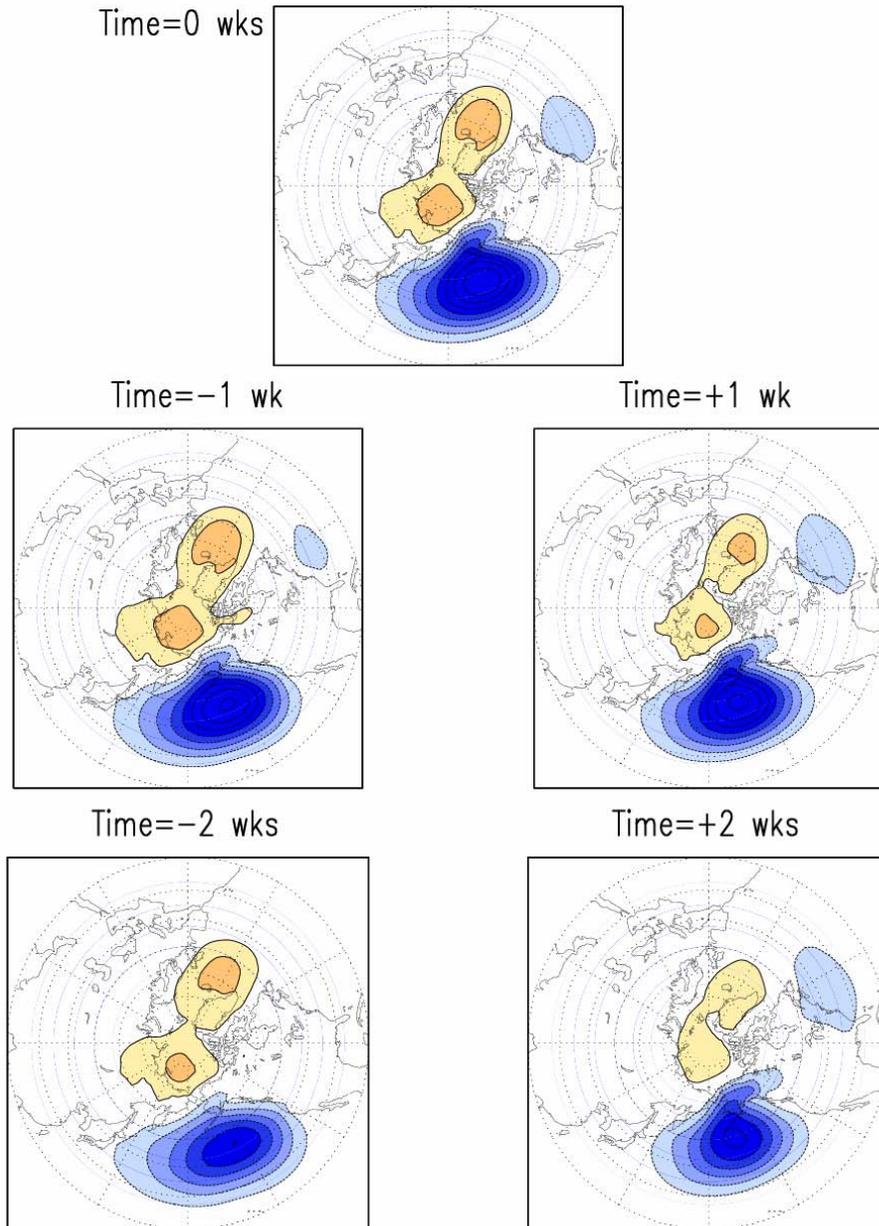
Figure 3.14: Lag-lead regressions of EEOF PC1 on weekly DJFM SLP for winters 1958-2001. SLP contouring shading follows figure 3.2.
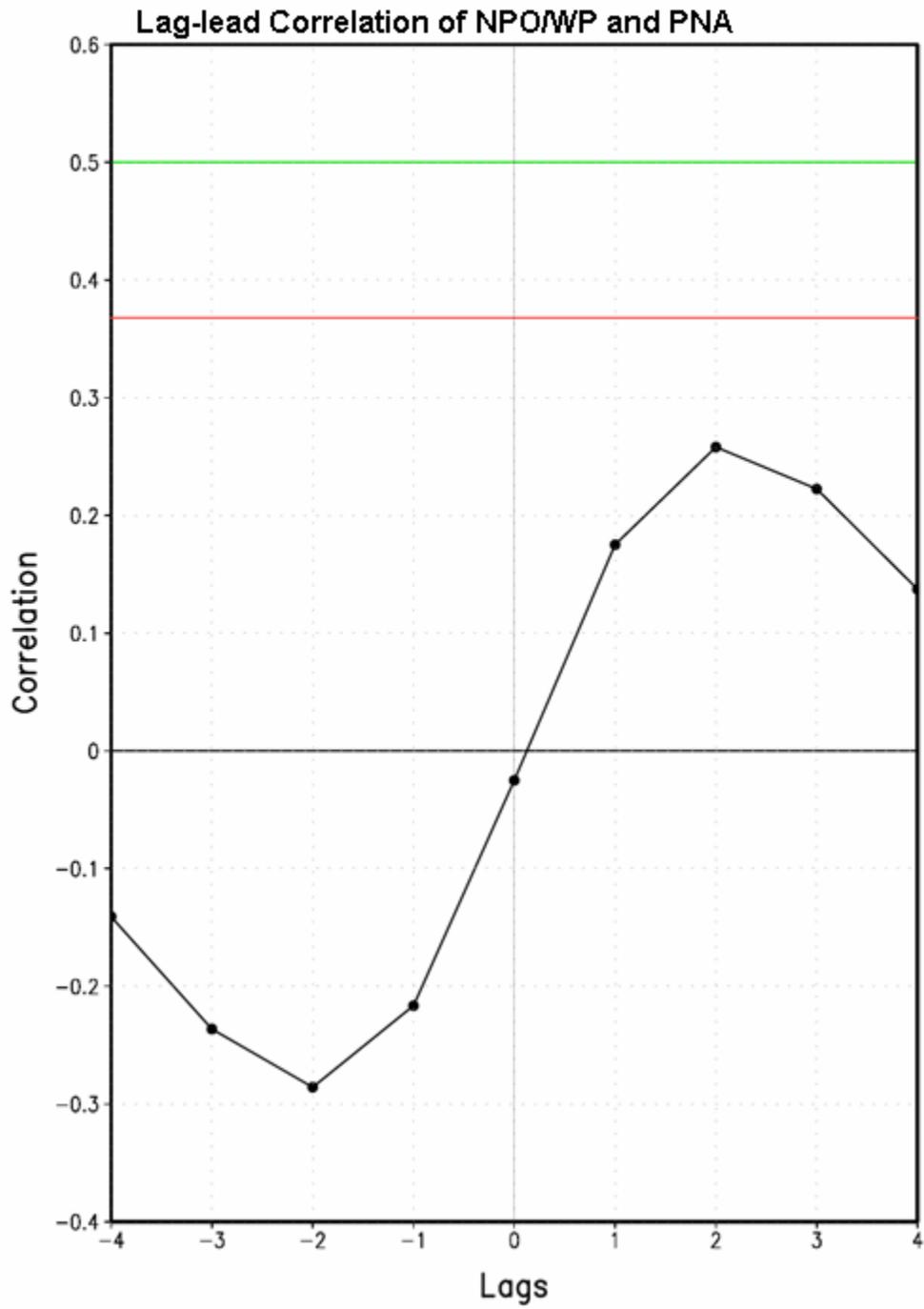
Figure 3.15: Average antecedent, contemporaneous and lagged correlation of Pacific Basin winter SLP EEOF PC1 and PC2 for DJFM 1958-2001. Green marks 0.5 correlation; red marks 1/e.
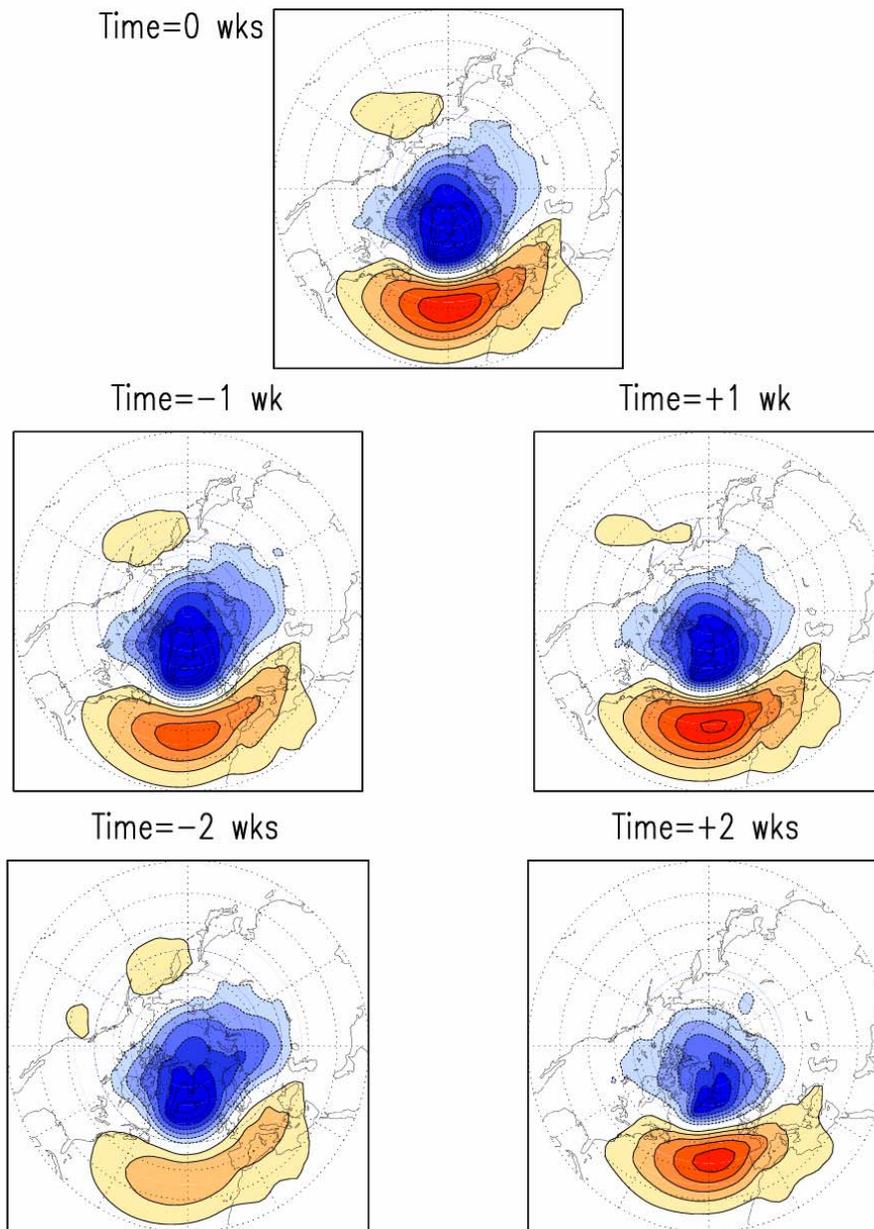
Figure 3.16: Lag-lead regressions of first PC from EEOF analysis of Atlantic Ocean (80ºW-0º) weekly winter SLP on weekly DJFM SLP for winters 1958-2001. SLP contouring shading follows figure 3.2.
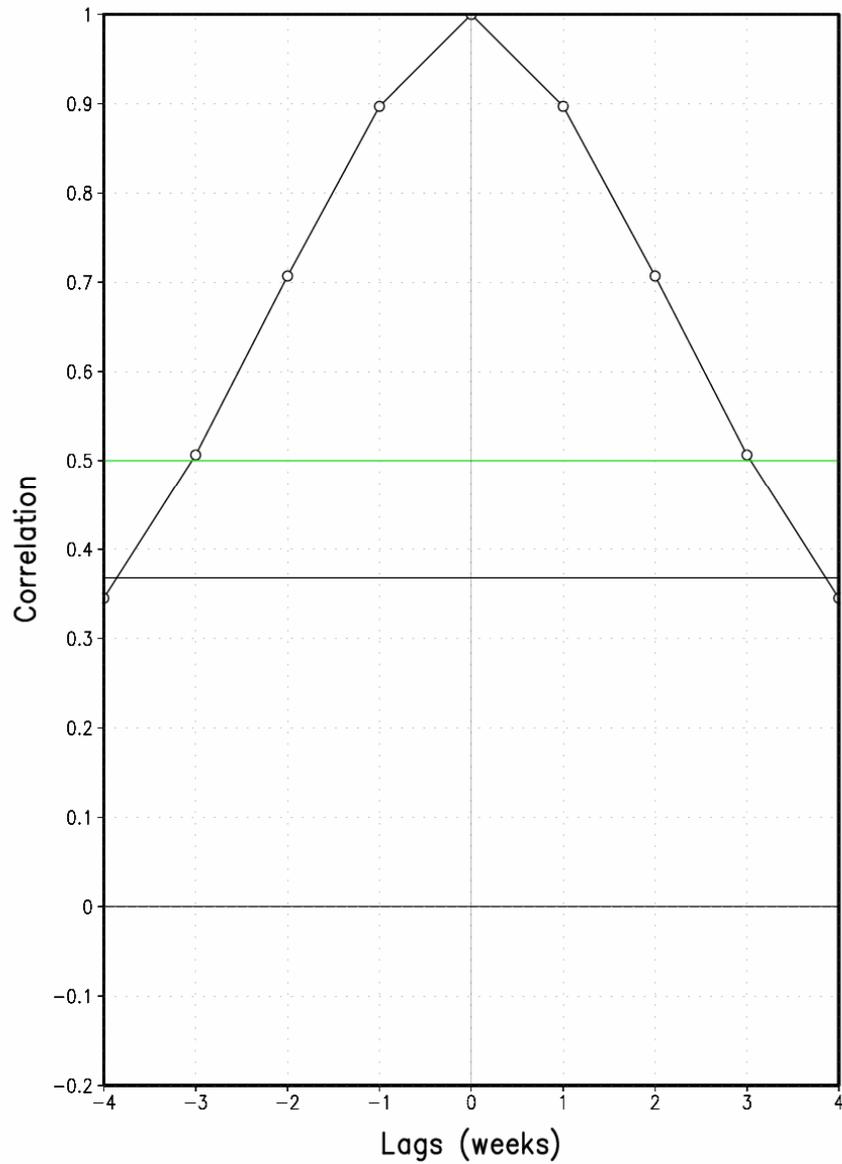
Figure 3.17: Average autocorrelation of Atlantic Basin EEOF PC1, the PC which is associated with NAO variability. The duration of an NAO episode based on the autocorrelation is approximately 5-6 weeks.
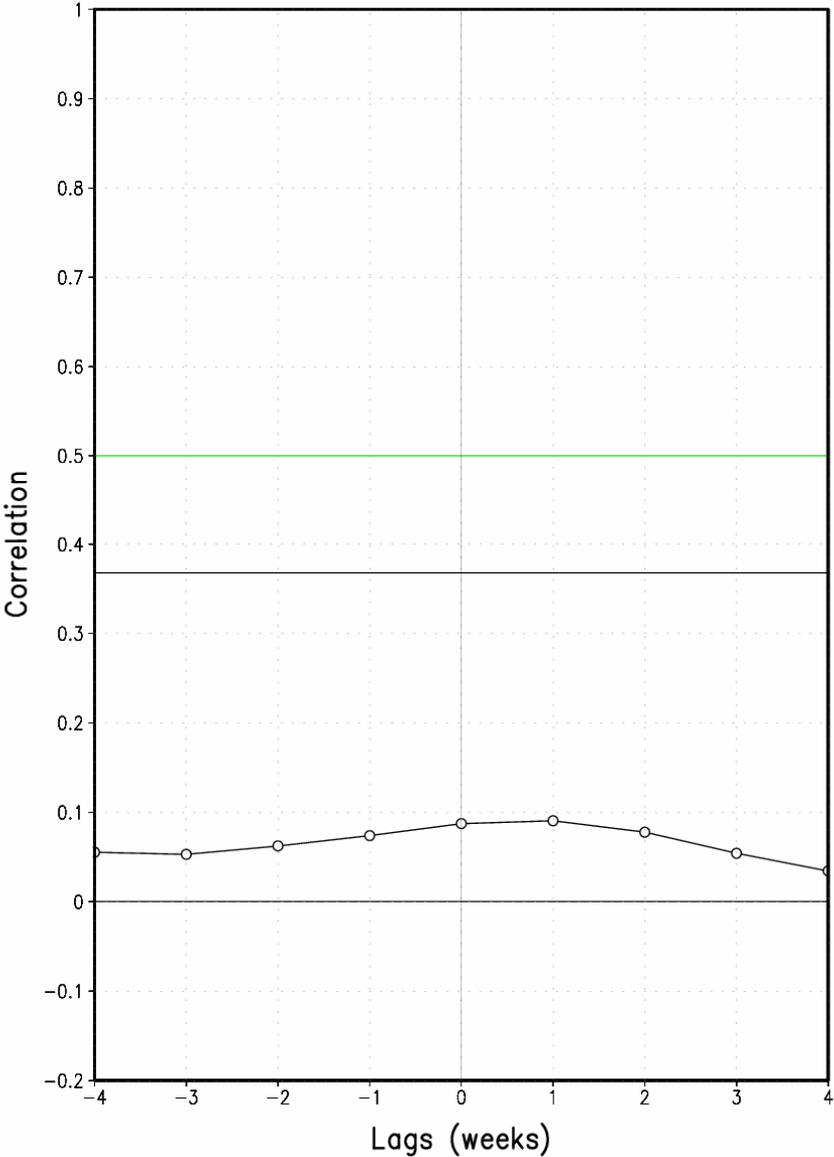
Figure 3.18: Average antecedent, contemporaneous and lagged correlation of Pacific Basin winter SLP EEOF PC2 and Atlantic Basin winter SLP PC1 for DJFM 1958-2001.

Chapter 4: Winter Atmospheric and Oceanic Variability and its Impact on Summertime Arctic Sea Ice Anomalies

Both earlier studies and this thesis work have demonstrated the importance of the lower tropospheric circulation on sea ice distribution in the Arctic. Sea ice responds dynamically to variations in the surface wind; caused both by the climatological seasonal cycle (figure 4.1) of SLP and interannual variability. This chapter parcels the observed summer ice decline into four components; winter teleconnections (NPO/WP, NAO and PNA), Pacific Ocean SST variability, localized summer atmospheric variability and the anthropogenic(?) signal. A case study of the summer melt season of 2007 is performed, and the compounding influence of the aforementioned factors is quantified.

4.1 – Summertime Arctic Sea Ice

4.1.1 – Climatology

The rapidly changing state of the Arctic, especially the summertime sea ice extent is both alarming and curious. Currently, the observed melt rate from summer to summer is accelerating, surpassing the ice melt projected by coupled climate models. The record for minimum September sea ice extent was set three times in the first decade of the 21st century (2002, 2005 and 2007), and the forecast for 2008 is grim: Another record-breaking sea ice minimum, besting the record set in September 2007 (Rigor 2008).

In an effort to understand how, why and where summertime sea ice is declining, a climatological picture of summertime (July-August-September; hereafter JAS) Arctic sea ice is presented. The most reliable records of sea ice concentration are derived from

satellite-based brightness temperatures beginning in 1979, but this relatively short sea ice

record prevents extraction of decadal/interdecadal variability present in the sea ice record.

A robust extraction of long-term sea ice variability would require analysis of an extended

record, dating back to the pre-satellite era. As mentioned earlier, the HadISST1.1 covers

this period, providing continuous coverage of sea ice for the last 50 years.[7] Comparison

of the winter (DJF) climatologies and standard deviations for the 1979-2004 subperiod

demonstrate that the HadISST1.1 accurately captures wintertime sea ice variability. A

similar comparison is performed for the summer months (JAS) and, as with the winter,

the two summertime climatologies are very close, with minor differences occurring along

the eastern coast of Greenland (figure 4.2*c*). No differences in standard deviation

between the two datasets occur. While both datasets use similar inputs of satellite data,

the HadISST1.1 is developed independently of the NASA satellite products. The ability

of the Hadley Centre to correctly compute sea ice concentrations independent of NASA

algorithms leads to the deduction that the methodologies for computation of sea ice

beyond 1979 sufficiently and realistically capture actual sea ice conditions. Furthermore,

Stroeve et al. (2008) pioneered use of this newly released reanalysis, relying on the

extended HadISST1.1 to place the 2007 melt season in context of September ice melts

since 1953.

JAS 1958-2007 climatology and standard deviation are plotted in figures 4.2*a* and

4.2*b* respectively. Much of the Arctic Ocean is covered with sea ice, although the area

that is completely covered is small, confined north of 70ºN. The north coasts of Siberia

and Alaska are partially ice covered all year, as is the Canadian Archipelago. The MIZ,

---

[7] Summers after 1957 are included in the analysis to restrict the data to the post IGY period. Non-uniform observing standards and geopolitical tensions preclude the use of data before this period.

diagnosed by the southern and northern bounds of the 10% standard deviation contour, is large in the summer, especially along the Siberian/Alaskan coast.

Figure 4.3 is a time series of normalized September sea ice extent during 1958-2007. The anomalies are calculated by removing the 1979-2000 September climatology and are normalized by dividing the anomalies by the September standard deviation. Sea ice extent is the most common metric for monitoring fluctuations in the Arctic sea ice pack since the quantity expresses the changes in the entire Arctic ice cap. A steep decline in September sea ice extent is evident, beginning in the early 1970s, and it is clear that in recent years, the decline has accelerated, with the summer of 2007 *five* standard deviations below average.

4.1.2 – Linear trend in September Arctic Sea Ice

As mentioned in the first chapter, the decline in summertime sea ice extent is not longitudinally uniform. Certain regions display little to no trend, while other regions display a marked trend. Figure 4.4 shows the trend for September 1958-2007 (panel *a*) and September 1979-2007 (panel *b*). During the longer 50 year period, sea ice is declining around the outer periphery of the Arctic, namely in the Barents Sea, Greenland Sea, Kara Sea, Laptev Sea, Eastern Siberian Sea and Chukchi Sea. Almost no decline is observed in the Beaufort Sea and Labrador Sea. The largest decline of 15% per decade occurs in the Eastern Siberian Sea, an area known to be influenced by the AO.

The situation during the satellite area (1979-present) is somewhat different. There is almost no trend in eastern Arctic[8] sea ice, and the trend in the western region is

---

[8] In the literature, "eastern" Arctic is taken as the sector beginning at the 90ºW meridian extending to the 90ºE meridian; conversely, "western" Arctic refers to the region beginning at the 90ºE meridian extending to the 90ºW meridian.

amplified and focused in the Eastern Siberian Sea, Beaufort Sea and Chukchi Sea. Sea

ice decline in this region is on the order of 30% per decade, a two fold increase from the

longer period. The area of sea ice decline is larger, extending into the central Arctic

basin. Panel *c* plots the average position of the 15% concentration line in September

1958 (blue) and September 2007 (red). Evidently, Arctic sea ice has undergone a lot of

changes in the last 50 years, and attribution of the observed changes to natural variability

and anthropogenic climate change is imperative if we are to improve our understanding

of the current state of Arctic climate.

4.3.1 – Detrending summer sea ice concentration

The goal of this chapter is to connect natural fluctuations in the winter climate to

the distribution of Arctic sea ice during the subsequent summer season and attribute a

fraction of the trend in the short satellite record to low frequency variations in the climate

and the persistent NAO conditions of the latter 20th century. To obtain the true linkages

between winter climate variability and summer sea ice concentration, both the PCs from

the analyses of SST and SLP (markers of climate variability) and sea ice concentration

must be detrended to prevent false footprints due to a trend in one or both of the records.

The secular trend in SST, discussed later in this chapter, is isolated in context of

natural variability; removal of the SST trend mode from the sea ice record detrends the

sea ice record. The following bullet points discuss the approach to removing the SST

trend from the sea ice record.

- Seasonal December-January-February SST trend mode PC regressed on

  seasonal July-August-September sea ice concentration to ascertain SST trend

  mode sea ice footprint.

- 50 year record of SST trend mode (TM) related anomalies developed.

  o $SICa_{TM}(t) = SICr_{TM} \times PC_{TM}(t)$ where $t = 1, 50$

- SST trend mode related anomalies are removed for each individual season,

  leaving synthetic sea ice concentration anomaly record containing *only* natural

  variability (detrended sea ice concentration; DT).

  o $SICa_{DT}(t) = SICa_{DT}(t) - SICa_{TM}(t)$ where $t = 1, 50$

4.2 – The Influence of Winter Teleconnections

4.2.1 – The North Pacific Oscillation/West Pacific Pattern and Pacific North American Pattern

The two previous chapters discuss the impact of the NPO/WP on the position of

winter MIZ. The circulation anomalies resulted in both a thermodynamic and dynamic

response of the MIZ in the Bering Sea and Sea of Okhotsk; however, the NPO/WP

circulation anomalies are not only limited to the two aforementioned marginal seas. The

circulation anomalies extend well into the Arctic, and an NPO/WP seasonal footprint on

the sea ice is possible. The circulation anomalies, cyclonic near the pole, favor the

development of new, thin sea ice in the fractures and leads open in the ice pack via

Ekman divergence. Regressions of the seasonally averaged NPO/WP index, obtained

from EOF analysis on monthly mean DJFM SLP anomalies between 1958 and 2004, on

seasonally averaged January-February-March (JFM), April-May-June (AMJ) and July-

August-September (JAS) sea ice concentrations (not shown) link the winter NPO/WP to a

5% decrease in summer sea ice concentration. The JFM regression pattern contains a signal in the Bering Sea, linking the NPO/WP to the earlier established extension of the MIZ in the Bering Sea. The hemispheric perspective reveals that the NPO/WP is also associated with less ice in the Barents and Greenland Seas. This could be related to the tertiary center over the Atlantic, where anticyclonic flow would advect warm, moist midlatitude air into the Arctic region, melting ice and stunting equatorward motion of the MIZ. Decreased sea ice concentration in the Atlantic sector persists into the subsequent AMJ and JAS seasons, based on the notion that if ice was not present there in the winter, then it is not going to be there during subsequent seasons. During JAS, there is a 5% decline in sea ice concentration in the East Siberia Sea and Laptev Sea, consistent with cyclonic anomalies and increased thin sea ice.

Like the NPO/WP, the PNA is linked to a decline in sea ice along the coast of Greenland for all three seasons. During the melt season, the PNA does not have the same effect in the East Siberia Sea that the NPO/WP does, with a small area experiencing a decline in sea ice. A moderate decline of 10% occurs in the Beaufort Sea following a winter with a positive PNA.

4.2.2 – The North Atlantic Oscillation

The footprint of the NAO on both winter and summer sea ice is somewhat better established. Studies link the NAO to both a dipole in sea ice near Greenland (Van Loon and Rogers 1979, Deser et al. 2000) and decreased summertime sea ice concentration in the Laptev Sea and East Siberia Sea (Rigor et al. 2002). Regressions of the seasonal NAO index derived from EOF analysis and correlated with Hurrell's index at 0.94 contain the features in the aforementioned studies. During JFM, the NAO is linked to a

15%-20% decrease in Barents Sea and Greenland Sea sea ice, and an equivalent increase in the Davis Strait. The sea ice response is caused by a variety of factors: stormtrack displacement, dynamic sea ice motion and low-level thermal advection.

Low sea ice concentration persists in the Greenland Sea for the subsequent months, and during JAS (figure 4.5), a large region of negative sea ice anomalies is present in the western Arctic. During winters with a positive NAO, the surface wind vector, and thus, sea ice motion vector is pointed away from the Siberian coast towards the Fram Strait (Rigor et al. 2002). A weakened Beaufort Gyre, a well-known consequence of a persistent positive NAO (figure 4.5), prevents ice recirculation, leading to losses of perennial ice through the Fram Strait (Rigor et al. 2002). This, coupled with Ekman divergence and thin sea ice development, leads to a drastic sea ice reduction in the western Arctic following winters with an active positive phase NAO.

4.2.3 – Analysis of detrended sea ice

The minor caveat of the current analysis is the presence of a trend in both summer sea ice and the NAO index (and possibly other teleconnection indexes; figure 4.7) which can produce false relationships. In addition, long-term means of the index need to be zero. To ascertain robust physical relationships, regressions must be calculated using both detrended indices and sea ice concentration. Figure 4.7 shows the patterns obtained by regressing the seasonal detrended winter teleconnection indexes on detrended seasonal sea ice concentrations. Detrending the sea ice removes the NPO/WP and PNA signals in the Greenland Sea and East Siberian Sea, implying a lack of causal mechanisms on seasonal to interannual timescales. To confirm the absence of a physical relationship between the NPO/WP, PNA and eastern Arctic sea ice, an analogous analysis is

performed regressing the total teleconnection indices on detrended sea ice concentration, and there is no NPO/WP or PNA signal in the eastern Arctic (not shown). Instead, the spurious results are likely due to presence of a linear trend in sea ice in that region.

Detrending both the NAO index and seasonal sea ice concentration removes the linkage between summertime sea ice concentration along the Greenland coast and the antecedent winter NAO conditions. However, a robust signal remains in the East Siberia and Laptev Seas, confirming that fluctuations in summer sea ice in this region are linked to the winter variations in the NAO. Both of these marginal seas display a negative linear trend over the last several decades; conversely, the NAO contains a substantial positive trend superimposed on the higher frequency variability, especially in the 1980s and 1990s. We will show in subsequent sections that a fraction of the trend in this region is related to the trend toward positive NAO conditions in the latter part of the 20th century.

4.3 – The Influence of Pacific Sea Surface Temperature Variability

4.3.1 – Pacific SST variability

Seven physical modes of SST variability are extracted when rotated EEOF analysis is applied to seasonal SST anomalies from the HadISST1.1 between 1958 and 2007. The seasons are the standard meteorological seasons, December-January-February (DJF), March-April-May (MAM), June-July-August (JJA) and September-October-November (SON). The modes are discussed in Guan and Nigam (2008), and the related PCs are shown in Fig. 4.8. The identified modes are

- ENSO+: The decay phase of El Nino

- ENSO-: The build-up phase of El Nino

- ENSO-NC: The non-canonical mode of ENSO, similar to the meridional mode in Chiang and Vimont (2004), which is more focused in the central Pacific Basin and displays lower-frequency variability than canonical ENSO

- The trend mode: The SST-trend extracted in context of natural variability. Implicit accommodation of natural variability leads to a non-stationary SST trend. Broadly similar to the linear trend.

- North Pacific-Pacific Decadal Variability (NP-PDV): A longitudinally vast region of SST anomalies in the Northern Pacific Ocean which is operative on decadal timescales. The NP-PDV is correlated with the Pacific Decadal Oscillation described by Manuta et al. (1997) and captures the 1976/77 "climate regime shift."

- Biennial: SST anomalies which originate in the eastern equatorial Pacific and propagate towards the dateline over three seasons.

- Pan Pacific-Pacific Decadal Variability (PP-PDV): Basin-wide SST anomalies, characterized by horseshoe shaped anomaly extending from the Bering Sea along the coast of North America and into the central tropical Pacific Ocean.

The changes in SST are related to variations in atmospheric circulation and the slowly-varying nature of SST results in the persistence of these circulation anomalies, perpetuating their influence on hydroclimate and sea ice. While not extensively studied, tropical SST variations, namely ENSO, are known to be related to sea ice extent in the Bering Sea during the winter months (Niebauer 1988; Niebauer 1998). Interestingly, the

effect of El Niño on sea ice in the Bering Sea changed after the climate regime shift

(Trenberth 1990), with El Niños before (after) 1976/77 increasing (decreasing) sea ice in

the Bering Sea during the winter months (Niebauer 1998). The ENSO sea ice footprint

changed after the climate regime shift due to an intensification and eastward

displacement of the climatological Aleutian Low in the decades following 1976/77. As

ENSO's effects are not confined to the winter months, the possibility exists that ENSO,

along with the other SST modes, affect the distribution of summertime sea ice, especially

in the marginal seas of the Pacific sector.

4.3.2 – Pacific SST variability and their relationships to sea ice

As mentioned earlier, the relative inertness of SST as compared to the atmosphere

results in little change in the influence of SST variability from season to season. Three

modes stand out as being influential for JAS Arctic sea ice: ENSO-NC, NP-PDV and the

trend mode. The linkage between the trend mode and a concentric decline in sea ice

(figure 4.9) is not surprising; regardless of the forcing behind the trends (anthropogenic

or otherwise), one would expect the two to be closely related. The near-global scale

increase in SST could be reflective of planetary warming, which could, in principle, also

result in sea ice loss, especially, along the periphery.

The regressions of the remaining SST PCs on the total sea ice concentration field

are not shown, but discussed in the following paragraphs. ENSO-NC and NP-PDV are

purely natural climate variations and would serve to exacerbate or offset the linear trend.

The anomalies associated with the ENSO-NC mode are similarly signed as the linear

trend. The anomalies are confined to two regions: the Eastern Siberian and Chukchi Seas

and the Greenland and Barents Seas. In the Greenland/Barents Seas, the decline is

minimal; a broad region experiences a 3% decrease with sea ice concentration decreasing up to 6% along the east coast of Greenland. In the Eastern Siberian and Chukchi Seas, the decline is larger; ice loss is as much as 9% in the Eastern Siberian Sea.

The effects of the NP-PDV are opposite of ENSO-NC in the Atlantic sector of the Arctic. Sea ice concentration increases in the Kara Sea, Barents Sea and Greenland Sea, up to 9% along the east coast of Greenland. There is also a 3% increase in the Laptev Sea and in the Canadian Archipelago. In the Chukchi and Beaufort Seas, there is a small region of ice decline of approximately 3%.

4.3.3 – Pacific SST variability and detrended sea ice concentration

Sea ice and SLP patterns derived from this analysis are presented in figure 4.10. Once again, both ENSO-NC and NP-PDV stand out as SST variabilities that are influential in the distribution of summertime Arctic sea ice. The sea ice footprints are similar to the footprints extracted using the full sea ice record. ENSO-NC is highly influential over the East Siberian Sea, Laptev Sea and Chukchi Sea, associated with a sea ice reduction of 9%. The circulation pattern associated with ENSO-NC features a low pressure anomaly centered over northern Siberia; the sea ice anomalies are consistent with the winter SLP anomalies. Southerly wind advects warmer air into the region, possibly stunting winter sea ice growth, and Ekman divergence forced by easterly flow would promote the development of new, thinner, less stable sea ice during the winter months. The newer, thin sea ice would melt rapidly the subsequent summer, leading to an overall loss in sea ice.

The influence of the NP-PDV is confined to the Atlantic sector of the Arctic, mainly in the Barents and Greenland Seas. An increase of 6-9% coincides with a zonal

dipole in SLP anomalies; higher pressure occurs to the west, over Greenland. The surface winds in this region would be northerly, favoring an extension of the MIZ in the winter and shifting the southern limit of ice sustainability equatorward. As the NP-PDV is operative on decadal timescales, the sea ice anomalies associated with the NP-PDV would persist for decades, if the NP-PDV was the only forcing in the region.

The obvious importance of low-frequency decadal-to-interdecadal SST variability on the distribution of summertime sea ice extent raises the question of linear trend vs. natural variability. How much of the linear trend calculated from the shorter term, satellite-based sea ice record is genuinely a trend and not the aliasing of natural variability having time scales longer than the satellite record? This question is especially intriguing given the importance of the NP-PDV for summertime sea ice, and the encapsulation of the climate regime shift by this particular mode. In the next section, we will show that the difference in sea ice trends in the Atlantic sector between the 26-year satellite period and the longer 50-year period is attributable to the NP-PDV.

4.4 – Winter Variability in the Sea Ice Trend

Trends in seasonal (JAS) sea ice concentration (figure 4.11) are, not surprisingly, similar to the trends in September sea ice concentration; the only difference is in the amplitude of the trend. During the longer period of 1958-2007, there is an annular decline in the Arctic ice cap. All the marginal seas are losing ice at a rate of 5-10% per decade, with the largest trend (10% per decade) occurring in the marginal seas which contain a natural variability signal, from the Greenland Sea eastward to the Eastern Siberian Sea. During the sub-period 1979-2007, the trend is even less zonally uniform (figure 4.11*b*). There is almost no decline in the Atlantic sector of the Arctic but the loss

of ice in Arctic's Pacific sector accelerates; reaching 20% per decade in regions. The Atlantic SLP analysis which extracts the NAO from the SLP field is updated through 2007 and the regression patterns associated with this longer analysis are presented in figure 4.12; panel *a* is the total regression, panel *b* is the regression of the full NAO index on detrended JAS sea ice concentration and panel *c* is the regression of the detrended NAO index on detrended JAS sea ice. The patterns are near identical to the regressions found in the 1958-2004 analysis with notable sea ice loss in the Eastern Siberian Sea; the analysis is updated to include the years 2005, 2006 and 2007. The regressions displayed in Fig. 4.12 indicate the importance of de-trending the SIC record prior to computation of regressions and correlations.

4.4.1 – Calculation of sea ice anomalies forced by natural winter variability

Seasonal sea ice anomalies related to natural variability are computed by multiplying the detrended sea ice regression patterns by the principal components of the six Pacific SST variability modes and the NAO; the SST-trend mode is excluded. The seven new sea ice records are summed together, and this new, synthetic seasonal sea ice data set is taken to represent natural variability of sea ice associated with natural atmospheric and oceanic variability. Here one is assuming that the trend implicit in the NAO record is part of natural variability, i.e., distinct from the anthropogenic signal. This interpretation is supported by the leveling off of the NAO trend, including hints of the beginning of a negative trend in the last decade (cf. Fig. 4.6). The anomalies are added together, linearly, as SST principal components are uncorrelated with each other (correlation is strictly zero), and also with the NAO index (largest correlation being 0.2;

table 4.1). The NPO/WP and PNA contributions to summertime sea ice are not included given their earlier documented insignificant influence. The steps are presented below.

- Regress the seasonal SST PCs and detrended NAO PC on detrended summer sea ice concentration, returning seven (6 SST PCs and the NAO) sea ice footprints.

- Correlate winter NAO index with SST PCs (table 4.1).

- Develop a synthetic sea ice anomaly record for each mode of natural variability by multiplying the raw PC time series by the regression pattern.

  o $SICa_n(t) = SICr_N \times PC_N(t)$ where $t = 1, 50$ and $N = 1, 7$

- Sum individual sea ice anomaly records to form new synthetic sea ice anomaly record containing sea ice anomalies related to 6 SST modes and NAO.

  o $\sum_{N=1}^{7} SICa(N)$ from $t = 1, 50$

4.4.2 – JAS 1958-2007

The summertime sea ice trend attributable to natural winter variability is depicted in Figs. 4.13a and c. In the Atlantic sector of the Arctic, natural winter variability serves to exacerbate loss of sea ice in summer. There is a 1-2% decline in sea ice per decade in the Barents Sea, Greenland Sea and Labrador Sea forced by winter variability, while a 5-10% loss per decade is related to additional forcings (anthropogenic or other). The trend

attributable to natural winter variability is not especially large, accounting for about a fifth of the linear trend in the same period

In the Pacific sector, namely the Eastern Siberian Sea, natural winter variability is forcing a 3-4% loss of sea ice per decade in the second half of the 20th century, or about 30-40% of the total sea ice trend during the 50-year period. Obviously sea ice loss is brought about by the trend towards positive NAO conditions during the latter 20th century; the NAO signal is largest in the Eastern Siberian Sea. Furthermore, while none of the ENSO indices display a trend, the indices are more frequently positive than negative. This too would favor sea ice decline, based on regression patterns of the ENSO modes, especially, the ENSO-NC mode (cf. Fig. 4.10).

4.4.3 – 1979-2007

The linear trend in summer sea ice attributable to natural winter variability is plotted in figure 4.13c, while the residual linear trend in shown in 4.13d. Evidently, natural winter variability has greatly modulated the summertime sea ice trend since the satellite era. In the Pacific sector of the Arctic, natural variability is responsible for a 4-6% per decade decline in sea ice, which is approximately a third of the total trend. This undoubtedly results, in part, from the positive NAO trend during the 1980s and 1990s. Sea ice variability in this region is also linked to the non-canonical mode of ENSO. The non-canonical mode of ENSO is particularly energetic since the climate regime shift (Guan and Nigam 2008), and close inspection of the time series reveals that the ENSO-NC PC is positive in 20 of the 29 analyzed seasons. The enhanced amplitude of the non-canonical ENSO mode coupled with a tendency towards positive NAO conditions is in some measure responsible for the decline in sea ice in the Eastern Siberian Sea during the

summer months of the satellite era sub-period. Furthermore, there is a trend towards warm ENSO events, with El Niños outnumbering La Niñas by a factor of 2 since 1979. The increasing El Niño frequency would advance decline in sea ice in the Chukchi Sea and Beaufort Sea (c.f. figure 4.10).

On the Atlantic side of the Arctic, the linear trend in sea ice due to natural winter variability is, interestingly, positive. If this was the only control on summertime sea ice distribution, sea ice in the Barents Sea and Greenland Sea would be increasing 6-8% per decade. It is noteworthy that only modes of Pacific Decadal Variability, one which encapsulate the climate regime shift of the 1970s, are linked to sea ice in this area. The NP-PDV index (not shown) between 1979 and 2007 contains a strong positive linear trend, indicative of a tendency towards sea ice growth, as opposed to loss, in the eastern Arctic. The circulation changes in the Atlantic Basin, prompted by a trend towards positive NP-PDV conditions in Pacific climate, are offsetting other influences which are driving the overall ice melt. The confinement of the satellite sea ice record to the post-Pacific climate regime shift years precluded characterization of Pacific Decadal Variability's influence on Arctic summer sea ice and its implicit inclusion and aliasing in computation of the total linear trend. Analysis using a sea ice record which extends beyond the Pacific climate regime shift into the earlier record, as here, allows for characterization of the influence of decadal variability. Removal of the NP-PDV influence from the sea ice record reveals a significantly more concentric negative linear trend in summer sea ice (fig. 4.13*d*). The implication that the circulation induced by the trend in the NP-PDV is currently compensating for sea ice loss forced by other factors is

troubling; when trend reverses or becomes near neutral, which is almost inevitable, sea ice loss will be exacerbated.

4.5 – Summertime Atmospheric Variability

The earlier sections demonstrate the importance of sea ice memory and the influence of winter circulation on sea ice, especially, in the subsequent summer. However, sea ice variability occurs on all timescales, from weekly to decadal. In this section, the response of the MIZ to contemporaneous atmospheric circulation anomalies is examined.

4.5.1 – Teleconnections in the summer circulation

Teleconnection patterns occur in the boreal summer circulation as well, albeit with weaker amplitude. The CPC finds eight to nine teleconnections to be prominent during the summer months. Most are seasonal counterparts to the better known winter teleconnections, while others are exclusive to the summer season. The CPC diagnoses teleconnections by applying rotated principal component analysis to monthly hemispheric 500 hPa height anomalies north of 20ºN. To remain consistent with our earlier analysis, we diagnose summer teleconnections by performing unrotated EOF analysis on Pacific (120ºE-120ºW) and Atlantic (80ºW-0º) monthly SLP anomalies during JAS 1958-2007. We focus on the July-September period – not the customary summer period (June-August) – in view of our interest in Arctic sea-ice decline which is most steep in September.

Our approach returns two of the CPC summer teleconnections: the PNA and NAO. The NAO is the first mode of summer SLP variability in the Atlantic, explaining

33% of the monthly variance (figure 4.14*a*). The PC corresponding to the NAO is correlated at 0.81 with the CPC's NAO index. The PNA is the first mode of Pacific SLP variability during summer months[9] (figure 4.14*b*), and it is correlated with the CPC PNA index at 0.68. Each consists of a meridional SLP dipole; the NAO dipole is a northeast shifted version of the winter structure. One center is located between Greenland and Iceland, and an oppositely signed center is immediately south situated at 30ºW, 45ºN. The PNA does not much resemble its winter counterpart; a longitudinally broad area of lower sea level pressure is centered along the 50th parallel, while a small anticyclonic circulation is situated southwest of the pole, centered at 150ºW, 80ºN. The higher-order EOFs in each basin cannot readily be identified as being counterpart of the established winter patterns. Without extensive analysis of robustness and physicality of the higher order modes, an effort beyond the scope of this thesis, we focus on the leading modes in each basin, to begin with.

Both the NAO and PNA contain centers in the Arctic region, and the surface circulation anomalies associated with each of them will further impact the distribution of Arctic sea ice. The sea ice footprint of summer teleconnections is investigated in the next section, and while these teleconnections are not as well defined as their winter counterparts, they do exert considerable influence on sea ice in the marginal seas of the Arctic Ocean.

4.5.2 – The effect of summer teleconnections on summer sea ice

---

[9] The PNA is identified as the first EOF of JAS Pacific SLP variability by correlating PC1 with the CPC PNA index for the summer months and regressing Pacific PC1 on 500 hPa geopotential heights (not shown) and visually comparing our results with the CPC teleconnections.

To remove the signal of winter variability in the sea ice record, the anomalies forced by winter variability are subtracted from the synthetic anomaly record developed by removing the SST trend mode JAS sea ice anomalies. The residual anomalies, then, only contain natural variability during the non-winter months.

Figure 4.15 shows SLP regressions and sea ice regressions obtained from regressing the detrended seasonal NAO and PNA indices on the new detrended summer sea ice record. The negative phase of the NAO is associated with a sea ice loss of 6-12% in the marginal seas of the Pacific. This is consistent with the findings of Ogi and Wallace (2007), who demonstrated that a negative AO phase during the summer season leads to sea ice reduction in this region. The sea ice loss decrease is caused by Ekman convergence towards the center of the anticyclone (i.e. towards northern Greenland); anticyclonic circulation anomalies force ice drift away from the coast into the central Arctic, reducing the already sparse sea ice concentration in the Eastern Siberian Sea, Chukchi Sea and Beaufort Sea.

The positive phase of the PNA is shown in figure 4.15*b*. Like the NAO, the depicted phase of the PNA leads to a loss of sea ice in the Eastern Siberian Sea, Chukchi Sea and Beaufort Sea. The reduction is modest compared to the NAO; approximately half the amplitude. Anomalous anticyclonic circulation anomalies near the Canadian Archipelago will advect sea ice away from the Siberian and Alaskan coasts towards the Canadian side of the Arctic, since ice moves to the right of the surface wind vector.

The impact of wind-induced ice drift varies from season to season. During the antecedent winter months, anomalous *cyclonic* circulation is detrimental to summer sea ice. Ekman divergence induced by the surface winds break sea ice apart and promotes

the development of thin sea ice in the leads and fractures opened in the winter ice pack.

Furthermore, ice divergence away from the center of the low implies an increase in sea ice immediately along the coast, where turbulence along the continental shelf will destroy sea ice. Finally, a weakened Beaufort high reduces sea ice re-circulation within the Beaufort Gyre, limiting sea ice growth via reduced ice packing and increasing sea ice advection out of the Arctic by a westward shift in the Transpolar Drift (Rigor et al. 2002). Thus, more of the ice pack consists of thinner, annual ice as opposed to thicker, perennial ice. This thin sea ice is significantly more unstable, and melts rapidly during the subsequent summer. During the contemporaneous summer months, *anticyclonic* circulation anomalies are unfavorable for sea ice extent. Easterly winds in the marginal Pacific seas prompt Ekman convergence and the movement of sea ice away from the coast, which is reflected as a decline in sea ice in these regions. If sea ice in the marginal seas falls below 15%, a reasonable possibility given that climatological summer sea ice concentration in this area is 40-60%, these regions will be neglected in the calculation of sea ice extent. The exclusion of the marginal seas in the sea ice extent calculation will be reflected as an overall reduction in sea ice extent, even though sea ice concentration in regions closer to the pole has increased.

4.5.3 – Summer variability in the sea ice trend

The summer NAO does not display the same strong linear trend that the winter NAO does, however, careful inspection of the PC shows a slightly negative trend (towards positive NAO conditions) in the first 30 years of the analysis (figure 4.14*c*). Conversely, the PNA PC exhibits an apparent negative trend from 1958 to 1993. As both of these modes in their depicted phase lead to ice decline, a trend towards opposite

conditions (conducive to sea ice growth) would act to offset the general decline in sea ice in the last 50 years.

NAO and PNA related sea ice anomalies are calculated using the same procedure described earlier; the PC at each time step is multiplied by the regression pattern. The anomalies related to the NAO and PNA are summed together, and then this record is detrended. Although the NAO and PNA are extracted during separate EOF analyses, the PCs are uncorrelated, allowing for the two modes and their impacts to be combined linearly. The summer trend is presented in figure 4.16*b*; the trend induced by winter variability is shown in 4.16*a* for context. Clearly, summertime variability is not responsible for a large fraction of the trend. A small trend, 1% per decade, occurs in the Chukchi Sea. Over the last 50 years, then, summertime variability increased sea ice concentration 5% in this region, not nearly enough to even partially offset sea ice loss. However, the lack of a linear trend in the summer NAO and PNA does not preclude the possibility that they are important during individual years, either intensifying or counterbalancing sea ice loss due to winter forcing or anthropogenic forcing.

4.6 – The melt of 2007

The summer of 2007 featured the smallest polar ice cap since the advent of modern record keeping. The sea ice loss was most pronounced in the Laptev, Eastern Siberian and Chukchi Seas (figure 4.17), with a sea ice anomalies as large as 70% in some regions. Sea ice distribution in these seas, in addition to containing much of the linear trend, is also strongly influenced by natural climate variability. This subsection presents the state of the polar atmosphere in 2007 and examines the influence of natural climate variability on the 2007 sea ice distribution.

4.6.1 – The Winter of 2006-2007

Figure 4.18 displays the average surface circulation anomalies during the winter of 2006-2007. The SLP anomalies over much of the Arctic were below normal during the winter, with one low pressure center to the northwest of Norway, near the Barents Sea, and a secondary center over the Eastern Siberian Sea (panel *a*). As the Pacific sector of the Arctic is the region that experienced the dramatic sea ice loss in 2007, this region is focused on in panel *b*, with surface SLP and wind anomalies plotted. The surface wind vectors are cyclonic, and a winter with cyclonic circulation anomalies forces Ekman divergence of sea ice and promotes the formation of thinner sea ice. The surface circulation during the winter of 2006-2007 was certainly favorable for the development of thinner sea ice, suggesting that a fraction of the severe sea ice loss was caused by the atmospheric conditions during the antecedent winter.

Since all natural variability is aliased into the anomaly field, individual contributions of teleconnections can not be deduced from the circulation anomalies alone. The winter of 2006-2007 was strongly influenced by both a moderate El Niño episode in the tropical Pacific and NAO conditions in the North Atlantic Ocean (CPC 2006; CPC 2008). The El Niño conditions persisted for 6 months, until January 2007, and for the most part, the NAO was in the positive phase, with an average value of 0.56 for the five month November to March period.

The remainder of the Pacific Ocean oceanic teleconnections is not discussed in the CPC winter outlook for 2007. However, the PCs for many of the remaining SST variabilities also favored a reduction in sea ice (table 4.2). Since these SST PCs are uncorrelated, and since the NAO index is not correlated contemporaneously with any of

the SST PCs, the total anomaly field pertaining to winter variability is calculated by multiplying the individual regression patterns by the PC corresponding to the '06-'07 winter and summing the anomalies.

The total 2007 summer sea ice anomaly forced by winter circulation reaches over 15% in the Eastern Siberian Sea, and extends into the Laptev and Chukchi Seas (figure 4.19*a*). Overall, variations in winter circulation account for a quarter to a third of the total sea ice loss (figure 4.17) in this region.

4.6.2 – The Summer of 2007

Winter is not the only season which affects summer sea ice distribution. Earlier subsections show the importance of the summer circulation and its variability on the distribution of Arctic sea ice. Figure 4.20*a* depicts the average SLP over the Arctic Ocean between the months of May and September 2007. The most distinctive feature is an anticyclone centered over the Beaufort Sea. Panel *b* focuses in on the vicinity of the anticyclone, and the Pacific sector of the Arctic. Consistent with the SLP, the surface winds are anticyclonic; the surface winds on the western side of the high contain a southerly component, leading to warm air advection over the Eastern Siberian and Chukchi Seas. Furthermore, Ekman convergence of sea ice will occur near the center of the high, and ice motion will then be out of the Eastern Siberian and Chukchi Seas towards the Beaufort Sea. The persistent southerly flow combined with a tendency for ice motion out of the Eastern Siberian and Chukchi Seas reduces sea ice in this region; an area already favorable for sea ice loss due to the preceding winter conditions.

The combination of the sea ice anomalies forced by the teleconnection patterns deemed important for summer sea ice distribution, the NAO and PNA, is pictured in

figure 4.19*b*. The region most affected by the summer NAO and PNA is westward

shifted with respect to the area affected by winter variability; most of the influence occurs

in the Beaufort and Chukchi Seas. A sea ice decline of 15% in the Chukchi Sea is forced

by contemporaneous atmospheric variability; this accounts for a third of the decline in

sea ice in this region (cf. figure 4.17). Along the northern Alaskan and Canadian coast,

summer variability is responsible for nearly half of the sea ice decline in this region.

Although summer teleconnections are not as prominent or as extensively studied as their

winter counterparts, the above discussion exemplifies why the influence they exert on the

summertime climate, especially sea ice distribution, can not be neglected.

4.6.3 – The total influence of natural variability

The troubling projection of an ice-free Arctic in during the twenty first century

raises geopolitical questions, scientific uncertainties and industrial adaptations. Many

cited the sea ice minimum in 2007 as a "tipping point," that the Arctic ice cap has

reached a point of no return, where recovery to pre-industrial, or even pre-satellite era

levels, is impossible (Associated Press 2007). Few express concern that the Arctic will

be nearly ice-free as soon as 2012, a mere four years from present. Some scientists

attribute the ice melting solely to anthropogenic activities, however this study has

demonstrated the necessity to quantify the effects of natural climate variability.

Atmospheric circulation and climate variability aligned during 2007 to greatly reduce sea

ice during the summer months; the interannual variability imposed on the long-term trend

resulted in a record-breaking sea ice minimum. Panel *c* of 4.19 is the remaining Arctic

sea ice anomalies during the summer of 2007 after the anomalies related to both winter

and summer climate variability are removed. The area with ice anomalies exceeding

50% is collapsed to just a small region in the Eastern Siberian Sea. Unquestionably, the state of the Arctic sea ice in 2007 was alarming, but perhaps future effects of anthropogenic climate change will be partially offset by natural variability. Reduced Arctic sea ice lessens to equator to pole temperature gradient, favoring negative NAO conditions (Francis, personal communication). Negative NAO conditions increase ice recirculation in the Arctic, actually increasing sea ice thickness. Furthermore, the current study does not account for the impact of natural variability occurring during the spring months, and as teleconnections are present in the boreal spring circulation, the possibility exists that a fraction of the sea ice decline is related to spring anomalies.

Chapter 4 Figures
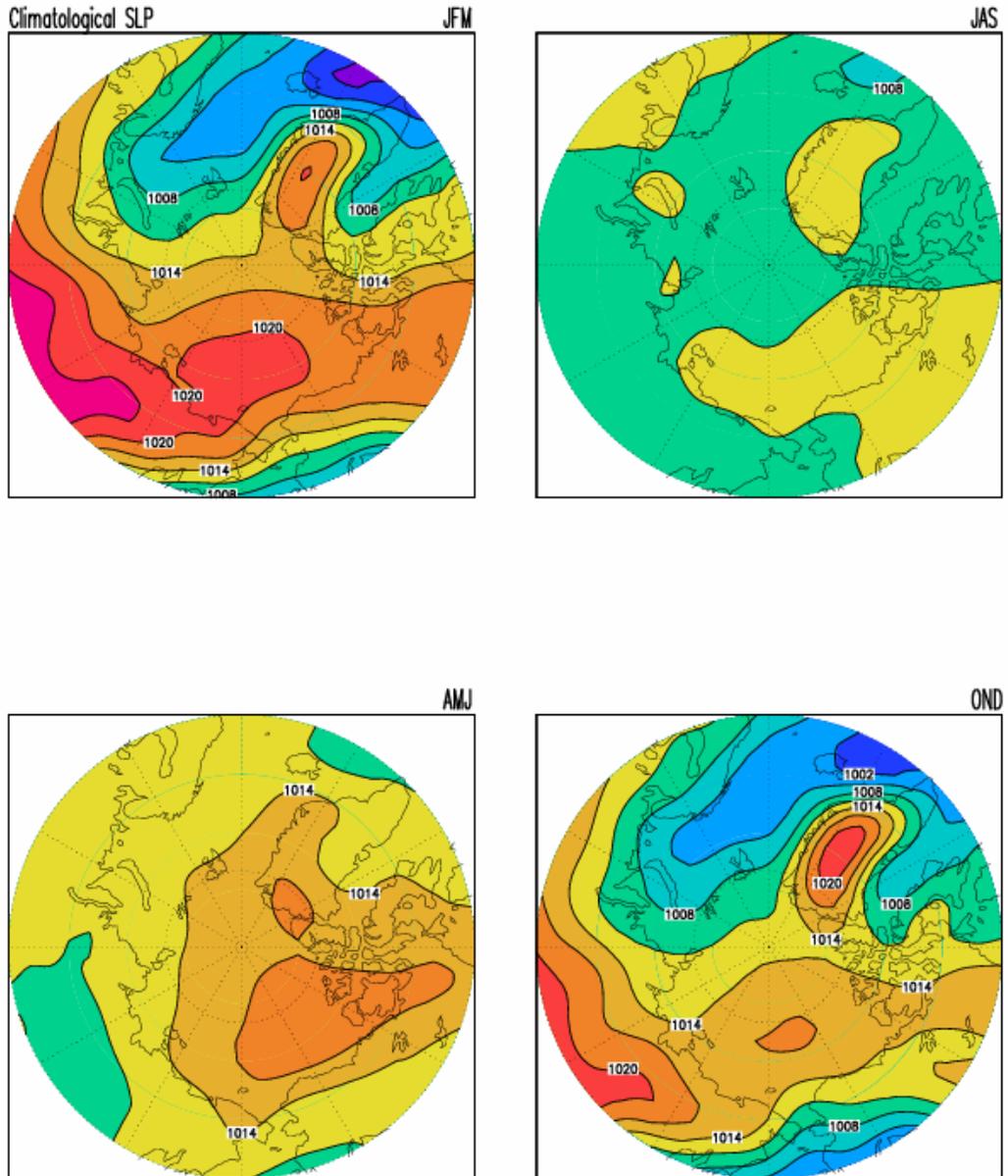
Figure 4.1: Climatological sea level pressure north of 60ºN from the NCEP/NCAR reanalysis between 1958 and 2007. The seasons are defined as winter (January-February-March), spring (April-May-June), summer (July-August-September) and autumn (October-November-December). The well established semi-permanent pressure systems, such as the Aleutian Low, Icelandic Low, Siberian High and Beaufort High are all present. SLP is contoured/shaded every 3 hPa beginning at 996 hPa.
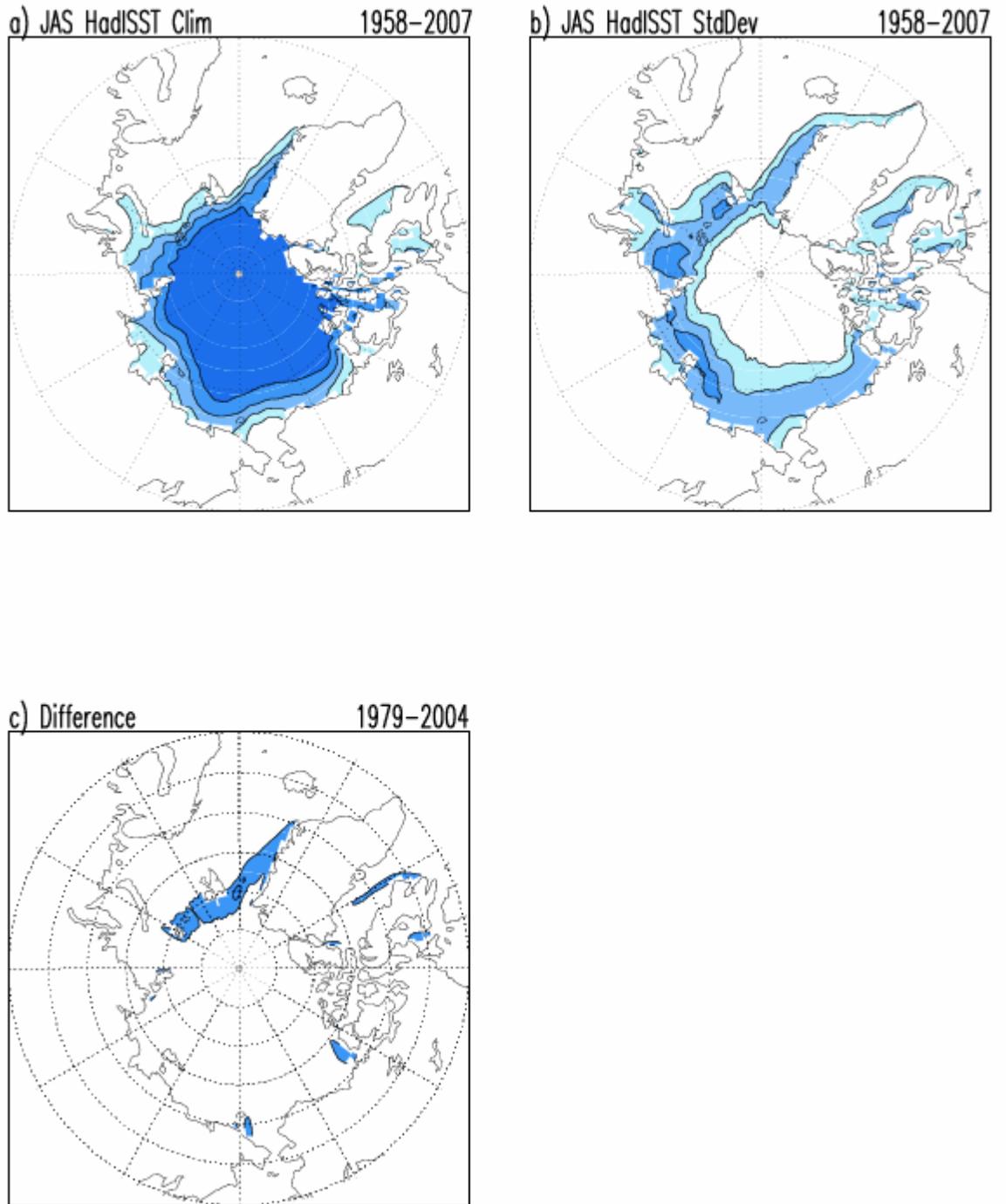
Figure 4.2: July-August-September sea ice concentration climatology (panel a) and standard deviation (panel b) between 1958 and 2007 from HadISST1.1. Difference between the two Had ISST1.1 and satellite-based JAS 1979-2004 climatologies is plotted in panel c. Shading/contouring is 20% (a), 10% (b and c) and the zero contour is suppressed.
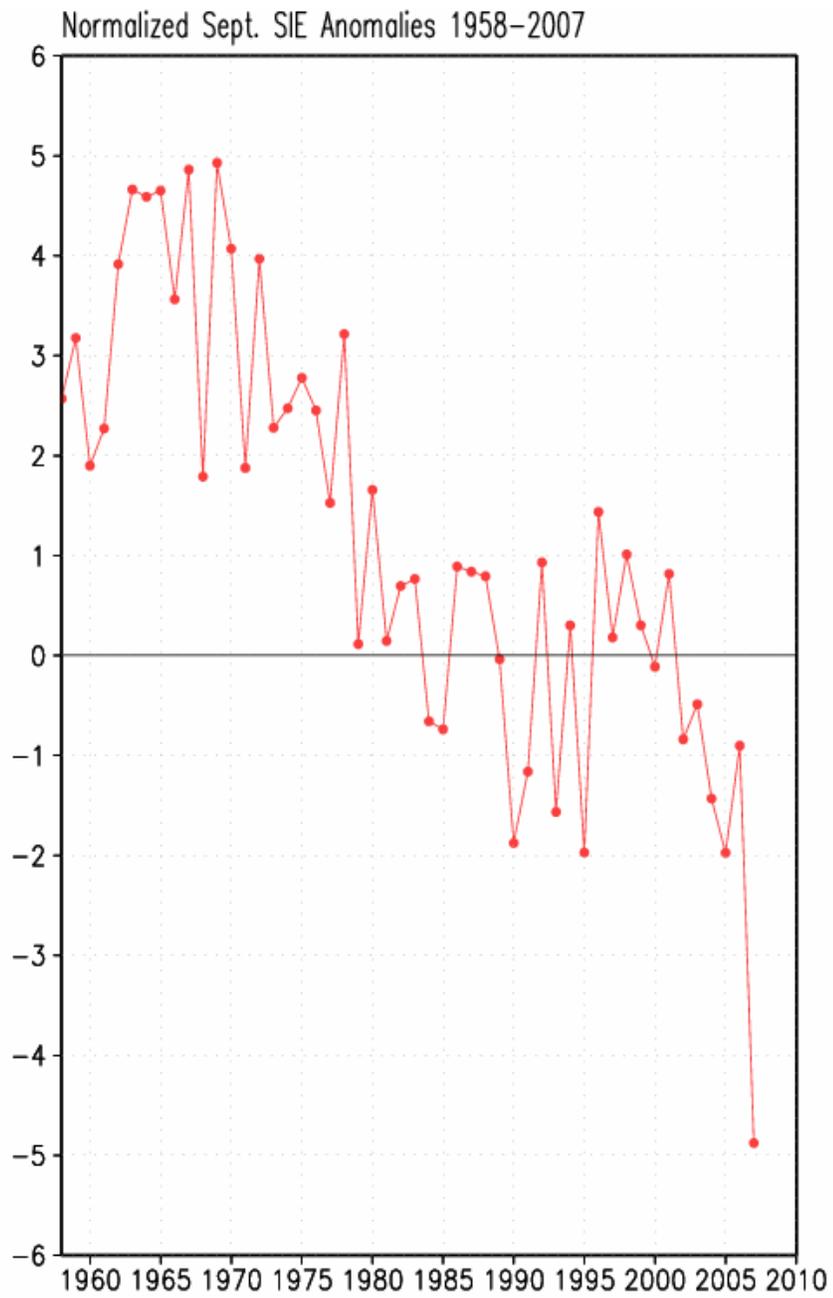
Figure 4.3: Normalized sea ice extent anomalies for Septembers 1958-2007 from HadISST1.1 sea ice concentration.
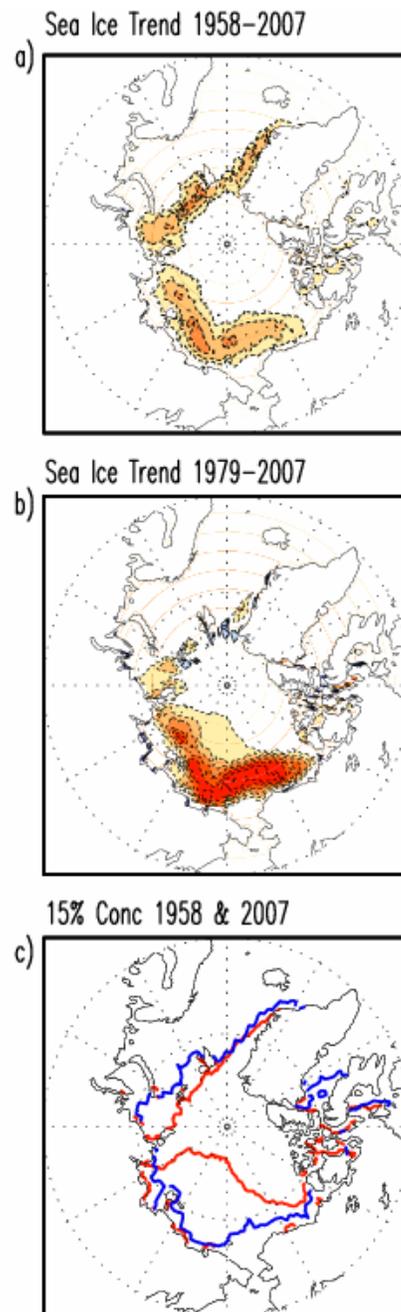
Figure 4.4: Linear trend in September sea ice concentration from 1958-2007 (panel a) and 1979-2007 (panel b) from HadISST1.1. Shading/contouring is 5% per decade; Red (blue) shading and dashed (solid) contours reflect negative (positive) values and the zero contour is suppressed. Location of the 15% concentration line in September 1958 (blue) and September 2007 (red) is plotted in panel c.

JFM NAO on JAS SIC
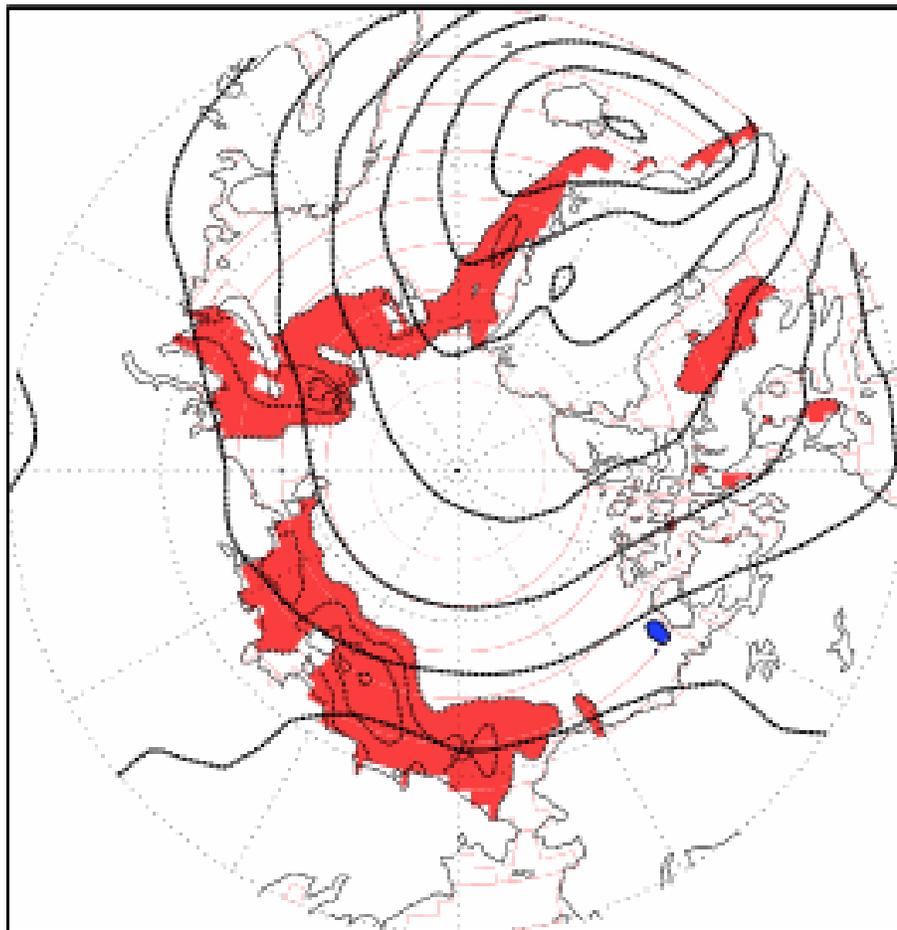
Figure 4.5: Regressions of the seasonal JFM NAO index on seasonal JAS sea ice concentrations from HadISST1.1 (shaded/contoured) and the monthly J-F-M NAO index on monthly J-F-M sea level pressure (thick contours) for 1958-2007. Sea ice regressions are shaded/contoured at 5%; red (blue) indicates sea ice increase (decrease). SLP anomalies are contoured at 1 hPa. Dashed (solid) contours correspond to negative (positive) values; zero contour is suppressed.
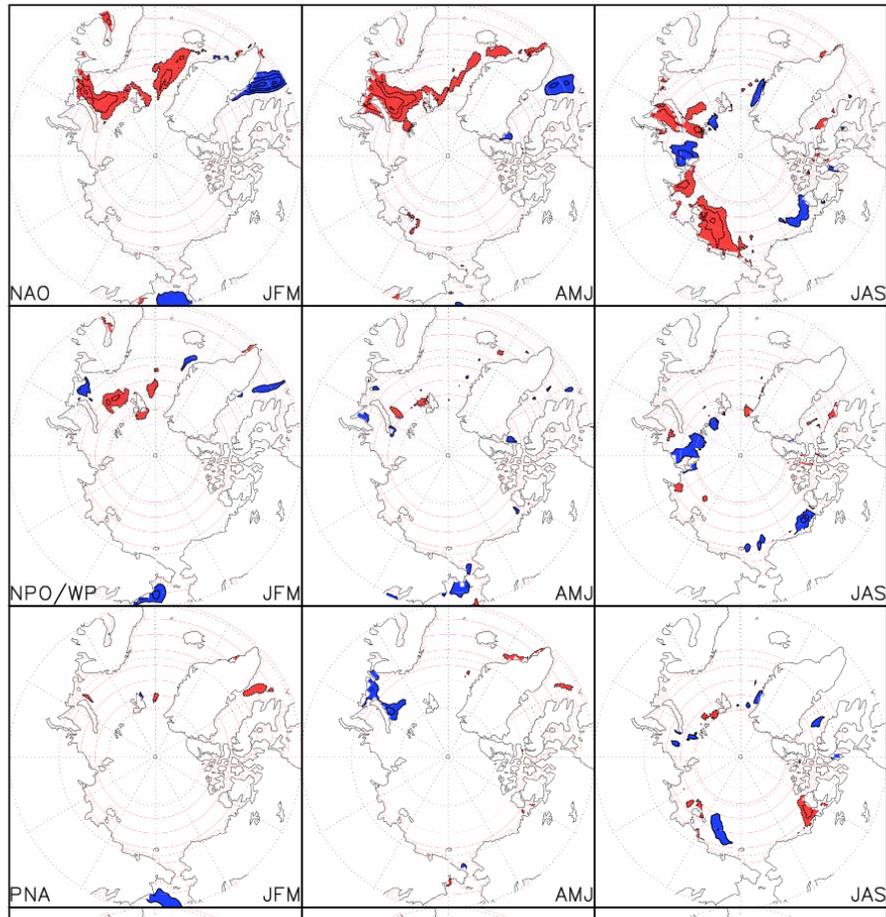
Figure 4.6: Regressions of the detrended seasonal JFM NAO (top), NPO/WP (middle) and PNA (bottom) indices on seasonal JAS sea ice concentration from the HadISST1.1 during 1958-2004. Red (blue) shading and dashed (solid) contouring indicates negative (positive) anomalies. Contour/shading interval is 5%; the zero contour is suppressed.
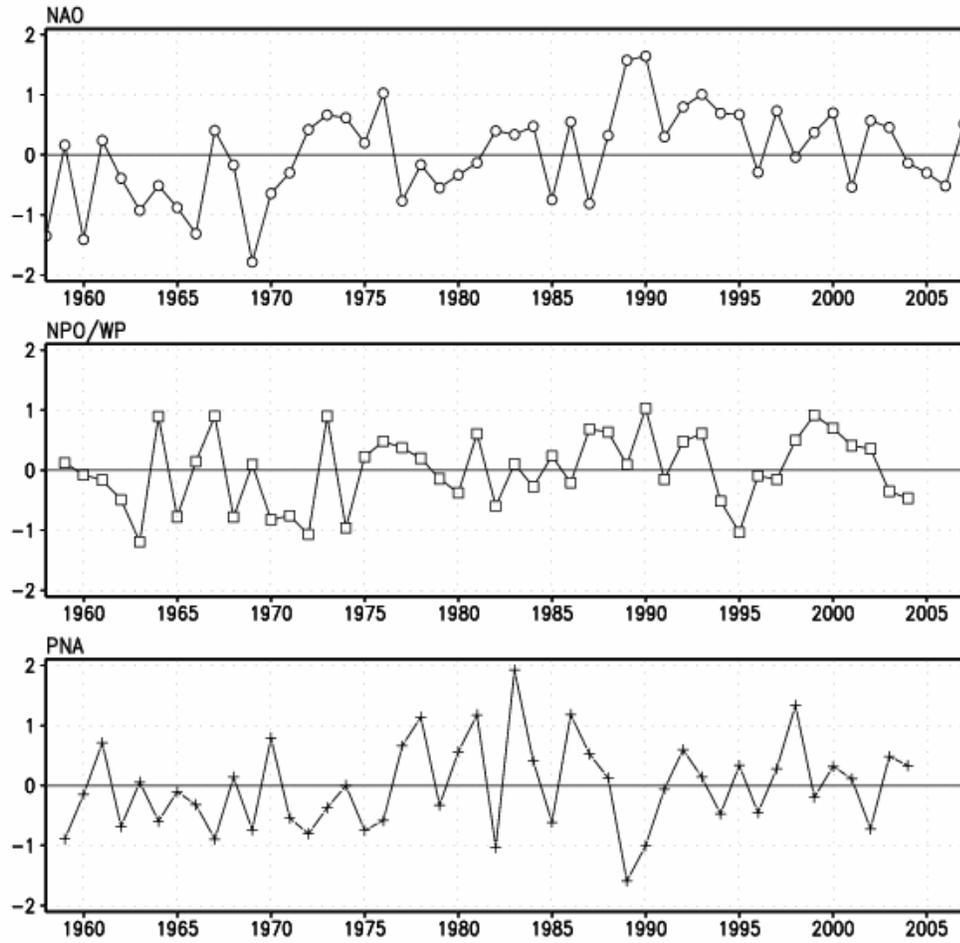
Figure 4.7: Seasonal JFM NAO (top), NPO/WP (middle) and PNA (bottom) indices derived from unrotated EOF analysis on monthly, basin-scale SLP anomalies for DJFM 1958-2007.
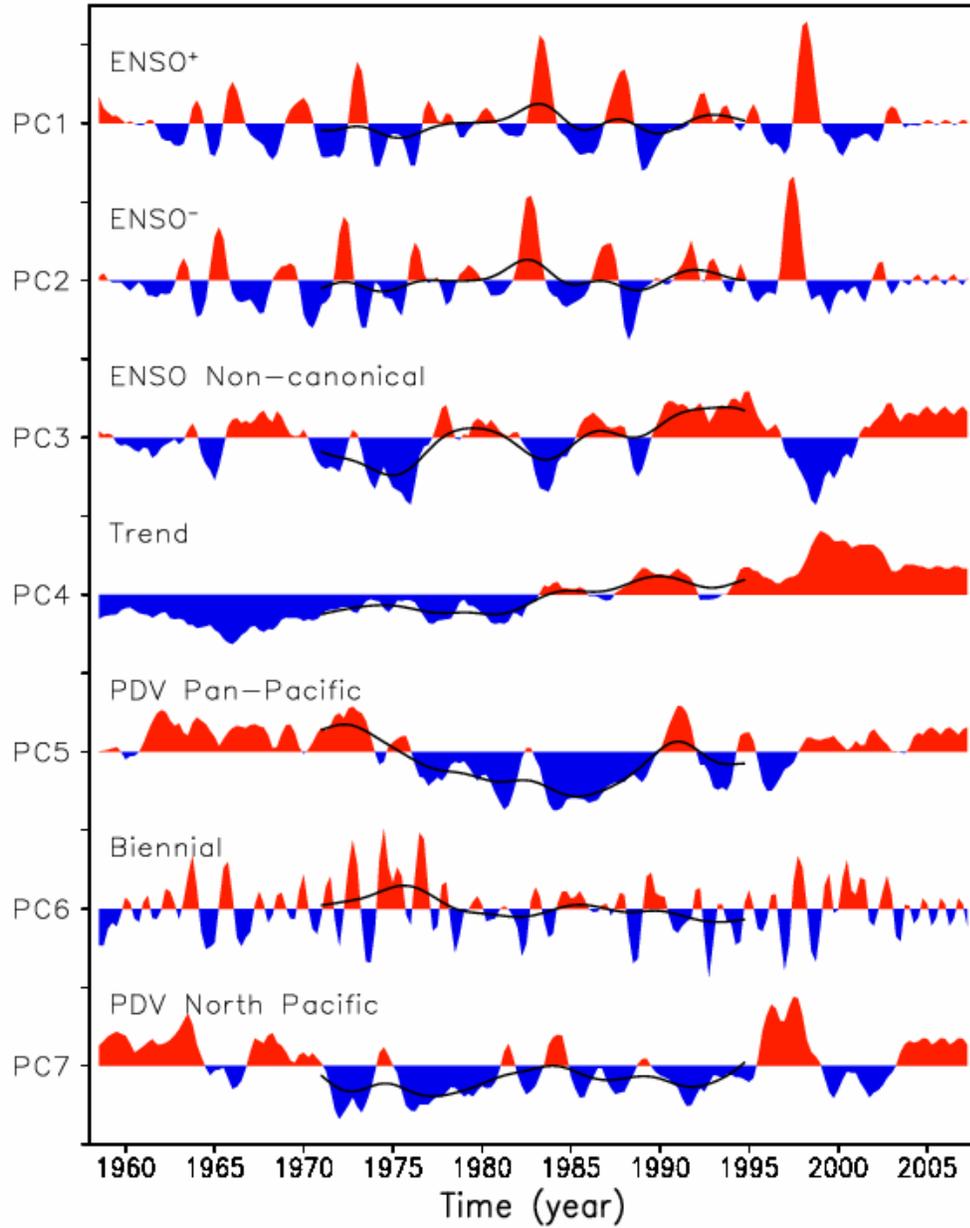
Figure 4.8: The seven leading principal components of Pacific SST variability derived from rotated EEOF analysis performed on seasonal HadISST1.1 SST anomalies between 1958 and 2007. The black curve represents the index after a 30-fold application of a one-two-one smoother.

PC4 Trend
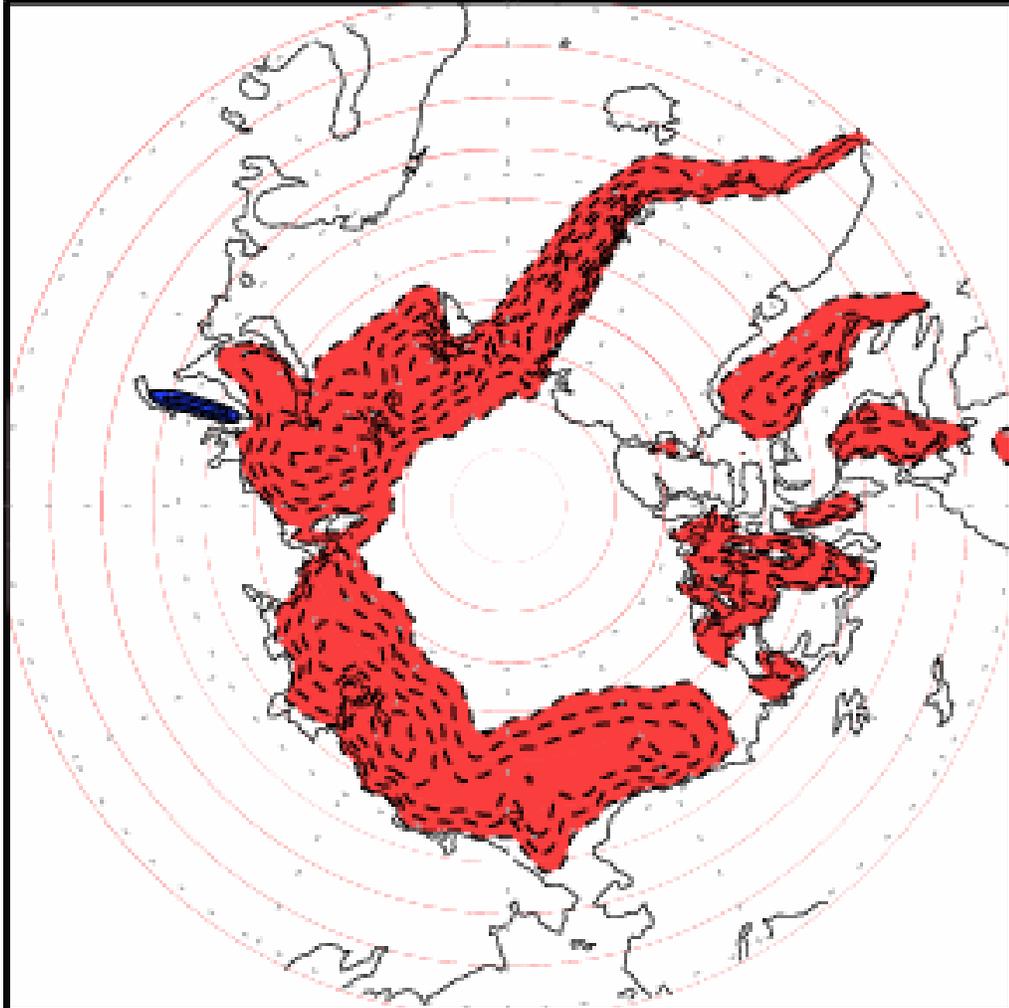
Figure 4.9: Regression of the seasonal DJF Pacific SST trend PC on seasonal JAS sea ice concentration during 1958-2007. Shading/contouring interval is 3%; red (blue) shading and dashed (solid) contours indicated negative (positive) values. The zero contour is suppressed.
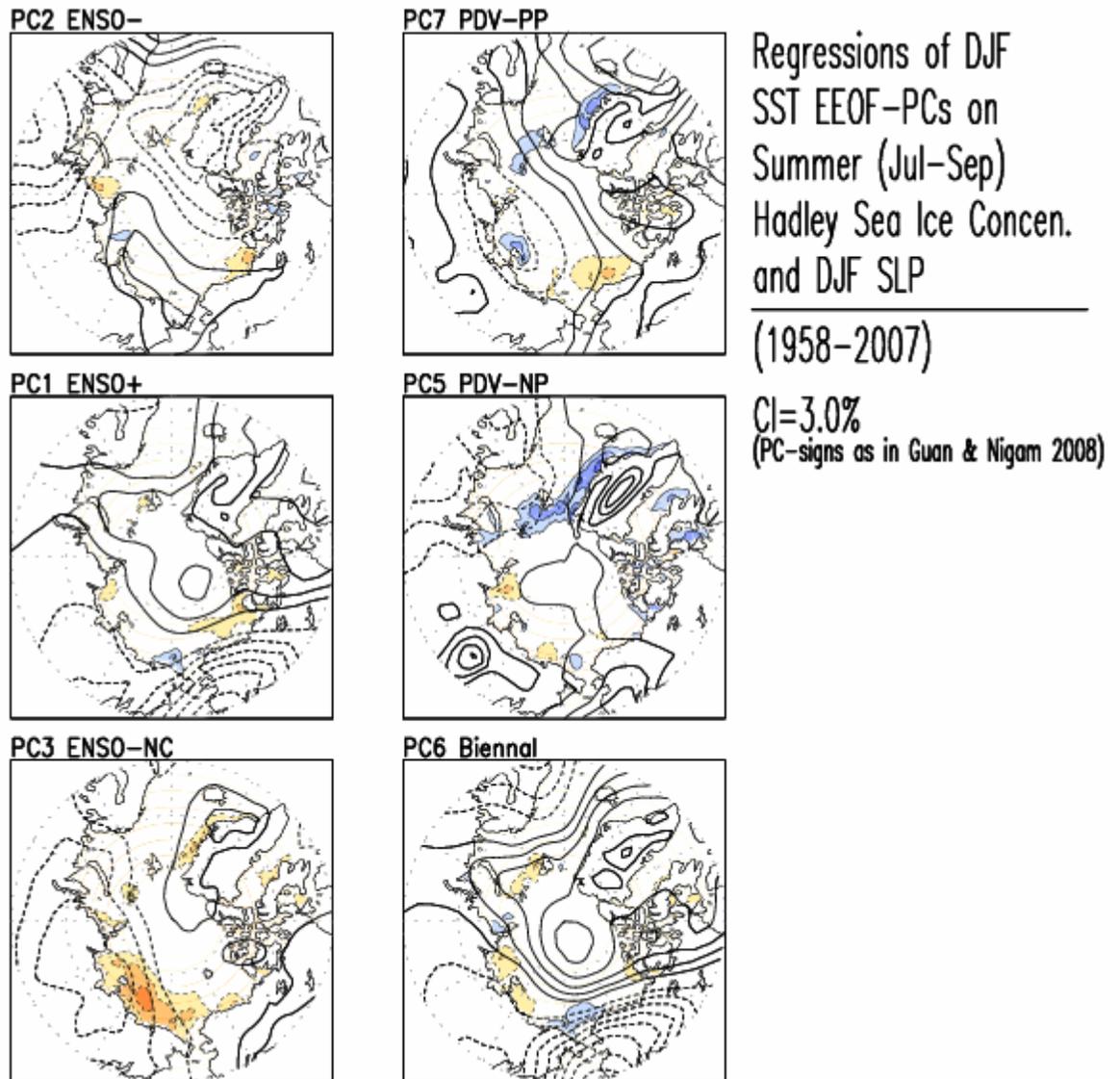
Figure 4.10: Regressions of seasonal DJF Pacific SST PCs on detrended seasonal JAS HadISST1.1 sea ice concentration (shaded/contoured) and detrended DJF NCEP/NCAR SLP (thick contours). Warm (cool) shading and dashed (solid) contours indicate negative (positive) values. Sea ice shading/contouring is 3%; SLP contouring is 0.5 hPa. The zero contour is suppressed in all plots.
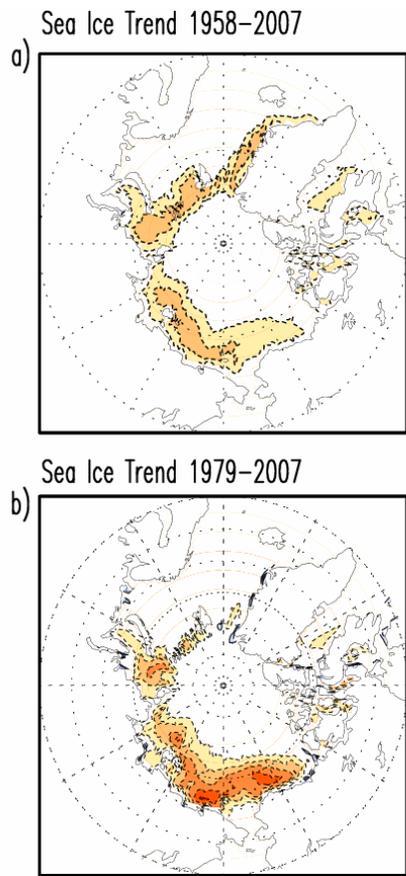
Figure 4.11: As in figure 4.4a and 4.4b, but for seasonal JAS sea ice concentration between 1958-2007.
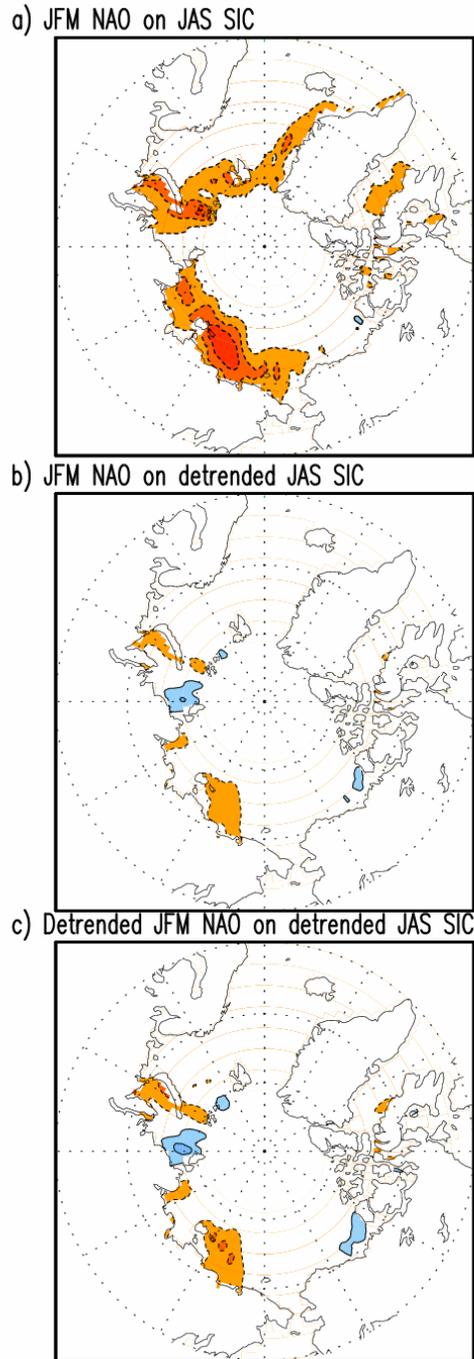
Figure 4.12: Regressions of the seasonal NAO PC on seasonal JAS sea ice anomalies (a), the seasonal NAO PC on detrended seasonal JAS sea ice anomalies (b) and the detrended seasonal NAO index on detrended seasonal JAS sea ice anomalies (c). All regressions are calculated for the 1958-2007 period; contouring/shading follow figure 4.6.

Correlation of NAO PC with SST PCs	1958-2007	1979-2007
Biennial	-0.2	-0.2
ENSO-	0.08	0.05
ENSO+	-0.15	-0.17
ENSO-NC	-0.07	-0.01
PP-PDV	-0.2	-0.12
NP-PDV	-0.1	0.03

Table 4.1: Correlation of the seasonal JFM NAO principal component from EOF analysis on monthly D-J-F-M 1958-2007 SLP anomalies over the Atlantic Basin (80ºW-0º; 20ºN-85ºN) with seasonal DJF SST principal components from rotated EEOF analysis on seasonal 1958-2007 SST anomalies over the Pacific Basin (120ºE-60ºW; 20ºS-60ºN) for the 50 year analysis period (left column) and 29 year satellite era (right column).
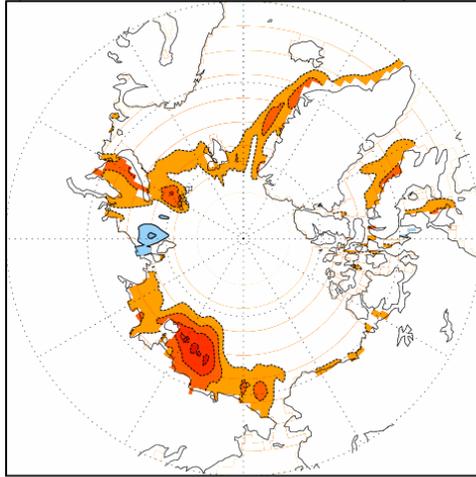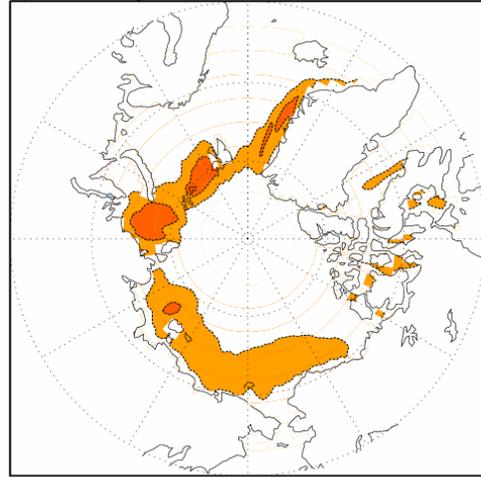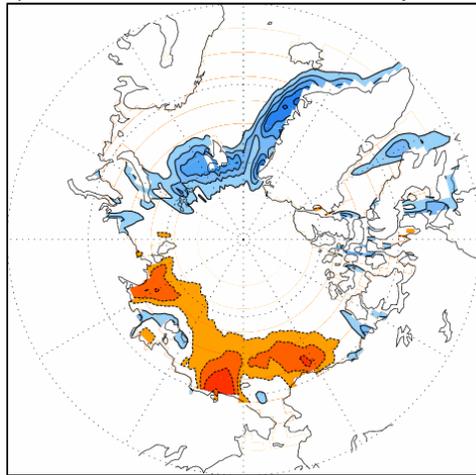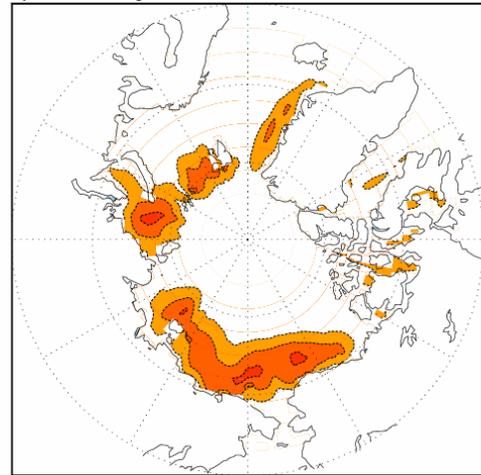
Figure 4.13: Linear trend in winter variability related sea ice anomalies for JAS 1958-2007 (a) and 1979-2007 (c). Warm (cool) colors and dashed (solid) contours indicate sea ice loss (gain). Contour/shading interval is 1% per decade for panel a, 2% per decade for panel c. Panels b and d are the linear trend in the remaining sea ice anomalies for the 1958-2007 and 1979-2007 periods respectively, and contour/shading interval is 5% per decade.
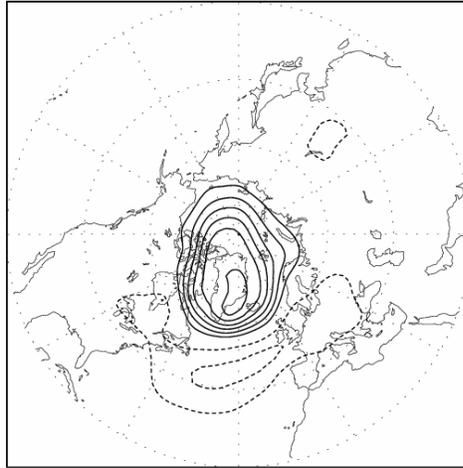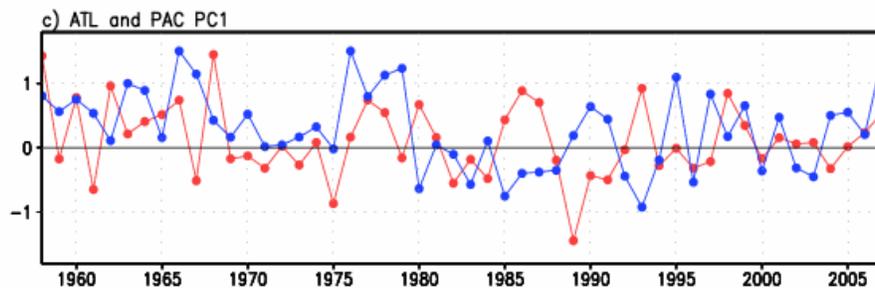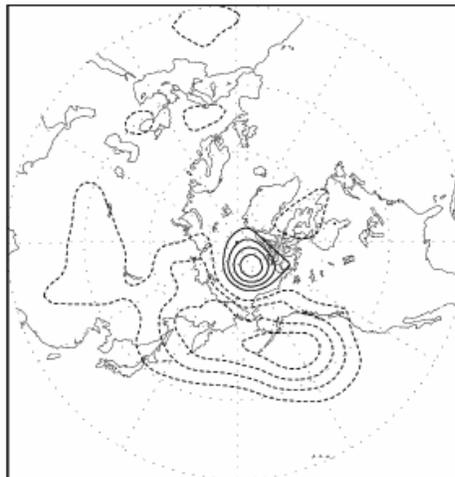
Figure 4.14: The first EOF of Atlantic July-August-September SLP anomalies from the NCEP/NCAR reanalysis between 1958 and 2007 (a) and the first EOF of Pacific July-August-September SLP anomalies from the NCEP/NCAR reanalysis between 1958 and 2007 (b). The first Atlantic EOF is the NAO; the first Pacific EOF is the PNA. Solid (dashed) contours are positive (negative) values. Contouring is 1 hPa, and the zero contour is suppressed. Panel c plots the corresponding seasonally averaged Atlantic (red) and Pacific (blue) principle components.

161

a) NAO Sea Ice and SLP regressions
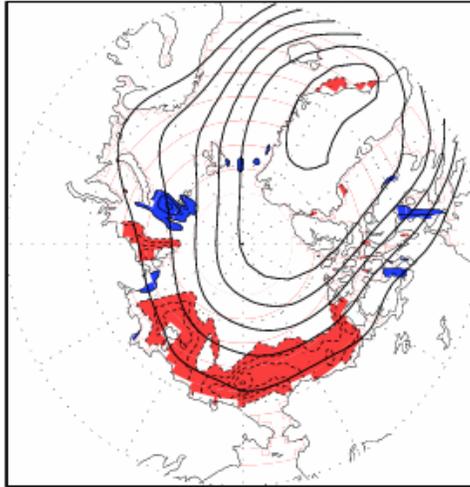
b) PNA Sea Ice and SLP regressions
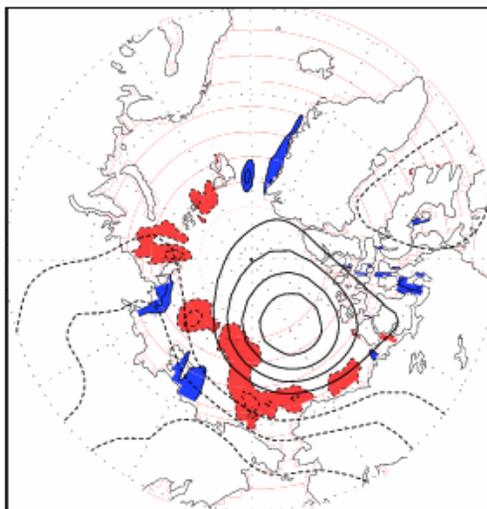
Figure 4.15: Regressions of detrended seasonal JAS summer teleconnection indices on detrended seasonal JAS summer sea ice concentration (shaded/contoured) and monthly J-A-S summer teleconnection indices on monthly J-A-S SLP (thick contours). Panel a are the NAO regressions; panel b is are the PNA regressions. Red (blue) shading and dashed (solid) contours indicate negative (positive) values; contour interval is 3% for sea ice; 1 hPa for SLP. The zero contour is suppressed.

a) JAS Sea Ice Trend related to Winter Variability
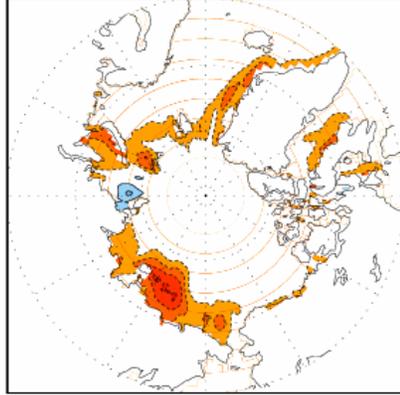
b) JAS Sea Ice Trend related to Summer Variability
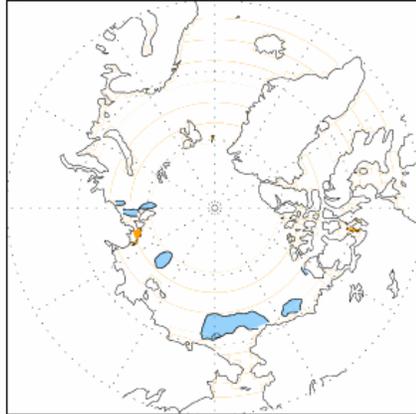
c) JAS Sea Ice Trend without Winter+Summer Variability
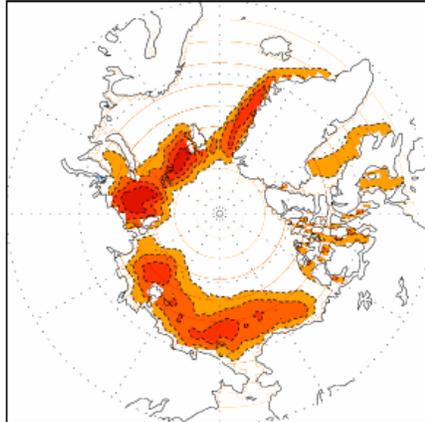
Figure 4.16: Linear trend in JAS sea ice concentration attributable to winter (a) and summer (b) natural climate variability and the linear trend in the remaining sea ice concentration (c) during the period 1958-2007. Red (blue) shading and dashed (solid) contours indicate sea ice decline (gain); contour interval is 1% per decade (5% per decade in panel c) and the zero contour is suppressed.
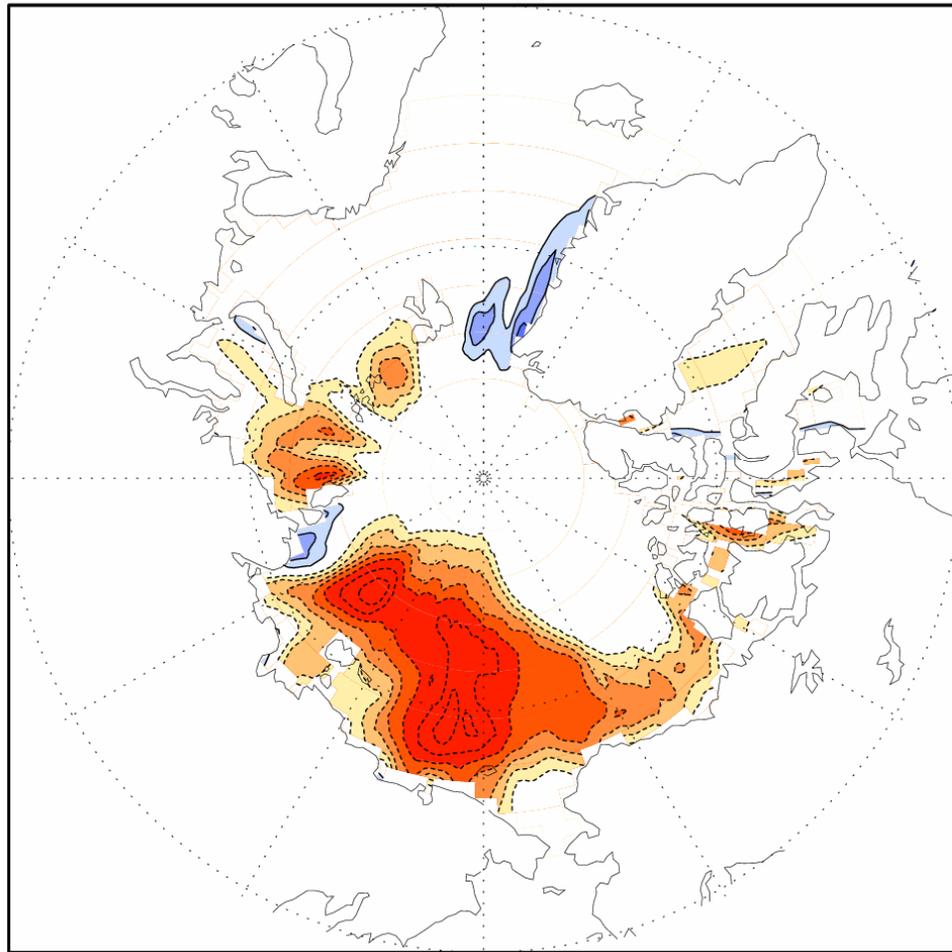
Figure 4.17: Seasonal sea ice concentration anomalies during JAS 2007 from the HadISST1.1. Shading/contouring follows previous figure, and the contour interval is 10%. The zero contour is suppressed.
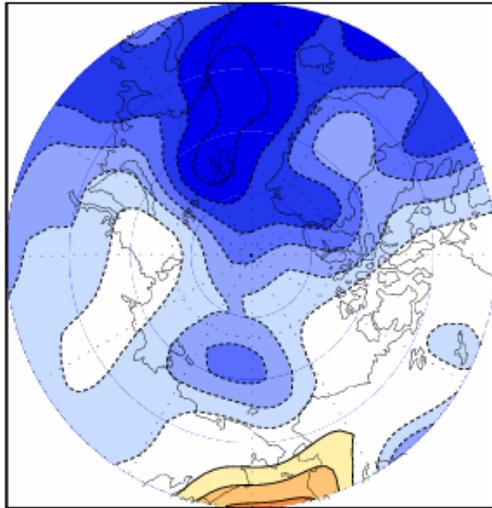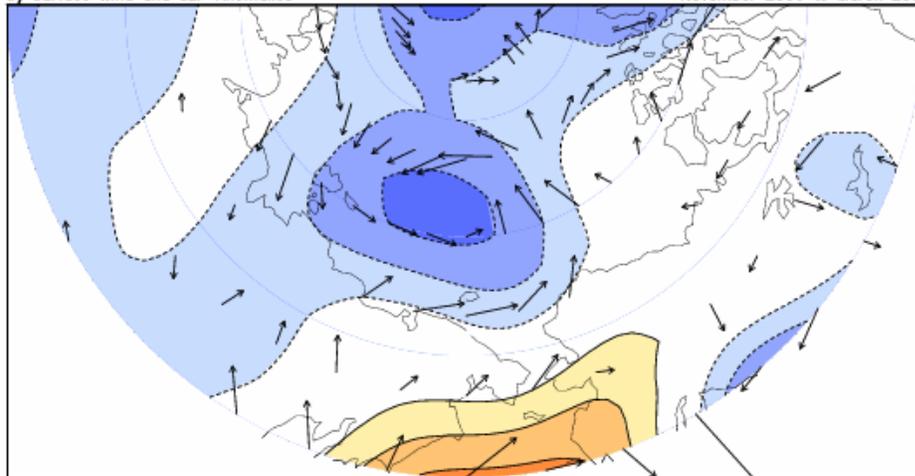
Figure 4.18: Hemispheric NCEP/NCAR SLP anomalies during November 2006 through March 2007 (a) and SLP (shading/contouring) and surface wind (vectors) anomalies in the Pacific sector of the Arctic for the same period (b). SLP anomalies are contoured 1 hPa; vector scale is plotted beneath panel b. Zero contour is suppressed.

Teleconnection	PC Value – Winter 2006/07
ENSO+	0.14
ENSO-	-0.17
ENSO-NC	1.2
NP-PDV	0.84
PP-PDV	1.03
Biennial	0.17
NAO	0.51

Table 4.2: Principal component values of the six natural modes of Pacific SST variability and the NAO during winter 2006/2007.
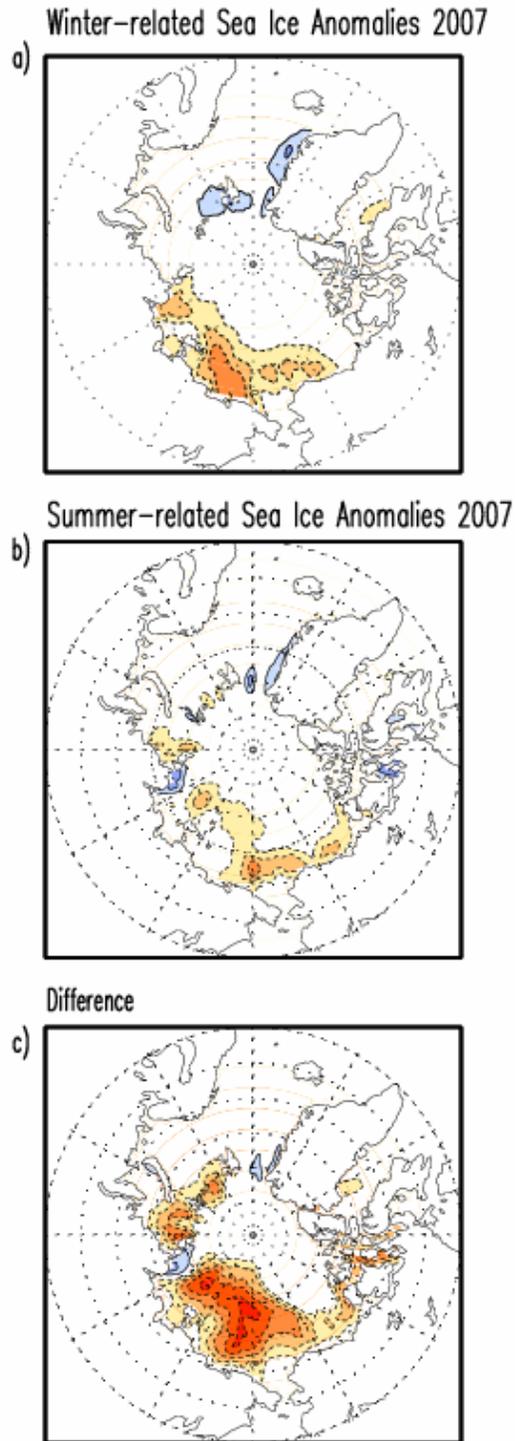
Figure 4.19: Seasonal sea ice concentration anomalies during JAS 2007 related to winter (a) and summer (b) natural climate variability. Panel c is the JAS sea ice anomalies remaining after the influences of natural climate variability are removed from the sea ice record. Panels a and b are contoured/shaded at 5%; panel c is contoured/shaded at 10%. The zero contour is suppressed; shading convention follows figure 4.14.
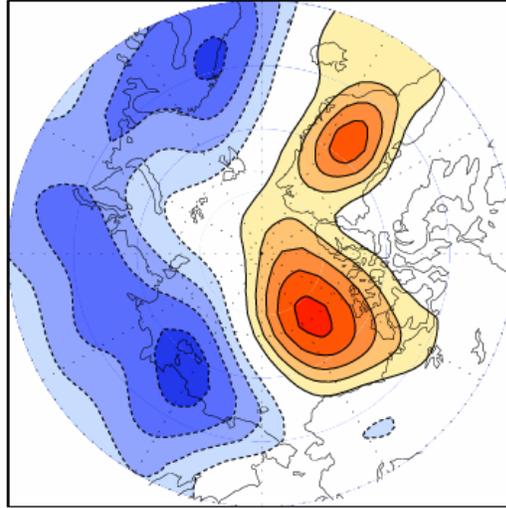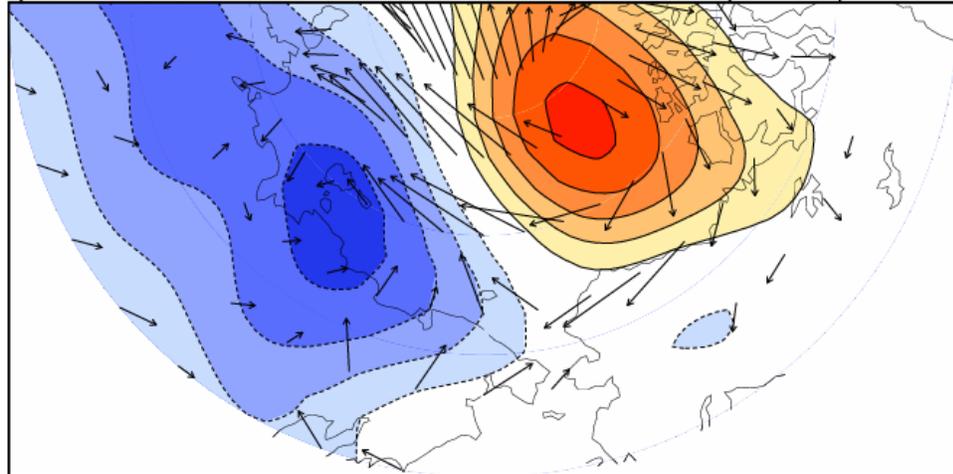
Figure 4.20: Hemispheric NCEP/NCAR SLP anomalies averaged between May 2007 and September 2007 (a) and SLP (shading/contouring) and surface wind (vectors) in the Pacific sector of the Arctic for the same period (b). SLP anomalies are contoured 3 hPa; vector scale is plotted beneath panel b.

Chapter 5: Conclusion

5.1 – The mature phase NPO/WP

The second chapter of this study presents a refined description of the North Pacific Oscillation (in winter sea-level pressure) and its upper-air signature, the West Pacific teleconnection pattern. The surface variability pattern has been known for almost a century (since 1916, see Walker and Bliss 1932), and by the NPO name since 1928. Yet, and despite its origin as a North American weather-influencing pattern in the far upstream region (with predictability implications), only a handful of studies have sought to further characterize the NPO structure and impacts in the intervening decades (Wallace and Gutzler 1981, Rogers 1981, Lau 1988, Nigam 2003). This is in stark contrast with the North Atlantic Oscillation, a basin analog of the NPO (a case made in Nigam 2003 and here), which has been more extensively studied because of its European weather and climate impacts (e.g., Hurrell et al. 2006) and influence on the trans-Atlantic shipping industry.

The study seeks to advance understanding of NPO/WP's spatio-temporal structure, variability mechanism(s), and Arctic sea-ice and North American hydroclimate impacts. The mature phase of variability is targeted first because it is easily identified in monthly-averages which are readily available; it fosters intercomparison with previous studies which are, by and large, based on monthly data; and because robust impacts anticipated in the mature phase can provide rationale and motivation for the subsequent weekly resolution and evolution focused analysis.

The principal findings of the monthly analysis are

- North Pacific Oscillation and the West Pacific teleconnection pattern are two faces of the same variability mode, the NPO/WP. While this link has been noted before (Wallace and Gutzler 1981, Hsu and Wallace 1985, Nigam 2003), it has hitherto not been firmly established from consistent analysis of long data records.

- NPO/WP is very influential on marginal ice zone extent in the Arctic Seas, with the western Bering Sea and Sea of Okhotsk ice zones significantly extended during the positive NPO/WP phase. The influence on the Arctic MIZ extent surpasses that of other Pacific variability modes (PNA, ENSO).

- NPO/WP exerts substantial influence on North American hydroclimate, leading to continent-wide warming and increased precipitation along the Alaskan/Canadian coast and over the south-central Great Plains. The hydroclimate impact is, at least, as significant as the winter PNA and ENSO impacts in these regions.

- NPO/WP is a basin analog of the NAO: Both exhibit similar dipolar SLP anomalies, perturb the climatological jet in their basin sectors similarly, and are connected to stormtrack modulation (Lau 1988). The parallel structure suggests that similar dynamical mechanisms may be operative as well, raising the possibility of dynamical analogs.

5.2 – Weekly analysis of the NPO/WP

Monthly analysis provides valuable insight into the mature-phase structure but little into variability evolution, i.e., genesis and decay of NPO/WP variability. The rapidity with which teleconnections grow and decay has been documented in earlier literature, using a variety of variables from unfiltered daily data (Feldstein 2000) to filtered weekly variances (Lau 1988). Furthermore, modeling studies (Hoskins and

Karoly 1981; Simmons et al. 1983) have demonstrated the decay scale of teleconnections and the energy propagation associated with them is 7-14 days, substantially shorter than a month. Using weekly winter 200 hPa geopotential height anomalies, Nigam established the waxing and waning of a PNA episode. A discernible signal was seen in 200 hPa geopotential height 2 weeks prior to the peak phase, and the 200 hPa height pattern 2 weeks after the mature phase bore virtually no resemblance to the nascent phase. Thus, to truly appreciate the evolutionary structure of teleconnections, namely the NPO/WP, submonthly quantities are analyzed.

EEOF analysis is the ideal statistical tool to isolate various modes of spatio-temporal variability, and applying this technique to weekly SLP anomalies during DJFM 1958-2001 returns the NPO/WP as the second mode of submonthly variability in the North Pacific. The NPO/WP undergoes significant evolution at the surface and in the middle to upper troposphere; the hydroclimate, SST and sea ice response to these rapid circulation changes is immediate. Furthermore, lag-lead relationships between the NPO/WP and other teleconnections are investigated; these lag-lead relationships can not be determined from an analysis of monthly quantities.

The significant findings of the weekly analysis are:

- The SLP signature of the NPO/WP displays a monopole-dipole-monopole structure over a five week period. The initial pressure perturbation occurs in the vicinity of the climatological Aleutian Low; the decay phase features a longitudinally broad region of high pressure extending across the midlatitude Pacific Basin.

- The NPO/WP displays an equivalent cold-core barotropic vertical structure over the Pacific Ocean during all five weeks; over the western North American continent, the

structure is baroclinic, consistent with the earlier findings of Hsu and Wallace (1985). The jet anomalies indicate initial jet intensification in the climatological exit region of the Asian Pacific jet, followed by a latitudinal displacement. The evolution of the jet anomalies, and therefore, stormtrack, resolve the earlier inconsistencies between the conclusions drawn by Lau (1988) and us.

- NPO/WP exerts substantial influence on weekly North American hydroclimate, decreasing precipitation over the Pacific Northwest, likely due to a disruption of the Sverdrup balance. Over the eastern United States, the NPO/WP is initially linked to a decline in precipitation, after the peak phase, the anomaly flips sign and precipitation increases in this region. The precipitation anomalies appear to be related to a weakening, and then intensification of the Atlantic jet. Like the monthly analysis, weekly analysis of the NPO/WP effect on temperature links it to a continental warming.

- Both SST and the MIZ respond to an NPO/WP episode on weekly timescales. A tripole in SST anomalies, related to the surface wind forcing, appears two weeks after the peak NPO/WP phase. This linkage is also found in Timlin and Deser (1997). An NPO/WP episode causes a net increase in sea ice in the Sea of Okhotsk and a net decrease in sea ice in the eastern Bering Sea. The MIZ in the western Bering Sea is extended south throughout an NPO/WP episode. The sea ice anomalies two weeks prior to the peak phase are described in Rogers (1981) as the NPO sea ice footprint; this discrepancy is due to Rogers defining the peak NPO phase as the SLP structure two weeks prior to the mature phase.

- The phase of the PNA at +2 weeks slightly resembles the initial NPO SLP perturbation; a lag-lead correlation calculated between the two PCs (the PNA is EEOF1 of weekly Pacific SLP) reveals that there is no strong linkage between the two.

- Interbasin connections to the NAO are sought; none are found. The NAO does display some similar evolutionary characteristics, with the northern node initially the strongest and the southern node amplified during the decay phase. The timescale of these two teleconnections differs; based on the autocorrelation of the NPO/WP PC, an episode lasts for approximately 2-3 weeks, while an NAO episode is more persistent, lasting 5-6 weeks. Furthermore, the correlation between the two PCs never exceeds 0.1.

5.3 – Natural variability in the Arctic sea ice record

The first two chapters of this study demonstrate the importance of atmospheric variability for sea ice distribution during the winter months. Sea ice contains a substantial amount of memory, so winter circulation variability can also leave a seasonal footprint on the sea ice that does not become evident until the summer months. Rigor et al. (2002) demonstrated this in their study which investigated the impacts of the winter AO on summer sea ice distribution; they found the polar cyclonic circulation anomalies associated with the high index phase of the AO forced Ekman divergence of sea ice and lead to thin ice growth in the leads and fractures of the older ice pack. During the subsequent summer, this newer ice melts faster, reducing sea ice concentration. This impact is most evident in the marginal seas along the Russian and North American northern coasts. The AO is not the only teleconnection which imposes circulation

anomalies at the air-ice interface; the other dominant winter teleconnections also impact polar circulation, leading to additional seasonal footprints. Furthermore, Pacific SST variability and summer teleconnections are also connected with high latitude circulation anomalies; these as well can contribute to sea ice anomalies. All of these teleconnections acting in concert can have a substantial effect on summer sea ice extent, causing severe ice loss in the Laptev Sea, Eastern Siberian Sea, Chukchi Sea and Beaufort Sea. These four seas contains much of the linear trend and we find that a fraction of the trend is attributable to natural variability in both the winter and summer climate. The important aspects are summarized below.

- September Arctic sea ice exhibits a concentric 5-15% decline per decade for the period 1958-2007; the sea ice trend during the satellite era is not uniform and is amplified in the Pacific marginal seas to 30% per decade. The seasonal trend in JAS summer sea ice is spatially identical, but the magnitude is reduced one-third to one-half.

- The winter variability patterns important for interannual sea ice variations are the NAO, the non-canonical mode of ENSO and North Pacific-Pacific Decadal Variability; the other modes are not highly influential individually. The Eastern Siberian Sea contains the largest natural variability signal.

- Trends in natural winter variability, especially the linear trend in the NAO index, account for a third of the total linear trend in JAS sea ice between 1958 and 2007. For 1979-2007, the trend induced by natural winter variability is also approximately a third of the total trend in the Pacific marginal seas. In the Atlantic, the linear trend related to winter variability is positive, offsetting the sea

ice loss related to alternative forcings. This is largely due to the NP-PDV, which captures the 1976/77 climate transition and switched to conditions favorable for sea ice growth.

- The two contemporaneous teleconnections most influential for summer sea ice distribution are the NAO and PNA. Both are influential in the Chukchi Sea and Beaufort Sea; neither index displays a significant linear trend and are only responsible for a sea ice gain of 1% per decade.

- The summer of 2007 featured the most substantial sea ice loss since modern record keeping began; both the winter and summer circulation was favorable for a drastic sea ice loss. Cyclonic anomalies were present during the winter of 2006-2007; a strong anticyclone was present during the late spring and summer of 2007. This led to thin ice growth and Ekman convergence, greatly reducing summer sea ice extent.

- The phases of all influential teleconnections in 2007 were conducive to a massive sea ice loss. The winter related anomalies were as large as 15-20% in the Eastern Siberian Sea; the summer related anomalies exceeded 10% in the Chukchi and Beaufort Seas. Removal of the anomalies related to natural variability from the total sea ice record greatly lessens the ice anomaly severity.

We do not account for variations in the ocean circulation which alter the flux of Atlantic and Pacific water into the Arctic via the Bering Strait, Fram Strait and Davis Strait (Williams 2004, Woodgate and Aagaard 2005). Multiple studies have demonstrated decadal to interdecadal variations in these currents (Dickson et al. 2008),

and like SST variability, the low frequency fluctuations in the sub-surface ocean circulation are possibly aliased into the short sea ice record as a trend.

The climate is undeniably changing, and one of the biggest challenges to the scientific community at large is to separate climate variability from climate change, and attribute these transformations to both natural climate variability and anthropogenic climate change. This work is an attempt to do just that. The first two-thirds detail an infrequently studied, but highly influential teleconnection pattern, the North Pacific Oscillation/West Pacific pattern. The NPO/WP exerts a large influence on the precipitation distribution in the Pacific Northwest, an area climatologically sensitive to slight changes in atmospheric circulation due to the strong seasonal cycle in precipitation. The NPO/WP is also linked to precipitation in the Great Plains and the southeast United States; the southeastern states are currently in the throws of one of the most severe droughts in history (CPC 2008). Parceling the precipitation anomaly into teleconnection-related anomalies and the residual will help decision-makers develop both short term and long term solutions to water management.

The last third of the thesis addresses a more important issue; the observed loss of Arctic sea ice during the latter part of the 20th century, continuing into the 21st. The loss of perennial sea ice in the Arctic during the summer months has enormous climatic and geopolitical consequences, and can potentially occur sooner than initially projected. However, not all of the Arctic sea ice loss is related to anthropogenic climate change. We demonstrated a fraction of the trend is attributable to a phasing of certain teleconnections, which are exacerbating or offsetting the sea ice loss. The actual trend in Arctic sea ice is uniform around the ice cap, with an average loss of 10% per decade.

Nonetheless, this work is merely a start; more analysis of the dynamics and thermodynamics governing Arctic sea ice and more comprehensive observations must be developed to isolate the trend related to anthropogenic climate change and the trend related to natural climate variations.

References

Ambaum, M. H. P., B. J. Hoskins and D. B. Stephenson, 2001: Arctic Oscillation or North Atlantic Oscillation? *J. Climate*, **14**, 3495-3507.

Alexander, M. A., I. Bladé, M., Newman, J. R. Lanzante, N.-C. Lau and J. D. Scott, 2004: The atmospheric bridge: The influence of ENSO teleconnections as air-sea interaction over the global oceans. *J. Climate*, **15**, 2205-2231.

Barnston, A. G. and R. E. Livezey, 1987: Classification, seasonality and persistence of low-frequency atmospheric circulation patterns**.** *Mon. Wea. Rev.*, **115**, 1083–1126.

Björnsson, H. and S. A. Venegas, 1997: A Manual for EOF and SVD analyses of climatic data.

Black, R. X. and R. M. Dole, 1993: The dynamics of large-scale cyclogenesis over the North Pacific Ocean. *J. Atmos. Sci.*, **50,** 421-442.

Cassou, C., L. Terray, J. W. Hurrell and C. Deser, 2004: North Atlantic winter climate regimes: Spatial asymmetry, stationary with time, and oceanic forcing. *J. Climate*, **17**, 1055-1068.

Cassou, C., C. Deser, L. Terray, J. W. Hurrell and M. Drévillon, 2004: Summer sea surface temperature conditions in the North Atlantic and their impact upon atmospheric circulation in early winter. *J. Climate*, **17**, 3349-3363.

Cavalieri, D. J. and C. L. Parkinson, 1987: On the relationship between atmospheric circulation and fluctuation in the sea ice extents of the Bering and Okhotsk Seas. *J. Geophys. Res.,* **92**, 7141-7162.

Cavalieri, D., C. Parkinson, P. Gloerson, and H. J. Zwally. 1997, updated 2006. *Sea ice concentrations from Nimbus-7 SMMR and DMSP SSM/I passive microwave data,*

January 1979 to December 2001. Boulder, CO, USA: National Snow and Ice Data Center. Digital media.

Cayan, D. R., 1992: Latent and sensible heat flux anomalies over the northern oceans: The connections to monthly atmospheric circulation. *J. Climate*, **5**, 354-369.

Chaing, J. C. H. and D. J. Vimont, 2004: Analogous Pacific and Atlantic meridional modes of tropical atmosphere-ocean variability. *J. Climate,* **17**, 4143-4158.

Chan S., and S. Nigam, 2007: Intercomparison of residually diagnosed diabatic heating from ERA-40, ERA-15 and NCEP Reanalyses. To be submitted to *Journal of Climate. Draft manuscript available.*

Chang, E. K. M., 1993: Downstream development of baroclinic waves as inferred from regression analysis. *J. Atmos. Sci.*, **50**, 2038-2053.

Chang, E. K. M., Lee, S. and Swanson, K. L, 2002: Storm track dynamics. *J. Climate*, **15**, 2163-2183.

Crantz, D. 1765: *History of Greenland*, 2nd ed., 2 vols., London, 1820, see p. 42.

Dannmeyer, F., 1948: Zur Frage der Gegensätzlichkeit der kalten winter in Grönland zu den Warmen Wintern in Deutschland. *Polarforsch.*, **2***,* 29-30.

Deser, C. and M. S. Timlin, 1997: Atmosphere-ocean interaction on weekly timescales in the North Atlantic and Pacific. *J. Climate*, **10**, 393-408.

Deser, C., J. E. Walsh and M. S. Timlin, 2000: Arctic sea ice variability in the context of recent atmospheric circulation trends. *J. Climate*, **13**, 617-633.

Dewey, K. F., and R. Heim, Jr. 1981. Satellite observations of variations in Northern Hemisphere seasonal snow cover. NOAA Technical Report NESS 87. 83 pp.

Dewey, K. F., and R. Heim Jr. 1982. New data base: a digital archive of Northern

   Hemisphere snow cover. Presented at Western Snow Conference, April 19-23.

   Reno, NV, 9 pp.

Dickson, B., J. Meincke and P. Rhines, 2008: Arctic-subarctic ocean fluxes: Defining the

   roles of northern seas in climate. Netherlands: Springer Netherlands.

Di Lorenzo, E., N. Schneider, K. M. Cobb, P. J. S. Franks, K. Chhak, A. J. Miller, J. C.

   McWilliams, S. J. Bograd, H. Arango, E. Curchitser, T. M. Powell and P. Riviere,

   2008: North Pacific Gyre Oscillation links ocean climate and ecosystem change.

   Geophys. Res. Lett., **35**, L08607, doi:10.1029/2007GL032838.

Dole, R. M. and N. D. Gordon, 1983: Persistent anomalies of the extratropical Northern

   Hemisphere wintertime circulation: Geographical distribution and regional persistence

   characteristics. *Mon. Wea. Rev.*, **111**, 1567-1586.

Dole, R. M., 1986: Persistent anomalies of the extratropical Northern Hemisphere

   wintertime circulation: Structure. *Mon. Wea. Rev.*, **114**, 178-207.

Dole, R. M. and R. X. Black, 1990: Life cycles of persistent anomalies. Part II: The

   development of persistent negative height anomalies over the North Pacific Ocean.

   Mon. Wea. Rev., **118**, 824-846.

Esbensen, S. K., 1984: A comparison of intermonthly and interannual teleconnections in

   the 700 mb geopotential height field during Northern Hemisphere winter. *Mon. Wea.

   Rev.*, **112**, 2016-2032.

Fang, Z. and J. M. Wallace, 1994: Arctic sea ice variability on a timescale of weeks and

   its relation to atmospheric forcing. *J. Climate*, **7**, 1897-1914.

Feldstein, S. B., 2000: The timescale, power spectra, and climate noise properties of teleconnection patterns. *J. Climate*, **13**, 4430-4440.

Fissel, D. B. and C. L. Tang, 1991: Response of sea ice drift to wind forcing on the northeastern Newfoundland shelf. *J. Geophys. Res.*, **96**, 18,397-18,409.

Green, P. M., D. M. Legler, C. J. Miranda V, and J. J. O'Brien (1997): The North American climate patterns associated with the El Niño-Southern Oscillation. *COAPS Project Report Series 97-1*. Published by the Center for Ocean-Atmosphere Prediction Studies, Florida State University, Tallahassee, FL. Retrieved from the world wide web February 2, 2007: http://www.coaps.fsu.edu/lib/booklet/

Guan, B., and S. Nigam, 2008: Pacific Sea Surface Temperatures in the Twentieth Century: An evolution-centric analysis of variability and trend. Submitted to *J Climate* on 3 June; under revision.)

Gudkovich, Z. M., 1961: Relation of the ice drift in the Arctic Basin to ice conditions in Soviet Arctic seas (in Russian), *Tr. Okeanogr. Kom. Akad. Nauk SSSR*, **11**, 14-21.

Higgins, R. W., W. Shi, E. Yarosh, R. Joyce, 2000: Improved United States precipitation quality control system and analysis. *NCEP/Climate Prediction Center ATLAS No. 7*. U.S. DEPARTMENT OF COMMERCE, National Oceanic and Atmospheric Administration, National Weather Service.

Horel, J. D., 1981: A rotated principal component analysis of the interannual variability of the Northern Hemisphere 500 mb height field. *Mon. Wea. Rev.*, **109**, 2080-2092.

Hoskins, B. J. and D. J. Karoly, 1981: The steady linear response of a spherical atmosphere to thermal and orographic forcing. *J. Atmos. Sci.*, **38**, 1179-1196.

Hoskins, B. J., H. H. Hsu, I. N. James, M. Masutani, P. D. Sardeshmukh, and G. H. White, 1989: Diagnostics of the global atmospheric circulation based on ECMWF analyses 1979-1989. *WCRP-27; WMO/TD-No. 326*, 217pp.

Hsu, H.-H. and J. M. Wallace, 1985: Vertical structure of wintertime teleconnection patterns. *J. Atmos. Sci.*, **42**, 1693-1710.

Hurrell, J.W., 1995: Decadal Trends in the North Atlantic Oscillation: Regional Temperatures and Precipitation**.** *Science,* **269**, 676-679.

Hurrell, J. W., M. Visbeck, A. Busalacchi, R. A. Clarke, T. L. Delworth, R. R. Dickson, W. E. Johns, K. P. Koltermann, Y. Kushnir, D. Marshall, C. Mauritzen, M. S. McCartney, A. Piola, C. Reason, G. Reverdin, F. Schott, R. Sutton, I. Wainer, and D. Wright, 2006: Atlantic climate variability and predictability: A CLIVAR perspective. *J. Climate*, **19**, 5100-5121.

Intergovernmental Panel on Climate Change, 2007: Climate change 2007. *Fourth Assessment Report.*

Johnson, C. M., 1980: Wintertime Arctic sea ice extremes and the simultaneous atmospheric Circulation. *Mon. Wea. Rev.*, **108**, 1782–1791.

Kaiser, H. F., 1958: The varimax criterion for analytic rotation in factor analysis. *Psychometrika*, **23**, 187-200.

Kalnay, E. and co-authors, 1996: The NCEP/NCAR 40 year reanalysis project. *Bull. Amer. Meteor. Soc.*, **77,** 437-471.

Kutzbach J. E., 1967: Empirical eigenvectors of sea-level pressure, surface temperature and precipitation complexes over North America. *J. App. Meteoro.*, **6**, 791–802.

Kutzbach, J. E., 1970: Large-scale features of monthly mean Northern Hemisphere anomaly maps of sea-level pressure. *Mon. Wea. Rev.*, **98**, 1166-1171.

Lau, N.-C., 1988: Variability of the observed midlatitude storm tracks in relation to low-frequency changes in the circulation pattern. *J. Atmos. Sci.*, **45**, 2718-2743.

Lau, N.-C. and M. J. Nath, 1991: Variability of the baroclinic and barotropic transient eddy forcing associated with monthly changes in the midlatitude storm tracks. *J. Atmos. Sci.*, **48**, 2589-2613.

Lau, N.-C. and M. J. Nath, 1996: The Role of the "Atmospheric Bridge" in linking tropical Pacific ENSO events to extratropical SST anomalies. *J. Climate*, **9**, 2036-2057.

Lau, N.-C., 1997: Interactions between global SST anomalies and the midlatitude atmospheric circulation. *Bull. Amer. Meteorolo. Soc.*, **78**, 21-33.

Madden, R. A. and P. R. Julian, 1971: Detection of a 40-50 day oscillation in the zonal wind in the Tropical Pacific. *J. Atmos. Sci.*, **28**, 702-708.

Madden, R. A. and P. R. Julian, 1972: Description of global-scale circulation cells in the Tropics with a 40-50 day period. *J. Atmos. Sci.*, **29**, 1109-1123.

Mantua, N.J., S.R. Hare, Y. Zhang, J.M. Wallace, and R.C. Francis, 1997: A Pacific decadal climate oscillation with impacts on salmon. *Bull. Amer Meteorol. Soc.*, **78**, 1069-1079.

Maslanik, J. S. Drobot, C. Fowler, W. Emery and R. Barry, 2007: On the Arctic climate paradox and the continuing role of atmospheric circulation in affecting sea ice conditions. *Geophys. Res. Lett.*, **34,** L03711, doi:10.1029/2006GL028269.

Meier, W., J. Stroeve, F. Fetterer and K. Knowles, 2005: Reductions in Arctic sea ice cover no longer limited to summer. *EOS*, **86**, 326-327.

Mesinger F. et al, 2006: North American Regional Reanalysis. *Bull. Amer. Meteoro. Soc., 87,* 343-360.

Mitchell, T.D. and P. D. Jones, 2005: An improved method of constructing a database of monthly climate observations and associated high resolution grids. *Inter. J. Climatolo.*, **25**, 693-712.

Nakamura, H. and J. M. Wallace, 1990: Observed changes in baroclinic wave activity during the life cycles of low-frequency circulation anomalies. *J. Atmos. Sci.*, **47**, 1100-1116.

National Snow and Ice Data Center, 2007: All about sea ice: Terminology. Found at http://www.nsidc.org/seaice/data/terminology.html. Retrieved from the World Wide Web on January 25, 2008.

National Snow and Ice Data Center, 2007: Arctic sea ice news, Fall 2007. Found at http://www.nsidc.org/news/press/2007_seaiceminimum/20070810_index.html. Retrieved from the World Wide Web on November 15th, 2007.

Niebauer, H. J., 1988: Effects of El Niño-Southern Oscillation and North Pacific weather patterns on interannual variability in the subarctic Bering Sea. *J. Geophys. Res.*, **93**, 5051-5068.

Niebauer, H. J., 1998: Variability in Bering Sea ice cover as affected by a "regime shift" in the north Pacific in the period 1947-96. *J. Geophys. Res.*, **103**, 27,717-27,737.

Niebauer, H. J., 1999: The 1997-98 El Niño in the Bering Sea as compared with previous ENSO events and the "regime shift" of the late 1970s. *Proceedings of the 1998 Science*

Board Symposium on the impacts of the 1997/98 El Niño event on the North Pacific Ocean and its marginal seas, **PICES Scientific Report No. 10**.

Nigam, S., and A. Ruiz-Barradas, 2006: Seasonal Hydroclimate Variability over North America in Global and Regional Reanalyses and AMIP Simulations: Varied Representation. *J. Climate*, 19, 815-837.

Nigam, S., 2003: Teleconnections. *Encyclopedia of Atmospheric Sciences*; Editors: J.R. Holton, J.A. Pyle & J.A. Curry; Academic Press, Elsevier Science, London, 2243-2269.

Nigam, S. and E. Deweaver, 2003: Stationary waves (Orographically and Thermally forced): Thermal *Encyclopedia of Atmospheric Sciences*; Editors: J.R. Holton, J.A. Pyle & J.A. Curry; Academic Press, Elsevier Science, London, 2121-2137.

Nigam, S, C. Chung, and E. DeWeaver, 2000: ENSO Diabatic Heating in ECMWF and NCEP Reanalyses, and NCAR CCM3 Simulation. *J. Climate,* **13,** 3152-3171.

Nigam, S., 1994: On the Dynamical Basis for the Asian Summer Monsoon Rainfall-El Niño Relationship. *J. Climate,* **7,** 1750-1771.

Nigam, S., and H. S. Shen, 1993: Structure of oceanic and atmospheric low-frequency variability over the tropical Pacific and Indian oceans. Part I: COADS observations. *J Climate,* **6,** 657-676.

Ogi, M., K. Yamazaki and Y. Tachibana, 2004: The summertime annular mode in the Northern Hemisphere and its linkage to the winter mode. *J. Geophys. Res.*, **109**,

Ogi, M. and J. M. Wallace, 2007: Summer minimum Arctic sea ice extent and the associated summer circulation. *Geophys. Res. Lett.*, **34**,

Orlanski, I., 2005: A new look at the Pacific storm track variability: Sensitivity to tropical SST and to upstream seeding. *J. Atmos. Sci.*, **62**, 1367-1390.

Parkinson, C. L. and A. J. Gratz, 1983: On the seasonal sea ice cover in the Sea of

    Okhotsk. *J. Geophys. Res.*, **88**, 2793-2802.

Pease, C. H., 1980: Eastern Bering Sea ice processes. *Mon. Wea. Rev.*, **108**, 2015–2023.

Preisendorfer R. W., 1988: *Principal Component Analysis in Meteorology and*

    oceanography, Mobley CD (ed). Elsevier: Amsterdam

Prinsenberg, S. J., I. K. Peterson, S. Narayanan, and J. U. Umoh, 1997: Interaction

    between atmosphere, ice cover, and ocean off Labrador and Newfoundland from 1962–

    1992. *Can. J. Aquat. Sci.,* **54,** 30–39.

Rayner, N. A., D. E. Parker, E. B. Horton, C. K. Folland, L. V. Alexander, D. P. Rowell,

    E. C. Kent, and A. Kaplan, 2003: Global analyses of sea surface temperature, sea ice,

    and night marine air temperature since the late nineteenth century. *J. Geophys. Res.,*

    108, 4407.

Rayner, N. A., P. Brohan, D. E. Parker, C. K. Folland, J. J. Kennedy, M. Vanicek, T. J.

    Ansell and S. F. B. Tett: Improved analysis of changes and uncertainties in sea surface

    temperature measured in situ since the mid-nineteenth century: The HadSST2 dataset.

    J. Climate, **19**, 446-469.

Renwick, J. A. and J. M. Wallace, 1996: Relationships between North Pacific blocking,

    El Niño and the PNA pattern. *Mon. Wea. Rev.*, **124**, 2071-2076.

Rex, D. F., 1950a: Blocking action in the middle troposphere and its effects on regional

    climate I. An aerological study of blocking. *Tellus*, **2**, 196-211.

Rex, D. F., 1950b: Blocking action in the middle troposphere and its effects on regional

    climate II. The climatology of blocking action. *Tellus*, **2**, 275-301.

Reynolds, R.W., N.A. Rayner, T.M. Smith, D.C. Stokes, and W. Wang, 2002: An improved in situ and satellite SST analysis for climate. *J. Climate*, **15**, 1609-1625.

Richman, M. B., and P. J. Lamb, 1985: Climatic pattern analysis of 3- and 7-day summer rainfall in the central United States: Some methodological considerations and a regionalization. *J. Clim. Appl. Meteor.*, **24**, 1325-1343.

Richman, M. B., 1986: Rotation of principal components. *Int'l J. Climatol.*, **6**, 293–335.

Rigor, I.G., J. M. Wallace and R. L. Colony, 2002: On the response of sea ice to the Arctic Oscillation, *J. Clim.*, **15**, 2546-2663.

Rigor, I. G., T. Arbetter, M. Ortmeyer, P. Clemente-Colón, and J. Woods, 2008: An assessment of Arctic sea ice forecasts on seasonal time scales. Presentation 7A.4 presented at the *24th Conference on IIPS* during the *88th Annual Meeting of the American Meteorological Society*. January 20-24, 2008, New Orleans, LA.

Rogers, J. C. and H. Van Loon, 1979: The seesaw in winter temperatures between Greenland and Northern Europe. Part II: Some oceanic and atmospheric effects in the middle and high latitudes. *Mon. Wea. Rev.*, **107**, 509-519.

Rogers, J. C., 1981: The North Pacific Oscillation. *J. Climatolo.*, **1**, 39-57.

Rogers, J. C., 1990: Patterns of low-frequency monthly sea level pressure variability (1899-1986) and associated wave cyclone frequencies. *J. Climate*, **3**, 1364-1379.

Rogers, J. C. and M. McHugh, 2002: On the separability of the North Atlantic Oscillation and Arctic Oscillation, *Clim. Dyn.*, **19**, 599-608.

Ropelewski, C. F. and M. S. Halpert, 1986: North American precipitation and temperature patterns associated with the El Niño/Southern Oscillation (ENSO). *Mon. Wea. Rev.*, **114**, 2352-2362.

Singarayer, J. S., J. L. Bamber and P. J. Valdes, 2006: Twenty-first-Century climate impacts from a declining Arctic sea ice cover. *J. Climate*, **19**, 1109-1125.

Schevchenko, G. V., A. B. Rabinovich and R. E. Thomson, 2004: Sea-ice drift on the northeastern shelf of Sakhalin Island. *J. Phys. Oceano.*, **34,** 2470-2491.

Simmons, A. J., J. M. Wallace and G. W. Branstator, 1983: Barotropic wave propagation and instability, and atmospheric teleconnection patterns. *J. Atmos. Sci.*, **40**, 1363-1392.

Stroeve, J., M. Serreze, S. Drobot, S. Gearheard, M. Holland, J. Maslanik, W. Meier and T. Scambos, 2008: Arctic sea ice extent plummets in 2007. *EOS*, **89**, 13-14.

Swanson, K. L., P. J. Kushner and I. M. Held, 1997: Dynamics of barotropic storm tracks. *J. Atmos. Sci.*, **54**, 791-810.

Thorndike, A. S. and R. Colony, 1982: Sea ice motion in response to geostrophic winds. *J. Geophys. Res.*, **87**, 5845-5852.

Thompson, D. W. J. and J. M. Wallace, 1998: The Arctic Oscillation signature in wintertime geopotential height and temperature fields. *Geophys. Res. Lett.*, **25**, 1297-1300.

Trenberth, K. E., 1990: Recent observed interdecadal climate changes in the Northern Hemisphere. *Bull. Amer. Meteor. Soc.*, 71, 988–993.

Uppala, S.M., Kållberg, P.W., Simmons, A.J., Andrae, U., da Costa Bechtold, V., Fiorino, M., Gibson, J.K., Haseler, J., Hernandez, A., Kelly, G.A., Li, X., Onogi, K., Saarinen, S., Sokka, N., Allan, R.P., Andersson, E., Arpe, K., Balmaseda, M.A., Beljaars, A.C.M., van de Berg, L., Bidlot, J., Bormann, N., Caires, S., Chevallier, F., Dethof, A., Dragosavac, M., Fisher, M., Fuentes, M., Hagemann, S., Hólm, E., Hoskins, B.J., Isaksen, L., Janssen, P.A.E.M., Jenne, R., McNally, A.P., Mahfouf, J.-F.,

Morcrette, J.-J., Rayner, N.A., Saunders, R.W., Simon, P., Sterl, A., Trenberth, K.E., Untch, A., Vasiljevic, D., Viterbo, P., and Woollen, J., 2005: The ERA-40 re-analysis. *Quart. J. R. Meteorol. Soc.,* **131**, 2961-3012.

Van Loon, H. and J. C. Rogers, 1978: The seesaw in winter temperatures between Greenland and Northern Europe. Part I: General description. *Mon. Wea. Rev.*, **106**, 296-310.

Vimont, D. J., D. S. Battisti and A. C. Hirst, 2001: Footprinting: A seasonal mechanism between the tropics and mid-latitudes. *Geophys. Res. Let.*, **28**, 3923-3926.

Vimont, D. J., D. S. Battisti and A. C. Hirst, 2002: Pacific interannual and interdecadal equatorial variability in a 1000-yr simulation of the CSIRO coupled general circulation model. *J. Climate*, **15**, 160-178.

Vimont, D. J., D. S. Battisti and A. C. Hirst, 2003a: The seasonal footprinting mechanism in the CSIRO general circulation models. *J. Climate*, **16**, 2653-2667.

Vimont, D. J., J. M. Wallace and D. S. Battisti, 2003b: The seasonal footprinting mechanism in the Pacific: Implications for ENSO. *J. Climate*, **16**, 2668-2675.

Walker, G. T., 1923: Correlation in the seasonal variations of weather, VIII: A preliminary study of world weather. *Mem. Indian Meterol. Dept.*, **21**, 75-131.

Wadhams, P., 2003: How does Arctic sea ice form and decay? Retrieved May 19, 2008 from Arctic Theme Page: http://www.arctic.noaa.gov/essay_wadhams.html

Walker, G. T., 1926: Correlation in the seasonal variations of weather, IX: A further study of world weather. *Mem. Indian Meterol. Dept.*, **24**, 275-332.

Walker, G. T. and E. W. Bliss, 1928: World weather III. *Mem. Roy. Meteorol. Soc.*, **2**, 96-134.

Walker, G. T. and E. W. Bliss, 1932: World weather V. *Mem. Roy. Meteorol. Soc.*, **4**, 53-84.

Wallace, J. M. and D. S. Gutzler, 1981: Teleconnections in the geopotential height field during the Northern Hemisphere winter. *Mon. Wea. Rev.,* **109**, 784–812.

Wang, J. and Co-Authors, 2005: Linking the Northern Hemisphere sea ice reduction trend and the quasi-decadal Arctic sea ice oscillation. *Clim. Dyn.*, **24**, 115-130.

Weare, B. C., and J. S. Nasstrom, 1982: Examples of extended empirical orthogonal function analyses. *Mon. Wea. Rev.*, **110**, 481–485.

Williams, C. E. 2004: The circulation and fluxes from the Arctic into the North Atlantic Ocean: 1979-2002 model results. *Naval Research Laboratory.*

Woodgate, R. A. and K. Aagaard, 2005: Revising the Bering Strait freshwater flux into the Arctic Ocean. *Geophys. Res. Lett.*, **32**, L02602, doi:10.1029/2004GL021747.

Wu, B. and Co-Authors, 2006: Dipole anomaly in the winter Arctic atmosphere and its association with sea ice motion. *J. Clim.*, **19**, 210-225.